Diverse intrusion modes during the construction of a high-silica magma reservoir: Evidence from La Obra–Cerro Blanco intrusive suite (central Chile)

Ítalo Payacán, María Alejandra Covarrubias, Nicolás Rodríguez, Lorenzo Tavazzani, Francisco Gutiérrez, Pierrick Roperch, Fernando Poblete, Martín Meyer

Research Paper

GEOSPHERE

GEOSPHERE, v. 20, no. 6

https://doi.org/10.1130/GES02746.1

15 figures; 1 set of supplemental files

CORRESPONDENCE: ipayacan@gmail.com

CITATION: Payacán, I, Covarrubias, M.A., Rodríguez, N., Tavazzani, L., Gutiérrez, F., Roperch, P., Poblete, F., and Meyer, M., 2024, Diverse intrusion modes during the construction of a high-silica magma reservoir: Evidence from La Obra–Cerro Blanco intrusive suite (central Chile): Geosphere, v. 20, no. 6, p. 1622–1654, https://doi.org/10.1130/GES02746.1.

Science Editor: Christopher J. Spencer
Associate Editor: G. Lang Farmer

Received 22 December 2023
Revision received 20 August 2024
Accepted 27 September 2024

Published online 30 October 2024

Diverse intrusion modes during the construction of a high-silica magma reservoir: Evidence from La Obra–Cerro Blanco intrusive suite (central Chile)

Ítalo Payacán[1], María Alejandra Covarrubias[2,*], Nicolás Rodríguez[3,*], Lorenzo Tavazzani[4], Francisco Gutiérrez[5], Pierrick Roperch[6], Fernando Poblete[7], and Martín Meyer[7]

[1]Facultad de Ingeniería, Arquitectura y Diseño, Universidad San Sebastián, Bellavista 7, Recoleta, Santiago 8420524, Chile
[2]Independent researcher, Santiago, Chile
[3]Departamento de Ingeniería Hidráulica y Ambiental, Pontificia Universidad Católica de Chile, Avenida Vicuña Mackenna 4860, Santiago 7820436, Chile
[4]Institute of Geochemistry and Petrology, Department of Earth Sciences, ETH Zürich, 8092 Zürich, Switzerland
[5]GeoExpedition, Las Palomas 25, Pirque, Santiago 9480000, Chile
[6]Géosciences Rennes, Université de Rennes I, 35042 Rennes Cedex, France
[7]Departamento de Geología, Universidad de Chile, Plaza Ercilla 803, Santiago 8370450, Chile

ABSTRACT

Several conceptual models have been proposed for the amalgamation of granitoid plutons, which range from incremental growth to single-stage emplacement of these systems. This diversity of views has led to intense debate about the thermomechanical state of silicic intrusions and the magma differentiation paths within the crust. In this contribution, we present a comprehensive petrologic, geochronologic, and magnetic fabric data set from the La Obra–Cerro Blanco intrusive suite, which allows us to explore the petrogenesis and magma emplacement processes in the upper crust.

This intrusive suite is composed of (1) a vertically zoned granitoid intrusion in spatial association with mafic layers and stocks and (2) a cupola-like high-silica granite. We interpret this intrusive suite as assembled by diverse but coexisting intrusion mechanisms over a time span of ~1.4 m.y. from 21.4 to 19.9 Ma. As indicated by the subhorizontal magnetic lineation, the first stage was dominated by horizontal emplacement of sheet-like intrusions of intermediate compositions, which became increasingly silicic after plagioclase and amphibole fractionation throughout the crustal column. The latest stage was instead dominated by cooling, crystallization, and differentiation of a thickened granitoid body and the formation of a high-silica magma chamber. The steep magnetic lineation and the abundance of aplite and rhyolitic dikes observed in the cupola-like, high-silica granites suggest that this portion acted as an evacuation channel of high-silica magma toward shallower levels, offering a rare opportunity to understand not only silicic magma accumulation and storage in the upper crust, but also the processes connecting the plutonic and volcanic environments.

Italo Payacan https://orcid.org/0000-0002-2198-709X
*Previously at Escuela de Geología, Universidad Mayor, Manuel Montt 367, Providencia, Santiago 7500994, Chile

INTRODUCTION

Deciphering the mechanisms of granitic pluton assembly is fundamental to understanding the conditions of magma storage, quantifying magmatic fluxes through the crust, and, ultimately, assessing if and how these reservoirs are related to volcanic plumbing systems (Bachmann and Huber, 2019; Cashman et al., 2017; Clemens, 1998; Moyen et al., 2021; Petford et al., 2000; Vigneresse and Clemens, 2000). Plutonic bodies represent a time-integrated record of the prolonged history of magma reservoirs, whereby multiple magmatic processes, such as crystal fractionation, continuous magma injection, magma mixing, and cumulate recycling, influence the terminal characteristics of the exposed plutonic rocks (Bergantz, 2000; Hawkins and Wiebe, 2004; Paterson et al., 2019; Sparks et al., 2019; Weinberg et al., 2021). The occurrence of early magmatic phenomena, such as lower- to middle-crustal mineral fractionation and crustal assimilation processes, can be reflected in the compositional variability of the magma batches that form upper-crustal plutons (Clemens et al., 2022a; DePaolo, 1981; Ducea et al. 2015; Kay et al., 2005; Moyen et al., 2021). In arc systems, changes in the source of crustal contamination, the input of terrigenous sediments, or abrupt changes in the tectonic regime affecting the crustal thickness can occur on the scale of a few million years (Alasino et al., 2022; Stern, 1991; Kay et al., 2005; Muñoz et al., 2012; Müntener et al., 2018) and can be recorded in a single magmatic system (Large et al., 2024; Silva et al., 2024). However, the fine-scale details of the magmatic events that produced magma reservoirs are often obscured, both due to the incomplete plutonic record (i.e., deeper levels of intrusions are rarely exposed) and because of overprinting of early magmatic events by late-stage equilibration processes (Cornejo and Mahood, 1997; Gutiérrez et al., 2013).

Over the last decades, combinations of geologic, petrologic, geochronologic, structural, and numerical modeling studies have argued for the incremental construction of granitic plutons, which are now thought to be

built by the amalgamation of multiple discrete magma pulses (Annen, 2009; Burchardt et al., 2012; Coleman et al., 2012; de Saint Blanquat et al., 2011; Karakas et al., 2017; Lipman, 2007; Matzel et al., 2006; Paterson et al., 2008; Rhodes et al., 2021; Schoene et al., 2012). The incremental growth model for construction of granitic magma reservoirs presents an alternative to the classic model advocating for the storage of large, crystal-poor volumes of mobile and eruptible magma in the crust (Glazner et al., 2004). In fact, numerical models of the thermal evolution of magma reservoirs indicate that the long-term cooling time scales expected for a single magma body stored in the upper crust are several orders of magnitude shorter than those obtained from geochronologic constraints on silicic plutons (Annen, 2009; Annen et al., 2014; Barboni et al., 2015; Menand et al., 2015; Morgan et al., 2008; Rhodes et al., 2021). This evidence has led to the proposal that most granitic plutons represent an amalgamation of discrete magma pulses rather than a large reservoir of crystal-poor, highly convective magma (Bartley et al., 2012; Glazner et al., 2004). The multiple magmatic injections that characterize the construction of granitic plutons are usually inferred as sheet-like intrusions (Menand et al., 2011). These incremental pulses may be preserved as subtle lithologic variations within plutons, enabling the identification of the discrete magma batches (Eddy et al., 2016; Farina et al., 2010, 2012; Leuthold et al., 2012; Liu et al., 2018; Wiebe and Collins, 1998). However, incremental constructions can occasionally record early mafic processes at the borders (Kruger and Latypov, 2020; Memeti et al., 2010) or zoned plutons, due to self-mixing and late liquid extraction (Aravena et al., 2017; Payacán et al., 2023; Tavazzani et al., 2024).

Most granitic intrusions exhibit long crystallization time scales (e.g., Alasino et al., 2017; Barboni et al., 2015; de Saint Blanquat et al., 2011; Eddy et al., 2016; Kaiser et al., 2017; Kern et al., 2016; Lipman, 2007; Michel et al., 2008; Paterson et al., 2011; Schoene et al., 2012; Tavazzani et al., 2023), which have been used in estimating magmatic fluxes during plutons assembly, with long-term average estimates for upper-crustal magma reservoirs inferred between 0.001 and 0.01 km^3/yr (Annen et al., 2014). The absolute magnitude and temporal fluctuations of magma injection rates control the thermal conditions of the crust and its ability to store large volumes of mobile magma capable of feeding rhyolitic volcanism. Thermal modeling shows that relatively high injection rates are needed to build and sustain reservoirs that can feed large eruptions (Annen, 2009; Barboni et al., 2015; Gelman et al., 2013; Townsend and Huber, 2020).

In parallel to the incremental assembly model, the crystal-mush paradigm, which states that upper-crustal magma reservoirs are constituted by crystal-rich magma hosting crystal-poor pockets (Bachmann and Bergantz, 2004, 2008), has been widely developed in the literature. This model ascribes the origin of high-SiO_2 rhyolitic melts within upper-crustal reservoirs to processes of crystal-melt separation, and it is supported by several lines of evidence, which are based on the plutonic and volcanic record (Dufek and Bachmann, 2010; Gelman et al., 2014; Lee et al., 2015; Lee and Morton, 2015; Schaen et al., 2018; Tavazzani et al., 2020). The redistribution of silicic melts within the magma reservoirs may result in the concentration of eruptible crystal-poor rhyolitic magma at certain levels (Bachmann and Bergantz, 2004), which can be recorded in the compositional variations of granitic plutons (Eddy et al., 2022; Payacán et al., 2023; Tavazzani et al., 2024). Some researchers, however, highlight the tenuous connection between upper-crustal granitic plutons and rhyolitic eruptions (Glazner et al., 2008), calling into question the role of upper-crustal magma reservoirs in feeding volcanism at the surface (Clemens et al., 2022a, 2022b). In order to shed new light on the nature of granitic plutons and the processes that control the transition between the plutonic and volcanic environments, it is necessary to access more well-documented natural cases of upper-crustal intrusive bodies, where the mechanisms that dominate assembly and magmatic evolution can be identified (Rhodes et al., 2021, 2024; Wallrich et al., 2023).

In this contribution, we present a comprehensive characterization of La Obra–Cerro Blanco intrusive suite, forming a batholith of dioritic to granitic composition, emplaced at upper-crustal levels through the West Andean thrust system in central Chile (33°S–34°S). The magmatic history of this intrusive suite is inferred from geologic mapping, petrographic observations, whole-rock geochemical data, and new in situ Hf isotopes and U-Pb zircon ages. The complex, multistage evolution of the system encompassed parental magma differentiation throughout the crust, initial construction of an upper-crustal reservoir through multiple magma injections, and late differentiation with the formation of a silica-rich magma chamber (a reservoir dominated by mobile magma). With this case study, we illustrate that diverse intrusion modes can occur within a single, albeit multistage, magmatic system and estimate time scales for the emplacement and crystallization of upper-crustal magma reservoirs. Last, by combining this data set with magnetic fabrics obtained via anisotropy of magnetic susceptibility measurements, we reconstruct the internal structure of a fossil magma reservoir that was likely the source for explosive volcanism recorded in the nearby Miocene strata.

GEOLOGIC BACKGROUND

Cenozoic Magmatic Arc in Central Chile

The Paleogene–Neogene magmatic arc in central Chile (33°S–34°S) is represented mainly by two volcanic formations (Abanico and Farellones Formations; Charrier et al., 2002; Nyström et al., 2003; Piquer et al., 2017, 2015; Vergara et al., 1988) and several intrusive bodies related to the Farallon-Nazca oceanic plate subduction (Kay et al., 2005; Kurtz et al., 1997; Muñoz et al., 2013). The arc-related rocks are arranged as north-south belts forming the western Principal Cordillera to the east of Santiago, delimited to the west by the west-vergent Infiernillo–San Ramón fault system (West Andean thrust system) and to the east by the Chacayes-Yesillo fault system (Fig. 1; Armijo et al., 2010; Farías et al., 2010; Piquer et al., 2016).

The evolution of the magmatic arc was characterized by the formation of an intra-arc basin under an extensional regime during the late Eocene–Oligocene,

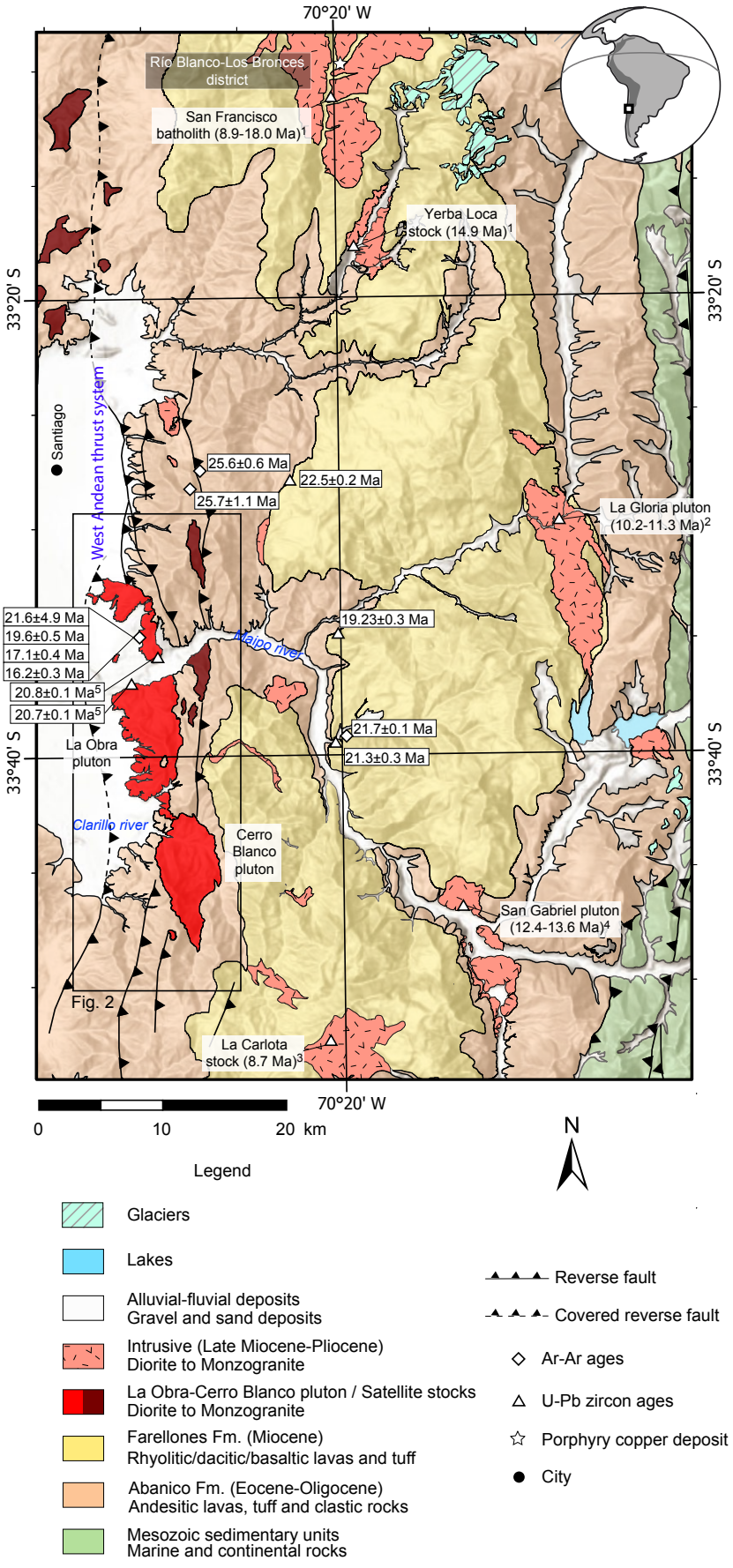

Figure 1. Geologic map of Miocene magmatic rocks in central Chile. La Obra–Cerro Blanco intrusive suite is emplaced in the western margin of the Abanico-Farellones volcanic belt, spatially related to the West Andean thrust system (Armijo et al., 2010). Map is based on Farías et al. (2008), Fock (2005), Piquer et al. (2015), Thiele (1980), and new observations from this study. Locations of samples dated by Ar-Ar methods and U-Pb in zircon in the host volcanic rocks are shown (Fock, 2005; Piquer et al., 2017; Vergara et al., 2004). Dates obtained by U-Pb zircon geochronology in plutonic rocks are also shown (1—Deckart et al., 2010; 2—Gutiérrez et al., 2018; 3—Muñoz et al., 2013; 4—Payacán et al., 2023; 5—Piquer et al., 2021).

where the Abanico Formation was deposited (referred as the Abanico basin; Charrier et al., 2002). This ~3-km-thick formation is composed of a lower member of pyroclastic breccias and tuff of dacitic composition, with subordinate sedimentary layers of lacustrine origin (Piquer et al., 2015; Thiele, 1980; Vergara et al., 1988). In contrast, the overlying member is composed of basic to intermediate volcanic rocks (Nyström et al., 2003). Radiometric ages based on several methods (e.g., Ar-Ar on multiple materials) have been reported for the volcanic rocks in the study area, ranging from 25.65 ± 1.1 Ma to 25.62 ± 0.6 Ma (Fig. 1; Vergara et al., 2004).

Short-lived deformation pulses allowed the tectonic inversion of the Abanico basin during the early Miocene (Charrier et al., 2005; Godoy et al., 1999; Jara et al., 2015). This deformation was accommodated by thrust systems located at the margins of the basin and migrating from west (West Andean thrust system) to the east (Farías et al., 2008). During this stage, the western cordilleran front would have been built adjacent to Santiago, resulting in small-wavelength folds affecting the volcanic rocks of the Abanico Formation (Armijo et al., 2010; Charrier et al., 2002; Farías et al., 2010).

The deposition of the ~2.5-km-thick volcanic Farellones Formation in the inner parts of the basin coincided with a contractional tectonic event. These volcanic rocks are divided into two members: the lower member, composed of intercalated sandstones to conglomerates (probably associated with alluvial deposits in a volcanic environment) and pyroclastic facies, followed by the overlying member, composed of intermediate to felsic lavas and pyroclastic breccias (probably recording block-and-ash deposits; Nyström et al., 2003; Piquer et al., 2017; Vergara et al., 2004). Radiometric ages from volcanic rocks have been reported in the study area, yielding ages of 21.7 ± 0.1 Ma in andesitic lavas (see references in Fock, 2005). U-Pb in zircon ages have also been reported in pyroclastic rocks to the east of the study area, corresponding to the lower member of the Farellones Formation, with ages of 22.5 ± 0.2 Ma, 21.3 ± 0.3 Ma, and 19.23 ± 0.26 Ma (Fock, 2005; Piquer et al., 2017). This prolonged interval of volcanism was dominated by both destructive and constructive episodes, which are recorded in the vicinity of the study area by volcanic morphologies such as volcanic maar-diatreme systems, rhyolitic dome complexes, and high-silica pyroclastic deposits associated with ash-fall and dome-collapse events.

The Miocene volcanism was accompanied by the emplacement of several discrete plutons that intruded the volcanic rocks of the Abanico Formation and the lower member of the Farellones Formation. The shape of the plutons is "similar to an overturned canoe" (Mahood and Cornejo, 1992, p. 65), and their main orientation is along the strike of the regional tectonic structures, suggesting a structural control on the space-making mechanism that allowed their emplacement (Gutiérrez et al., 2018; Payacán et al., 2023). The plutons' crystallization ages show latitudinal variations, ranging from ca. 20 Ma in plutons emplaced in the western margin of the Abanico-Farellones belt (recorded in La Obra pluton; Kurtz et al., 1997; Piquer et al., 2021) to ages of ca. 15 Ma in the mafic Yerba Loca stock (Deckart et al., 2010), while in the eastern margin of the Abanico-Farellones belt, 13–12 Ma ages are recorded in the San Gabriel pluton, and an age of ca. 10 Ma is recorded in the La Gloria pluton (Gutiérrez et al., 2018; Payacán et al., 2023). Then, during the late Miocene (<8–4 Ma), the plutonic activity returned westward, forming porphyries associated with the mineralization of the giant Cu-porphyry deposit in the Rio Blanco–Los Bronces district (Deckart et al., 2010; Muñoz et al., 2013).

Geologic Background of La Obra–Cerro Blanco Intrusive Suite

Previous studies have mentioned La Obra pluton, outcrops of which can be found by the Maipo River, to the southeast of Santiago (Fig. 1). It has been described as a hornblende- and biotite-bearing leucogranodiorite (Kurtz et al., 1997) and quartz-monzonite to granodiorite (Piquer et al., 2021). Geochemically, this intrusive body is characterized on average by 69.8 wt% SiO_2 and a relatively low La/Yb ratio compared to the rest of the Tertiary plutons in the area (Kurtz et al., 1997; López-Escobar et al., 1979). According to crystallization pressure estimates from the Al-in-hornblende geobarometer, this pluton was emplaced at a depth of 3.1–4 km (Kurtz et al., 1997).

Radiometric dates have been obtained from samples collected near the Maipo River through a variety of methods (Fig. 1), with ages ranging from 22 ± 0.6 Ma (K-Ar dating; Selles and Gana, 2001) to 21.6 ± 0.5 Ma, 19.6 ± 0.5 Ma, 17.1 ± 0.4 Ma, and 16.2 ± 0.3 Ma (Ar-Ar in hornblende, biotite, plagioclase, and K-feldspar, respectively; Kurtz et al., 1997). A more recent study reported U-Pb in zircon data from the same area (Fig. 2), yielding crystallization ages of 20.8 ± 0.1 Ma and 20.7 ± 0.1 Ma for a granodiorite and a quartz-monzonite, respectively (Piquer et al., 2021).

In addition to La Obra pluton, several poorly characterized intrusions were emplaced in the western margin of the Abanico-Farellones volcanic belt, spatially associated with deformed volcanic rocks and the San Ramón thrust system, which allowed the formation of the western Principal Cordillera (Figs. 2 and 3). The Cerro Blanco pluton is a granitic body that outcrops in the southern part of this structural corridor, in the area of the Clarillo River (Fig. 4), and it appears as the most prominent part of the intrusive suite, being the highest elevation where the granites can be observed (1400 m above the river incision). In addition, mafic stocks with dioritic to quartz-monzodioritic compositions are observed in the eastern margin of La Obra pluton and in the northern part of the study area (San Juan and Minillas stocks; Fig. 2).

ANALYTICAL METHODS

During geologic mapping of the lithologic variations in La Obra–Cerro Blanco plutonic suite, we collected 77 hand samples for petrographic description of the mineral content and rock textures. From this collection, a subset of 50 samples was selected to be described using transmitted-light microscopy and for preparation of nonoriented thin sections.

Whole-rock compositions of 47 samples were determined by Bureau Veritas Mineral Commodities, Vancouver, British Columbia, Canada. Approximately

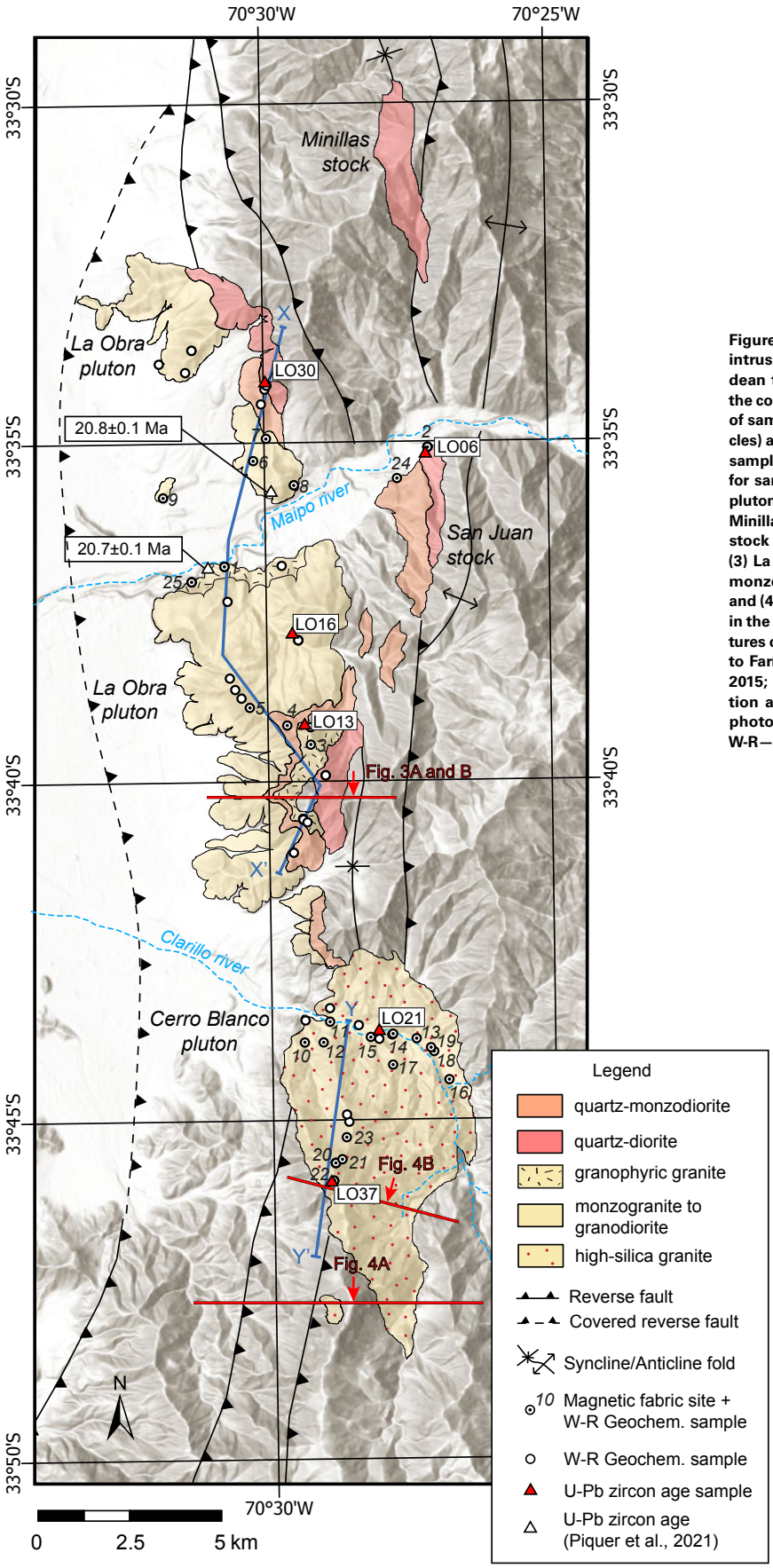

Figure 2. Geologic map of the early Miocene intrusive rocks emplaced along the West Andean thrust system in central Chile, showing the compositional and textural facies, locations of samples for geochemical analyses (white circles) and U-Pb zircon dating (white triangles for samples from Piquer et al., 2021; red triangles for samples obtained in this study). Individual plutons are labeled, from north to south: (1) the Minillas stock (quartz-diorite), (2) the San Juan stock (quartz-diorite to quartz-monzodiorite), (3) La Obra pluton in the central part (quartz-monzodiorite, granodiorite to monzogranite), and (4) Cerro Blanco pluton (high-silica granite) in the southern part of the area. The main structures of the host rock are shown too (according to Farías et al., 2008; Fock, 2005; Piquer et al., 2015; Thiele, 1980). Also shown are the location and orientation (red arrows) where the photographs in Figures 3 and 4 were taken. W-R—whole rock.

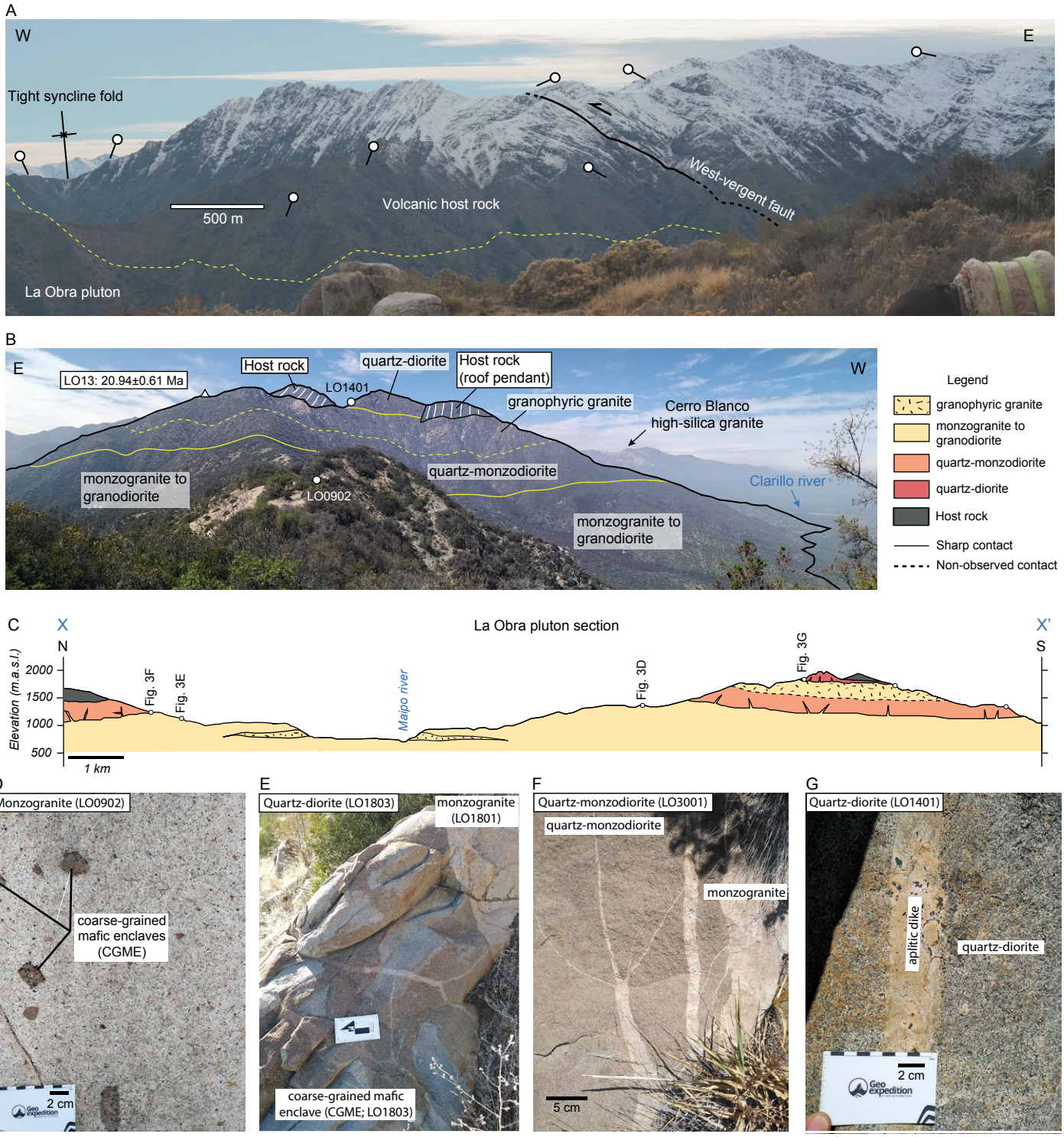

Figure 3. Field photographs illustrating the compositional variations and internal contacts within La Obra pluton. (A) View from the summit of Cerro Blanco pluton, showing the host-rocks structures observed at the eastern margin of La Obra pluton. The west-vergent fault and the axis of a tight syncline fold are marked. Granitic rocks crop out at the lower parts of the slopes of the Clarillo River. (B) Panoramic view and interpreted contacts according to field mapping of the roof zone of La Obra pluton. A roof pendant with steep shape is observed in the central part, concordant with the pluton's layering, but exhibiting stratification discordant with the borders. (C) Schematic N-S cross section in the longitudinal direction of La Obra pluton (X-X' in Fig. 2). The vertical continuity of magmatic domains on both slopes of the Maipo River valley showcases the overall elongated dome shape of the intrusion and the sheet-like nature of the single magmatic domains. Location of the following photos is marked on the cross section; m.a.s.l.—meters above sea level. (D) Outcrop of the monzogranite containing centimeter-sized mafic enclaves. (E) Metric-scale mafic enclave contained in the monzogranite that is crosscut by granitic veins as observed in the northern part of the pluton. (F) Centimeter-wide monzogranitic dikes that intrude the quartz-monzodiorite layer. (G) Aplitic dike intruding the quartz-diorite layer in the upper part of La Obra pluton.

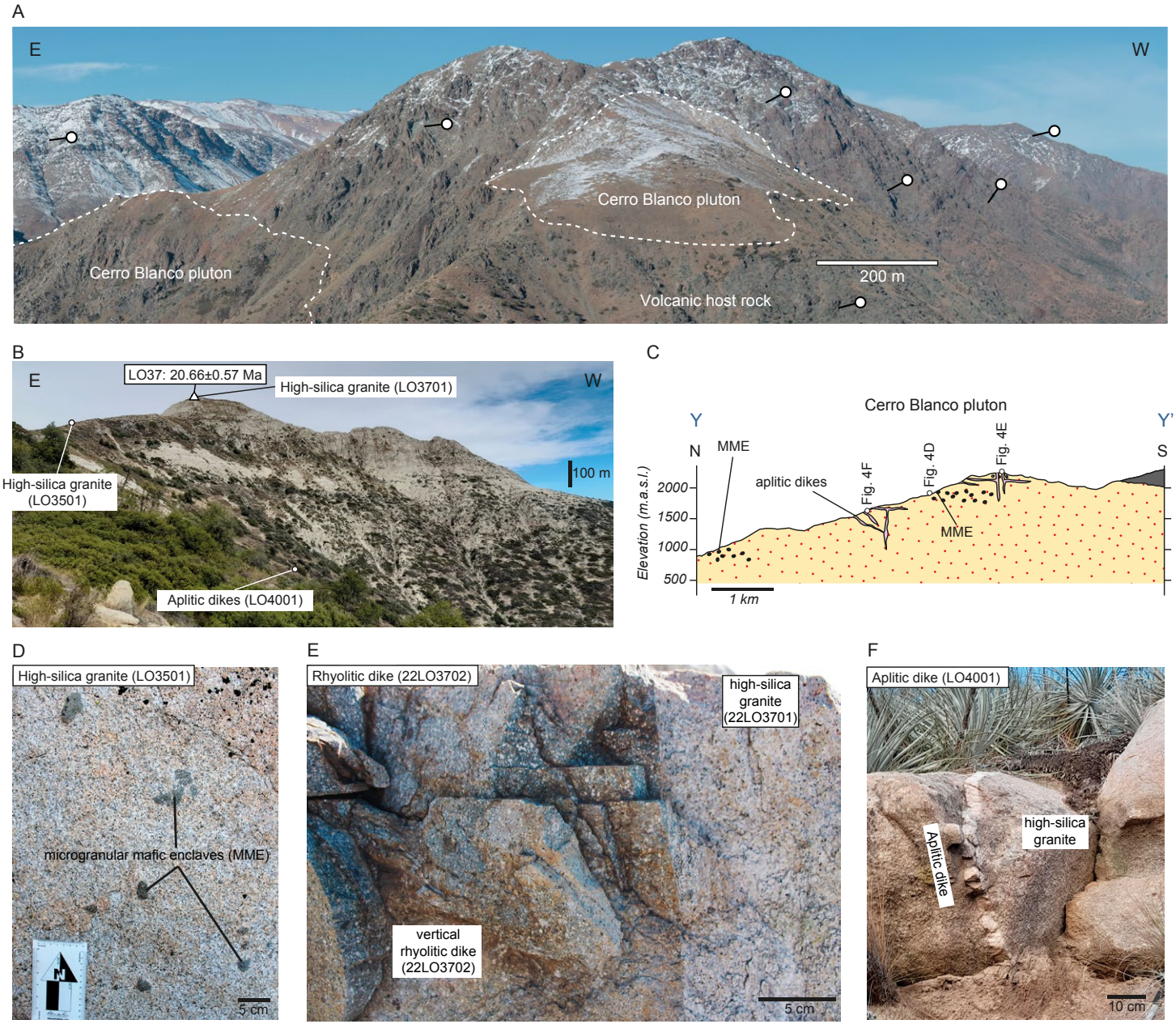

Figure 4. Field photographs from Cerro Blanco pluton. (A) Photograph of the view to the south of Cerro Blanco pluton, where the southwestern margin of the pluton is observed. Note the irregular geometry of the contact and its discordant relationship to the host-rock stratification. (B) General view of Cerro Blanco pluton, showing the most prominent outcrops of the granitic rocks in the Clarillo River area. Locations of representative samples are shown. (C) Cross section in longitudinal direction of Cerro Blanco pluton (Y-Y′ in Fig. 2); The pluton is nearly homogeneous in composition, with isolated aplitic dikes concentrated in the middle and upper portions of the pluton. MME—microgranular mafic enclaves; m.a.s.l.—meters above sea level. (D) Outcrop of the high-silica granite in the middle levels of Cerro Blanco pluton, containing centimeter-scale mafic enclaves. (E) Vertical rhyolitic dike intruding the high-silica granite in the upper levels of the pluton, showing porphyritic textures with quartz and plagioclase phenocrysts. (F) Outcrop of one of the several aplitic dikes intruding the high-silica granites in the middle levels of the pluton.

200–300 g of rock per sample were analyzed for major elements using inductively coupled plasma–atomic emission spectrometry (ICP-AES) and for trace elements using inductively coupled plasma–mass spectrometry (ICP-MS). Analyses were performed on lithium borate fused material through the LF200 package. Measurements were performed using OREAS 908, OREAS 181, and SY-4 as reference materials according to the laboratory procedures (for details, including the limits of detection, see https://commodities.bureauveritas.com/). The precision and accuracy values, and standards measurements, are presented in Table S1.[1]

For U-Pb dating, we selected six samples from different magmatic domains and spatially distributed through the plutons. Rock samples were crushed and sieved, and zircon crystals were separated by means of heavy liquid and magnetic separation processes. Zircon crystals were then mounted in epoxy resin, polished, and imaged with cathodoluminescence (CL). Following CL imaging, we used laser ablation–inductively coupled plasma–mass spectrometry (LA-ICP-MS) techniques to determine trace-element abundances and U-Pb crystallization ages at ETH Zürich. A 193 nm Resonetics Resolution S155 laser-ablation system coupled to a Thermo Element XR sector-field single-collector ICP-MS (Guillong et al., 2014) was used. Laser parameters included a spot size of 20 µm, a repetition rate of 5 Hz, and an energy density of ~2 J cm^{-2}. The ablation aerosol was mixed in the fast washout S-155 ablation cell (Laurin Technic) with carrier gas consisting of helium (~0.5 L min^{-1}) and make-up gas consisting of argon (~1 L min^{-1}) and nitrogen (2 mL min^{-1}). The ablated aerosol was then homogenized by flushing it through a squid device before introduction into the plasma torch. The single-collector sector-field MS is equipped with a high-capacity (80 m^3 h^{-1}) interface pump to improve sensitivity. Before each analytical session, the instrument was optimized on NIST SRM612 glass to achieve a detection efficiency in the range of 1% (on Pb, Th, U) while keeping low oxide production ($^{248}ThO^+/^{232}Th^+ \leq 0.25\%$) and a U/Th ratio of ~1. Intensities were recorded for the following isotopes: ^{27}Al, ^{29}Si, ^{31}P, ^{49}Ti, ^{89}Y, ^{91}Zr, ^{93}Nb, ^{137}Ba, ^{139}La, ^{140}Ce, ^{141}Pr, ^{146}Nd, ^{147}Sm, ^{153}Eu, ^{157}Gd, ^{159}Tb, ^{163}Dy, ^{165}Ho, ^{167}Er, ^{169}Tm, ^{173}Yb, ^{175}Lu, ^{178}Hf, ^{181}Ta, ^{202}Hg, ^{204}Pb, ^{206}Pb, ^{207}Pb, ^{208}Pb, ^{232}Th, ^{235}U, and ^{238}U. Detailed parameters can be found in Table S2 following the community-derived guidelines (Horstwood et al., 2016). For U-Pb dating, GJ-1 was used as calibration reference material (CRM). Validating reference materials (VRM) included Plešovice (337 Ma; Sláma et al., 2008), Temora (417 Ma; Black et al., 2003), and zircon 91500 (1065 Ma; Wiedenbeck et al., 1995). The data were reduced using the software Iolite version 4.5 (Paton et al., 2010, 2011) with VizualAge (Petrus and Kamber, 2012). No common-Pb correction was applied, but integration intervals were set to exclude inclusions, common Pb, and discordant parts of the signal. Unknown ages are reported as 2 standard error (S.E.) absolute. Reproducibility of validation reference materials and systematic long-term uncertainty were propagated to the weighted average uncertainty by quadratic addition (i.e., total external uncertainty). The VRM results show the achievable precision and accuracy of the method, which are in the range of 1.0%. The long-term external uncertainty is in the range 0.5% for $^{206}Pb/^{238}U$ ages and is composed of the uncertainty from the applied corrections, uncertainty of the decay constants, lack of common-Pb correction, the uncertainty on the true $^{206}Pb/^{238}U$ ratio of the primary standard GJ-1, and possible uncertainty from matrix effects (Sliwinski et al., 2022). For trace-element quantification, we used Si as an internal standard at 15.2 wt% SiO_2 in zircons, and NIST 610 as external CRM. Ti was quantified by zircon 91500 (Ti: 4.73 ± 0.15 mg g^{-1}) as suggested by Szymanowski et al. (2018).

Zircon Lu-Hf isotopic analyses were carried out on the same zircon grains analyzed for U-Pb and trace elements by laser ablation–multicollection–inductively coupled plasma–mass spectrometry (LA-MC-ICP-MS) at ETH Zürich using a RESOlution (ASI/Applied Spectra) excimer ArF (193 nm wavelength) LA system equipped with the dual-volume S-155 ablation cell (Laurin Technic), attached to a Nu Plasma 2 (Nu Instruments) multicollector sector-field MS. A laser spot size of ~50 µm, a repetition rate of 5 Hz, and an energy density of ~3.5 J·cm^{-2} were used for static spot analyses. The carrier gas consisted of high-purity helium (~0.35 L·min^{-1}) and argon sample gas from the MC-ICP-MS (~1.0 L·min^{-1}). The MC-ICP-MS was optimized for maximum sensitivity on Hf isotopes and peak alignment throughout the investigated mass range. We acquired intensities for the following isotopes (corresponding Faraday cup indicated between brackets): ^{171}Yb (L4), ^{173}Yb (L2), ^{175}Lu (Ax), $^{176}(Yb + Lu + Hf)$ (H1), ^{177}Hf (H2), ^{178}Hf (H3), ^{179}Hf (H4), ^{180}Hf (H5), and ^{181}Ta (H6). The data were processed offline with the software Iolite version 4.5 (Paton et al., 2010, 2011), using an in-house data reduction scheme. Instrumental mass bias for Yb and Hf isotopes was corrected to the natural abundance ratios of $^{173}Yb/^{171}Yb$ and $^{179}Hf/^{177}Hf$, and the isobaric interferences of ^{176}Yb and ^{176}Lu on ^{176}Hf were corrected using the natural abundance ratios of $^{176}Yb/^{173}Yb$ and $^{176}Lu/^{175}Lu$, with all natural abundance ratios taken from Chu et al. (2002). The mass bias correction factor obtained for Yb isotopes was applied to Lu isotopes. Accuracy and external reproducibility of the method were controlled by repeated analyses of reference zircon standards GJ-1 (Morel et al., 2008), Plešovice (Sláma et al., 2008), GHR1 (Eddy et al., 2019), and Temora (Woodhead and Hergt, 2005). The $^{176}Hf/^{177}Hf$ ratios obtained on all reference materials were within uncertainties identical to the recommended values (see also Table S1). The initial $^{176}Hf/^{177}Hf$ ratios were calculated for each analysis using a ^{176}Lu decay constant of 1.865×10^{-11} (Scherer et al., 2001), the measured $^{176}Lu/^{177}Hf$ ratio, and an average crystallization age of 21 Ma as constrained by LA-ICP-MS U-Pb ages on the same samples. The initial εHf values were calculated using the parameters for chondritic uniform reservoir (CHUR) recommended by Bouvier et al. (2008). The quoted uncertainties on initial isotopic compositions of unknowns include the analytical uncertainty (2 S.E.) and the average intrasession reproducibility (2 standard deviation [2σ]) of initial isotopic compositions of reference

[1]Supplemental Material. Table S1: Whole-rock geochemistry for samples from the La Obra–Cerro Blanco suite (ICP-MS-ES data) and standards. Table S2: Procedure for LA-ICP-MS analysis of zircon, U-Pb dating and trace element in zircon results, and Hf data and corresponding reference material. Table S3: Fe-Ti oxides compositions determined by using SEM-EDS. Table S4: Results of the anisotropy of the magnetic susceptibility from La Obra–Cerro Blanco intrusive suite. Table S5: Geochemical modeling of trace element partitioning. Text S1: Contains additional trace element plots of the rocks of La Obra–Cerro Blanco suite. Please visit https://doi.org/10.1130/GEOS.S.27166185 to view the supplemental material. Contact editing@geosociety.org with questions.

materials (typically ~1 εHf unit), propagated by quadratic addition. The data are reported in Table S2.

In total, 25 sites were sampled for magnetic fabric measurements, each consisting of 8–14 oriented cores (255 in total) obtained with a portable drilling machine used for paleomagnetic studies. We prioritized sampling of the main intrusive units, avoiding mafic enclaves and dikes. The spatial distribution of sampling was conditioned by the weathering, alteration, and integrity of the rock and the presence of nonrotated blocks (which is common due to the vegetation and weathering in the area). The magnetic fabric was determined by anisotropy of magnetic susceptibility measurements using an AGICO KLY-3S Kappabridge at the Laboratory of Magnetic Mineralogy and Paleomagnetism of the Universidad de Chile (Chile) and at the Laboratory of Paleomagnetism in the Université de Rennes (France). Each specimen measurement was normalized to the bulk susceptibility value (K_{bulk}).

The magnetic mineralogy was characterized through transmitted- and reflected-light observations under a petrographic microscope. We complemented the characterization of the magnetic mineralogy by using a scanning electron microscope (SEM), model GeminiSEM 360 with NanoVP (Electron Microscopy Laboratory of the Universidad Tecnológica Metropolitana, Chile). We obtained backscattered electron (BSE) images of the Fe-Ti oxides from representative samples. The chemical composition of the Fe-Ti oxides was characterized using an energy-dispersive spectrometry (EDS) system (model AZtecLive Lite, Oxford Instruments) with an Ultim Max silicon drift detector (SDD) analytical detector with a window of 40 mm^2. Elemental analyses were performed at 15 kV and 10^{-6} mbar.

PETROGRAPHY AND ARCHITECTURE OF LA OBRA–CERRO BLANCO INTRUSIVE SUITE

La Obra Pluton: Monzogranites, Granodiorites, Quartz-Monzodiorites, and Quartz-Diorites

La Obra pluton displays an elongated dome shape, with the main length of the pluton trending to the north (Fig. 2). The western contact with the host rock is covered by alluvial deposits, while the eastern margin is characterized by vertical to steeply eastward-dipping contacts (Figs. 3A and 3B). The roof of the pluton is exposed in its central part, with an increase in elevation from north to the south, from 1390 up to 2050 m above sea level, recognized as a gently dipping contact with the host rocks and a small roof pendant with stepped shape (Fig. 3B). The roof is concordant with the horizontal compositional layering of the pluton (see the following paragraphs). However, the stratification of the volcanic host rock is discordant with the pluton's margin, and this is most notable in the roof contact (Fig. 3A). On the pluton east side, the host-rock lithologies are highly deformed, as indicated by the steep dips and the presence of a tight syncline fold, where the axial plane is cut by the margins of the pluton (Fig. 3A).

La Obra pluton has a vertical zoning pattern, composed of subhorizontal sheet-like intrusions of variable composition (Fig. 3C). From bottom to top, these units are as follows:

(1) An ~600-m-thick layer (with unexposed base) that consists of monzogranites and granodiorites showing gradational contacts. These are medium- to coarse-grained rocks composed of euhedral plagioclase, subhedral to anhedral K-feldspar (with occasional perthitic texture), and medium- to fine-grained anhedral interstitial quartz (Fig. 5A). Zoned euhedral plagioclase crystals with poorly preserved cores are observed in these rocks. Major mafic phases are fine-grained biotite and minor amphibole, sometimes forming mafic mineral clots. Fe-Ti oxides (in spatial association with biotite and hornblende clots), titanite, zircon, and apatite are present as accessory minerals. At the base of this layer, monzogranites with finer crystal size and smaller amounts of mafic minerals can be observed with granophyric textures covering up to 50% of the rocks, which are slightly richer in hornblende content compared to the rest of the monzogranites and minor granodiorites. Field mapping suggests a tabular shape of this intrusion, which is arranged horizontally, following the vertical zoning pattern of the compositional domains (Fig. 3C).

(2) Quartz-dioritic (and less dioritic) mafic enclaves are observed within the monzogranites and granodiorites, displaying both microgranular and porphyritic textures. The mafic enclaves are a few centimeters in size, covering up to 7% of the outcrops, and commonly rounded to subangular in shape (Fig. 3D). They are composed of subhedral plagioclase crystals, which commonly present sieve texture, and they are accompanied by pyroxene and amphibole crystals as the major mafic phases (up to 35–40 vol%). In the middle levels of the monzogranitic domain, some metric medium- to coarse-grained mafic enclaves (sample LO1803) are preserved, presenting felsic veins and a few-centimeter-wide dikes (Fig. 3E). Texturally, these enclaves are similar to the larger mafic layers observed in the upper parts of La Obra pluton and the satellite stocks (which will be described in the Minillas and San Juan Satellite Stocks: Quartz-Diorites and Quartz-Monzodiorites section below).

(3) An ~250-m-thick layer of quartz-monzodiorites overlies the monzogranites and granodiorites unit. Near the base, quartz-monzodiorites are intruded by several centimeter-scale monzogranitic dikes with sharp margins, with this crosscutting relationship suggesting that the monzogranites are relatively younger (Fig. 3F). Quartz-monzodiorites are medium- to coarse-grained rocks, mainly composed of euhedral plagioclase crystals, with anhedral K-feldspar and quartz crystals. The major mafic phase is subhedral clinopyroxene, associated with minor hornblende (Fig. 5B).

(4) An ~250-m-thick layer of granophyric granites crops out above the quartz-monzodiorites, formed by discrete outcrops exposed in the upper levels of the pluton. These granites are coarse grained and consist of euhedral plagioclase crystals surrounded by subhedral K-feldspar and fine anhedral quartz (Fig. 5D). The granophyric texture is well developed in this unit and covers a higher proportion of the rock volume compared to the basal granophyric granites. Biotite is the dominant mafic mineral (<5 vol%), and

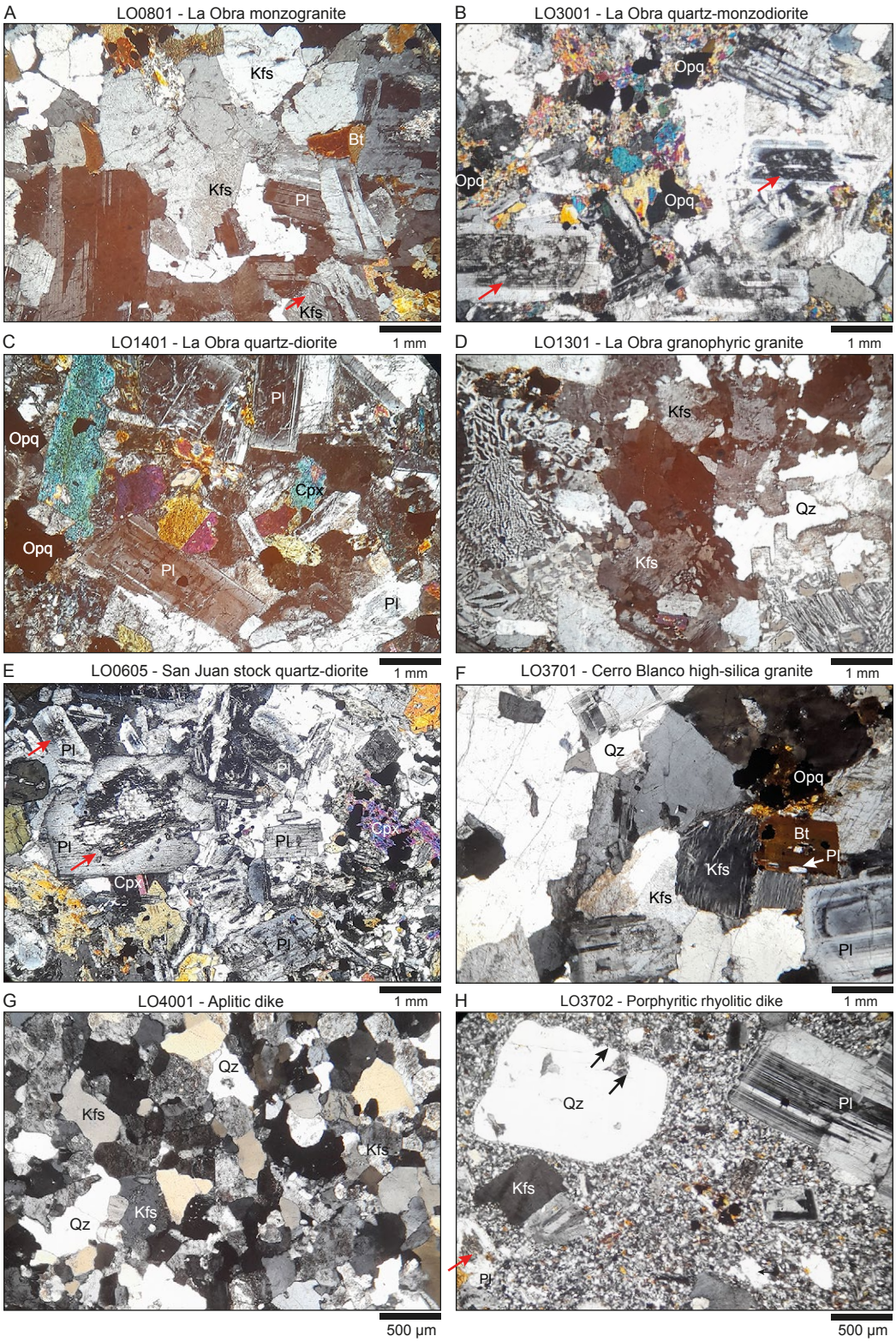

Figure 5. (A–D) Photomicrographs of representative samples from the diverse rock types observed in La Obra pluton. (A) Medium- to coarse-grained biotite monzogranite from the lower level. (B) Medium-grained quartz-monzodiorite from the upper level with sieve-textured plagioclase. (C) Coarse-grained quartz-diorite from the upper level. (D) Granophyric granite from the upper level of the pluton displaying anhedral crystal intergrowths. (E) Representative coarse quartz-diorite from the San Juan stock, where sieve textures are observed in plagioclase crystals. Similar features to quartz-monzodiorite are highlighted by red arrows. (F–H) Photomicrographs of representative samples from Cerro Blanco pluton. (F) Representative high-silica granite from the upper part of the pluton. (G) Representative aplitic dike observed in the middle part. (H) Porphyritic rhyolite dike from the upper part of the pluton. Medium-grained felsic phenocrysts are contained in a granophyric groundmass. Embayments in quartz crystals are highlighted by arrows. Mineral abbreviations are listed according to Whitney and Evans (2010).

it is commonly found as fine crystals around plagioclase and K-feldspar crystals (Fig. 5D) in spatial association with Fe-Ti oxide.

(5) An ~100-m-thick layer of quartz-diorite is exposed at the highest levels of La Obra pluton, above the granophyric granites (Fig. 3B). This is the most mafic unit within the pluton and corresponds to coarse-grained rocks composed of euhedral plagioclase crystals, medium-grained quartz, and subordinate K-feldspar. Sieve textures are infrequently observed in plagioclase crystals (Fig. 5C). Clinopyroxene is the major mafic phase (>20 vol%; Fig. 5C), and it displays subhedral prismatic crystals with a seriate texture. Minor hornblende is also observed. Fe-Ti oxides are abundant, occurring as fine- to medium-grained crystals grown in interstitial spaces between plagioclase grains. This unit is intruded by fine- to medium-grained aplitic dikes, which are just a few centimeters wide and display sharp contacts with the host rock (Fig. 3G), overall suggesting that the quartz-dioritic magmas were one of the earliest intruded phases.

Cerro Blanco Pluton: High-Silica Granites

The Cerro Blanco pluton, located in the southern part of the batholith, has a bell-shaped geometry. The intrusion's cupola is close to the summit of Cerro Blanco hill with a vertical exposure of ~1300 m (Fig. 4B). The cupola has an elongated shape oriented in a N-S direction, similar to the orientation of the rest of the plutons. The western contact is well exposed and follows a NW-SE trend with an irregular shape, while the eastern contact is mostly covered by scree and vegetation (Fig. 2). The southern limit of the intrusion is affected by intense hydrothermal alteration; nevertheless, it is recognized that the stratification of the host rocks, which is predominantly dipping to the east, is discordant with the pluton's margin (Fig. 4A).

The Cerro Blanco pluton is markedly homogeneous, without clear internal contacts as seen in La Obra pluton (Figs. 4B and 4C). It is composed of high-silica granites, which we consider here as monzogranites richer in quartz than those from La Obra pluton (i.e., richer in SiO_2 as shown in the geochemical results). The high-silica granites are coarse grained and present anhedral quartz, subhedral K-feldspar, and euhedral plagioclase crystals (Fig. 5F). Mafic phases are dominated by subhedral fine-grained biotite (up to 10 vol%), forming mafic mineral clots with Fe-Ti–oxide crystals. Occasionally, biotite crystals present small plagioclase and Fe-Ti–oxide inclusions. Plagioclase is present in lower percentages compared to granites from La Obra pluton, so we consider the Cerro Blanco pluton to be composed of high-silica granites. K-feldspar crystals seldom show perthitic texture with irregular lamellae (Fig. 5F).

Mafic enclaves are abundant in discrete levels of Cerro Blanco pluton, especially at the base and the upper part of the intrusion (Fig. 4C). In general, the mafic enclaves are rounded microgranular diorites and quartz-diorites only a few centimeters in size (Fig. 4D). The enclaves' mineralogy is characterized by the presence of prismatic clinopyroxene and hornblende crystals, randomly oriented and intergrown with subhedral plagioclase crystals. Some medium-grained felsic crystals are observed within the enclaves, forming a porphyritic texture, usually accompanied by disequilibrium textures. Fine-grained mafic mineral concentrations are also observed within the high-silica granite, with mineralogy similar to that observed within mafic enclaves.

Aplitic dikes observed intruding high-silica granite are especially abundant in the middle and the uppermost levels of the pluton (Fig. 4C). Dikes are generally a few centimeters wide with sharp margins (Fig. 4F) and display aplitic texture, showing intergrown felsic crystals with irregular edges and predominantly quartz content (Fig. 5G). Additionally, in the uppermost levels of the pluton, some gray-colored porphyritic dikes are observed, intruding the high-silica granites. These dikes are at high angle to and show sharp contacts with the host high-silica granites (Fig. 4E). The groundmass is composed of intergrown microgranular felsic minerals (quartz + K-feldspar ± plagioclase), with limited presence of biotite. The phenocrysts are 0.5–2 mm in size and comprise ~30 vol% of the dike, consisting of quartz, plagioclase, and K-feldspar (some of them with plagioclase inclusions). The phenocrysts commonly have rounded shape and, in some cases, rounded embayment, indicating a thermal and/or chemical disequilibrium with the groundmass (Fig. 5H). Clusters of fine-grained mafic minerals, analogous to those observed in mafic enclaves, are also observed within the dikes (Fig. 5H).

Minillas and San Juan Satellite Stocks: Quartz-Diorites and Quartz-Monzodiorites

The main satellite stocks described in this work are two intrusions located to the north and east of La Obra pluton, which are smaller than the main intrusions (Fig. 2). They intrude the volcanic rocks of the Abanico Formation and present an elongated shape with a NNW trend, consistent with the tectonic structures of the thrust system. The Minillas stock is a 3-km-long sheet-like intrusion with a vertical arrangement and NNW trend composed of quartz-diorites. The San Juan stock, located to the east of La Obra pluton, is a composite pluton that shows dominantly quartz-monzodioritic composition grading to quartz-diorite toward its eastern margin. This intrusion contains several decametric enclaves, chiefly microgranular diorites and quartz-diorites with variable color index, although a subordinate group of coarse-grained enclaves is also seen (sample LO0603). In general, the mafic enclaves present an elongated shape, with both sinuous and sharp margins, many of which show gradation in mafic mineral concentrations.

In general, both stocks are composed of fine- to medium-grained quartz-diorites to quartz-monzodiorites, with ~40–50 vol% of euhedral plagioclase surrounded by minor intergranular quartz (~10–15 vol%; Fig. 4). The original zoning in plagioclase crystals is poorly preserved, and they commonly show sieve textures with fine quartz and Fe-Ti–oxide inclusions (Fig. 5E). Clinopyroxene and amphiboles are the main mafic phases, showing poor preservation, with several Fe-Ti–oxide crystals as inclusions. However, mafic phases show relicts of prismatic habit and occasionally are present as inclusions within

quartz and plagioclase crystals, indicating that they crystallized during early stages of the magma crystallization.

GEOCHEMISTRY AND GEOCHRONOLOGY

Whole-Rock Geochemistry

The results for whole-rock analyses are presented in Table S1. La Obra–Cerro Blanco intrusive suite displays a wide range of compositions, with SiO_2 contents ranging from 54 to 80 wt% (Fig. 6A). In general, the rocks studied here have metaluminous and calc-alkaline signatures, consistent with the arc-related character (Figs. 6B and 6C). Compositions can be divided into discrete groups according to the magmatic domains to which they belong. Mafic enclaves and diorites to quartz-monzodiorites are grouped in a first cluster with 54–59 wt% of SiO_2 and variable alkali content, which also includes two samples from the San Juan stock (Fig. 6A). Four samples of quartz-monzodiorite cluster around 63–65 wt% SiO_2, including samples from La Obra pluton and the San Juan stock. Granitic compositions are predominant, ranging from 68 to nearly 80 wt% SiO_2, with the majority of samples between 70 and 75 wt% (Fig. 6A). In general, the Cerro Blanco monzogranites are richer in silica than the La Obra monzogranites, so we refer to them here as high-silica granites.

Most major elements show linear patterns of variation, suggesting that all the rocks belong to a common liquid line of descent (Fig. 7). Samples from Cerro Blanco pluton deviate slightly from the main array and show depletion in most major elements, probably due to their SiO_2 enrichment (Fig. 7). Two samples from Cerro Blanco pluton, which show slight hydrothermal alteration by oxidation, are anomalously rich in total Fe content. However, in these two

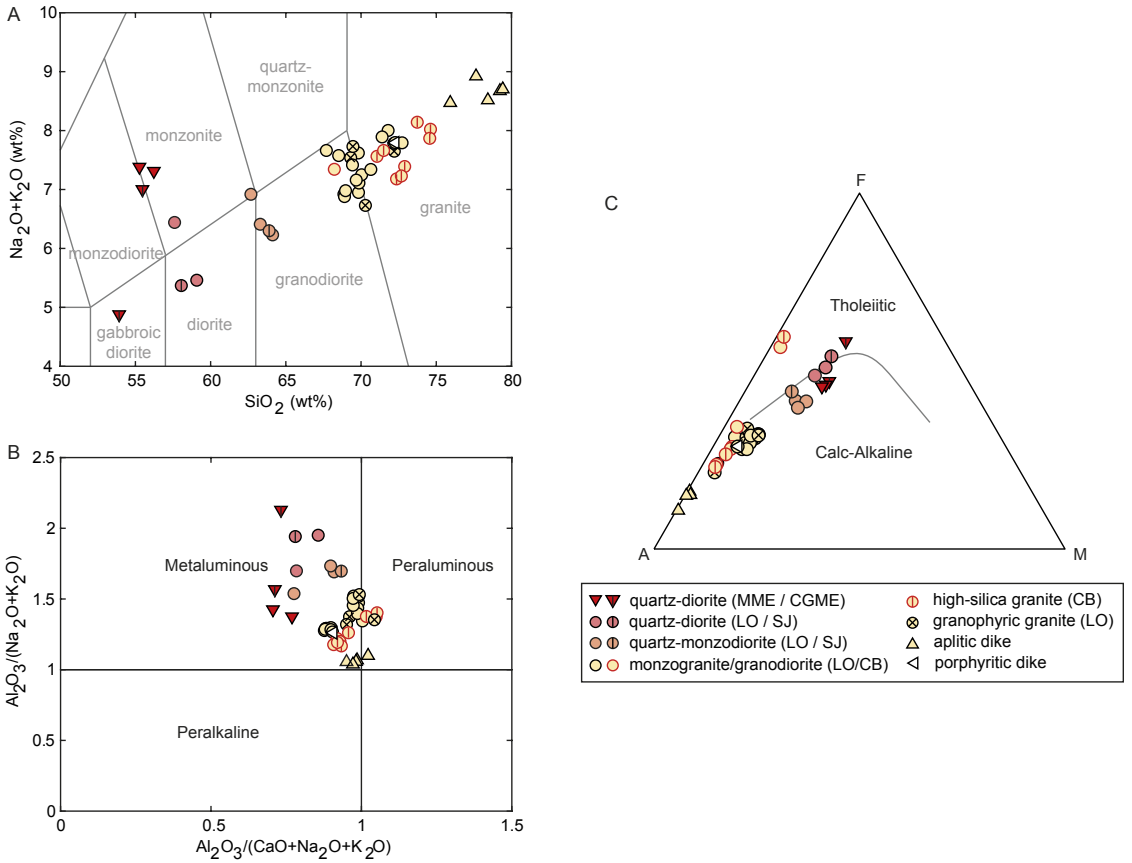

Figure 6. Chemical classification of samples from La Obra–Cerro Blanco intrusive suite, based on whole-rock composition. (A) Total alkalis–silica diagram (Middlemost, 1994), showing the range in silica content from 54 to 80 wt%, with a predominance of granitic compositions. Mafic enclaves, quartz-diorites, and quartz-monzodiorites are a minority and form discrete groups. (B) Alumina/alkali index diagram showing the metaluminous character of La Obra–Cerro Blanco plutonic system (Shand, 1927). (C) AFM plot (where A = Na_2O + K_2O; F = total iron as FeO; M = MgO) showing the mostly calc-alkaline signature of the rocks from La Obra–Cerro Blanco (according to Irvine and Baragar, 1971). Abbreviations: LO—La Obra pluton; CB—Cerro Blanco; SJ—San Juan stock; MME—microgranular mafic enclaves; CGME—coarse-grained mafic enclaves. The 2σ analytical error is smaller than the symbol size.

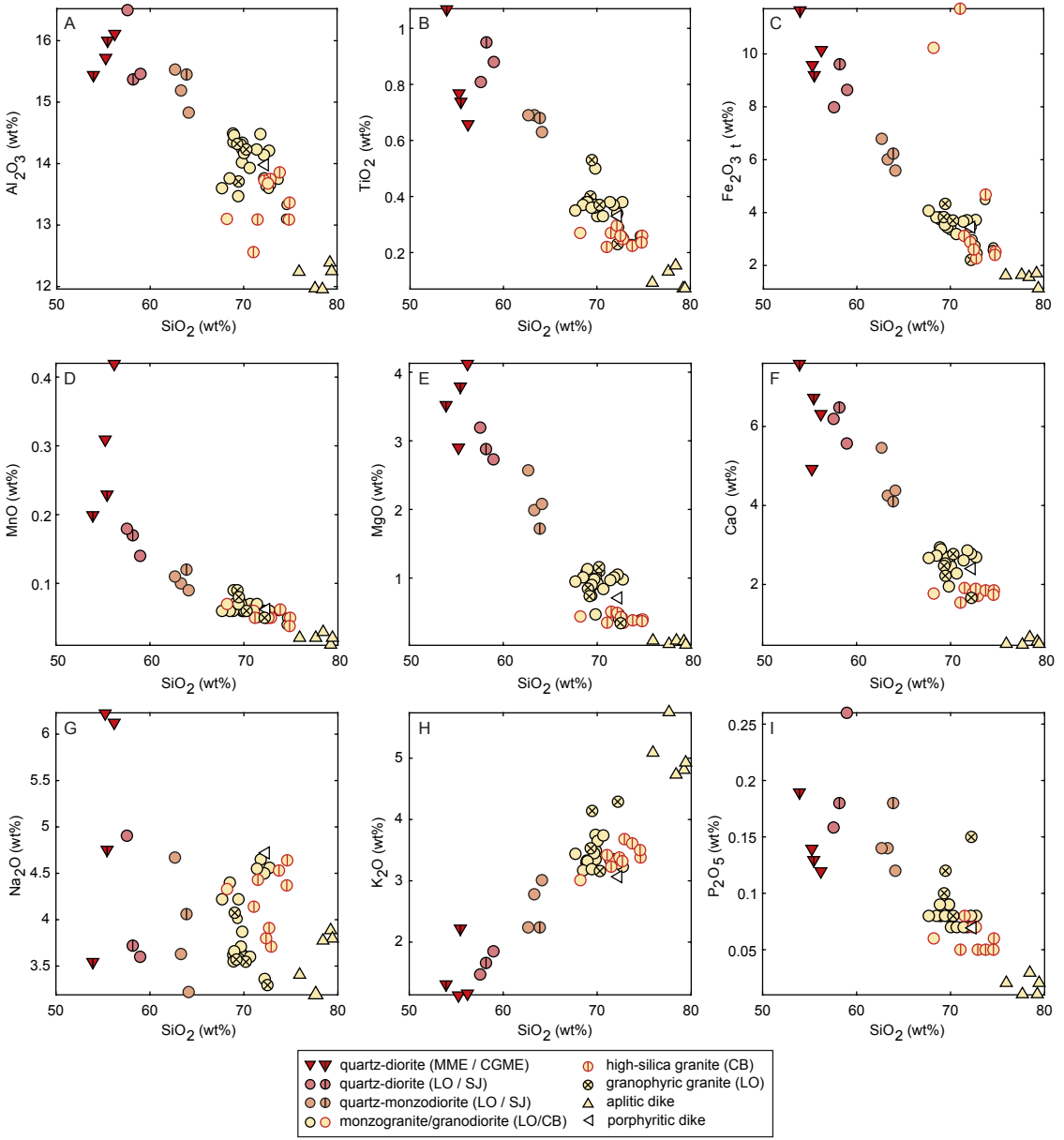

Figure 7. Variation of major elements vs. silica content in samples from La Obra–Cerro Blanco intrusive suite. Two altered samples (abundant Fe-oxides) from Cerro Blanco pluton are shown, which exhibit a Fe enrichment, but the general trends of the other elements are not modified. Abbreviations: LO—La Obra pluton; CB—Cerro Blanco; SJ—San Juan stock; MME—microgranular mafic enclaves; CGME—coarse-grained mafic enclaves. The 2σ analytical error is smaller than the symbol size.

samples, the abundance of all other major elements is still consistent with the general patterns (Fig. 7).

The mafic enclaves follow the same geochemical trend defined by the main intrusive suite, but, individually, they are enriched in MgO and depleted in Al_2O_3, TiO_2, and P_2O_5 (Fig. 7). However, the coarse-grained mafic enclaves (samples LO0603 and LO1805) present compositions similar to the quartz-diorites from the mafic units from La Obra pluton and San Juan stock. Felsic dikes follow the same linear pattern as the entire intrusive suite in terms of major elements. Specifically, the sample from one of the porphyritic dikes observed in the upper part of Cerro Blanco pluton shows ~72 wt% SiO_2 content, a composition consistent with the most silica-rich samples from La Obra pluton (Figs. 6 and 7).

Trace elements exhibit trends that reflect compositional changes between different magmatic domains. Among the most notable trends, Rb displays a typical increasing tendency with respect to SiO_2 content (Fig. 8A). Ba content also shows an increasing tendency; however, aplites have lower contents than granites and show a wider range in Ba content (Fig. 8B). Sr decreases as lithologies become more felsic, as is typically observed in magmatic suites (Fig. 8C). Values of Ba/Th ratio vary between 40 and 80 for the magmatic domains, showing a slight decrease as silica content increases (Fig. 8D). Incompatible elements, such as La and Nb, show little SiO_2 dependence (see Fig. S1 for additional plots). In addition, the magmatic suite presents Sr/Y ratios between 1 and 20, which are lower than those related to adakite-like magmas and chiefly reflect the changing Sr contents in the magmatic suite (Y remains almost constant; Fig. 8E). Aplite samples show a wider range of Y, with values up to 60 ppm; a pair of mafic enclaves also shows higher Y contents.

In general, the rare earth element (REE) distribution is nearly invariant with respect to SiO_2 (except for mafic enclaves and dikes), showing relatively flat patterns in chondrite-normalized spider diagrams (see Fig. S2). Monzogranites and high-silica granites present a slightly more pronounced spoon-shape pattern than quartz-diorites and quartz-monzodiorites. These variations are evidenced by the relatively narrow variation of La/Yb ratios (between 4 and 10 for the main magmatic domains), where the SiO_2 dependence is not noticeable; on the contrary, La/Sm shows a slight increasing tendency and Dy/Yb shows a decreasing tendency as SiO_2 becomes higher (Figs. 8G–8I). This indicates a depletion in medium rare earth elements (MREEs). The tendency of Eu/Eu* is also highlighted, which typically presents values between 0.1 and 0.8 for most of the rocks, representing pronounced negative Eu anomalies, the values of which tend to increase as the rocks become more siliceous (Fig. 8F). Aplitic dikes display more pronounced negative Eu anomalies and are enriched in heavy rare earth elements (HREEs; Fig. S2). The distribution of REEs in mafic enclaves is characterized by a wider range of La/Yb, La/Sm, and Dy/Yb ratios (Figs. 8G–8I). The two samples corresponding to coarse-grained mafic enclaves show a flat pattern similar to that exhibited by the quartz-diorites and quartz-monzodiorites, while microgranular mafic enclaves from the Cerro Blanco pluton present a flatter REE pattern, with marked enrichment in HREEs and a pronounced negative Eu anomaly (see Fig. S2 for additional plots).

Zircon Petrochronology

U-Pb Crystallization Ages

In total, 469 zircon crystals from six samples were analyzed for U-Pb geochronology. Dated samples are from the San Juan stock quartz-diorite (LO06), the marginal quartz-monzodiorite (LO30), the basal monzogranite (LO16), the upper granophyric granite of La Obra pluton (LO13), and the basal monzogranite (LO21) and high-silica granite (LO37) of Cerro Blanco pluton (Fig. 9A; refer to Table S1 for the coordinates of each sample and their associated whole-rock geochemistry). The weighted mean ages obtained from both La Obra and Cerro Blanco plutons are comparable. The complete U-Pb data set is presented in the Supplemental Material (Table S2). Based on their weighted mean age (±2σ uncertainty) and spatial distribution in the plutonic system, three groups of samples can be distinguished:

(I) The San Juan quartz-diorite (LO06; $N = 63$) shows the oldest weighted mean age of 21.37 ± 0.55 Ma with a mean square of weighted deviates (MSWD) of 0.78 (Fig. 9B). The range of single zircon ages spans between 22.78 ± 0.83 Ma and 20.63 ± 0.81 Ma.

(II) The samples located near the margins of the plutons, corresponding to samples LO30 (La Obra pluton; $N = 54$), LO13 (La Obra pluton; $N = 18$), and LO37 (Cerro Blanco pluton; $N = 52$), have intermediate weighted mean ages of 20.59 ± 0.55 Ma, 20.94 ± 0.61 Ma, and 20.66 ± 0.57 Ma (MSWD = 1.1, 0.76, and 2, respectively). It is interesting to note that these samples differ in composition, ranging from 64 wt% SiO_2 (LO30) to 74 wt% SiO_2 (LO37).

(III) Granitic samples from the inner parts of the plutons show the youngest weighted mean ages. Sample LO16 (La Obra pluton; $N = 45$) has a weighted mean age of 19.92 ± 0.55 Ma with an MSWD of 1.3, while sample LO21 (Cerro Blanco pluton; $N = 45$) has a weighted mean age of 19.93 ± 0.57 Ma (MSWD = 1.8). Both samples are similar in whole-rock composition and texture, with ~69 wt% SiO_2 content (Fig. 9C). Statistically, weighted mean ages for both these samples are significantly younger than the oldest sample LO06.

The new U-Pb zircon ages presented here are consistent with those previously published by Piquer et al. (2021), also acquired by means of LA-ICP-MS analyses. The samples were obtained from the inner parts of the lower levels of La Obra pluton, corresponding to monzogranite and granodiorite (consistent with our geologic mapping) and yielded weighted mean ages of 20.79 ± 0.13 Ma (20.79 ± 0.44 Ma, with propagated excess uncertainty) and 20.69 ± 0.07 Ma (20.69 ± 0.42 Ma, with propagated excess uncertainty), respectively, similar to the weighted mean ages reported in this study for samples LO30, LO13, and LO37 (Fig. 9C).

Trace-Element Geochemistry

The full set of trace-element contents from zircon analyzed for U-Pb ages is presented in the Supplemental Material (Table S2). Individual samples

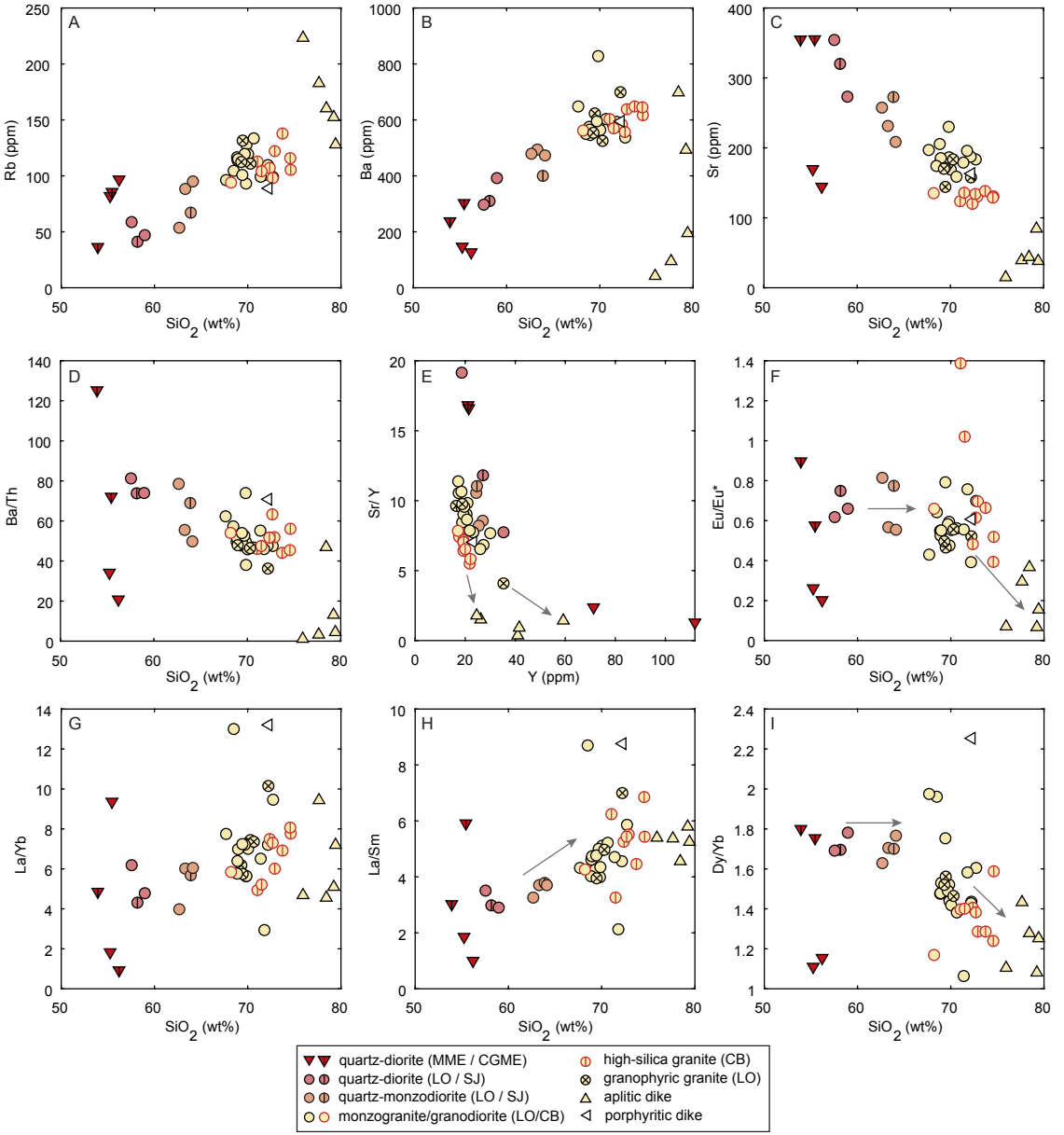

Figure 8. Variations in trace-element contents and trace-element ratios of samples from La Obra–Cerro Blanco intrusive suite. Abbreviations: LO—La Obra pluton; CB—Cerro Blanco; SJ—San Juan stock; MME—microgranular mafic enclaves; CGME—coarse-grained mafic enclaves. The 2σ analytical error is smaller than the symbol size. Gray arrows show the general trend for elements or ratios emphasized in the text.

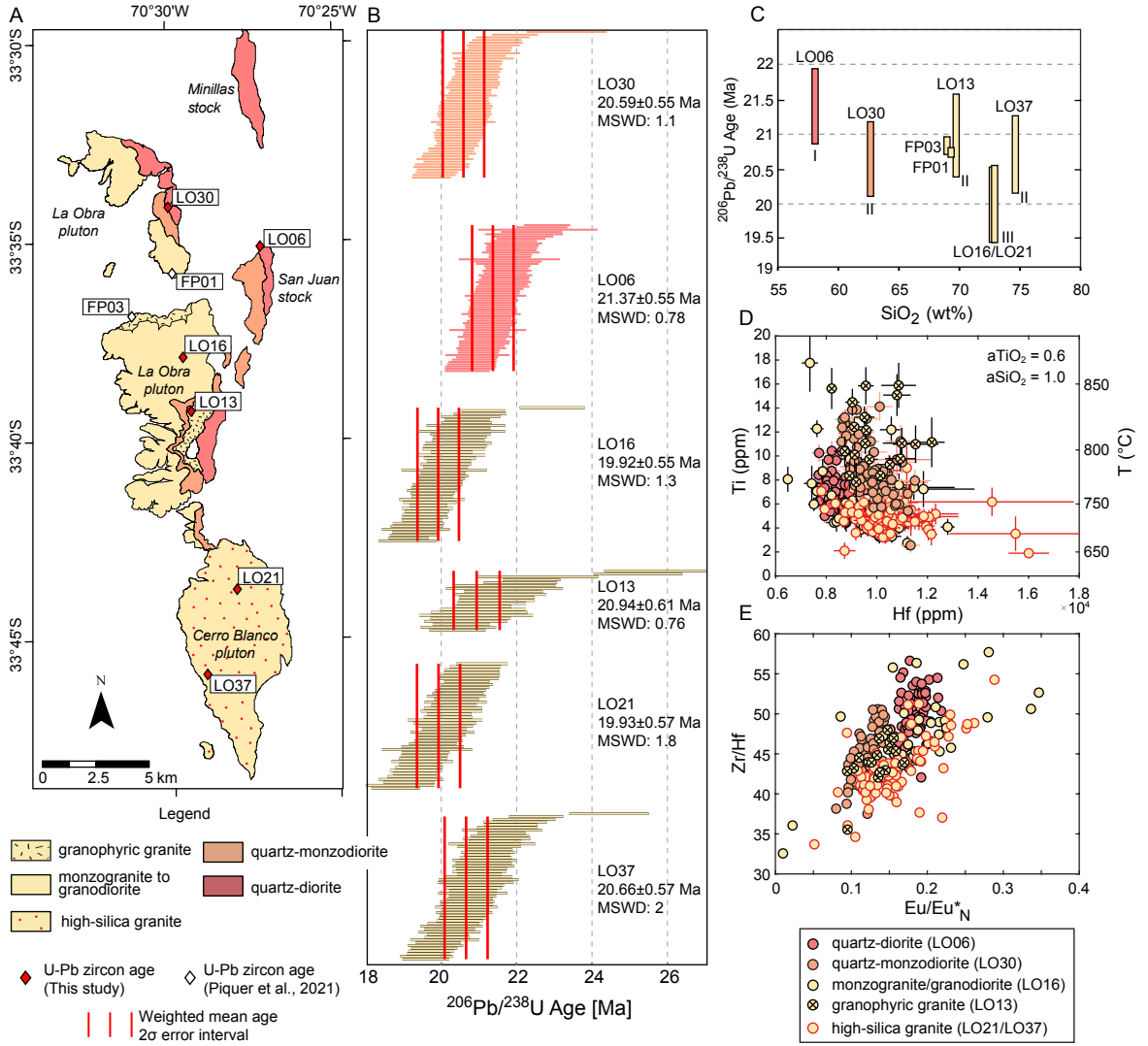

Figure 9. U-Pb zircon geochronology results. (A) Map with the locations of samples collected for U-Pb dating. (B) Rank-ordered $^{206}Pb/^{238}U$ zircon spot dates (2σ uncertainty). Samples are ordered according to their map location, from north to south. Weighted means and mean square of weighted deviates (MSWD) values were calculated with IsoplotR 4.15 (Vermeesch, 2018). (C) Weighted mean $^{206}Pb/^{238}U$ zircon ages vs. whole-rock SiO_2 for each dated sample. This plot highlights that the most mafic sample (I: LO06 from the San Juan stock) is statistically older than monzogranitic samples from the lower parts of La Obra and Cerro Blanco plutons (III: LO16 and LO21, respectively), while the rest of the samples (II: LO13, LO30, LO37), located close to the margins of the plutons are statistically coeval to the rest of the samples. Ages obtained by Piquer et al. (2021) from La Obra pluton are plotted in the same sample (FP01 and FP03) using a whole-rock composition chosen according to the closest representative sample obtained in this study. (D) Ti and Hf content in zircon crystals. Ti-in-zircon crystallization temperatures estimates used the model of Ferry and Watson (2007). Error bars represent 2σ analytical uncertainty. (E) Zr/Hf and Eu/Eu^*_N in zircon crystals. Analytical error interval for the compositions is equal to the symbol size.

showed continuous ranges in zircon trace-element compositions. Zircons from the quartz-diorite San Juan stock, the quartz-monzodiorite sheet, and the granophyric granite in the upper part of La Obra pluton (LO13) are richer in Ti compared to the rest of the samples (Ti = 6–14 ppm). In contrast, zircon grains from monzogranite (LO16 and LO21) and high-silica granite (LO37) samples are relatively Ti-poor (Ti = 2–6 ppm; Fig. 9D). Zr/Hf ratios of zircons change with bulk-rock composition, with lower ratios for the silicic samples in a good correlation with the Eu anomaly $(Eu/Eu^*)_N$.

Hf Isotopes

In a subset of zircon grains analyzed for U-Pb ages and trace elements, we also collected Hf isotopes; all Hf values are included in the Supplemental Material (Table S2). La Obra and Cerro Blanco zircons showed initial εHf values from +8.0 to +12.4 and from +7.5 to +13.5, respectively, with weighted mean values for individual samples enclosed in a tight interval between +10.2 and +11.2 (Fig. 10A).

MAGNETIC FABRIC OF LA OBRA–CERRO BLANCO INTRUSIVE SUITE

Magnetic Mineralogy

Petrographic observations under transmitted and reflected light show that most of the opaque minerals correspond to titanomagnetite (near the magnetite end member) with brownish gray homogeneous crystals, and minor titanohematite crystals. In general, opaque minerals are more abundant in mafic samples and occur as subhedral to anhedral crystals occupying the intercrystalline interstices, especially surrounding mafic minerals and, to a lesser extent, plagioclase (Figs. 11A–11D). These crystals are typically cubic or with low aspect ratios. A subordinate group occurs as inclusions within biotite, amphibole, and plagioclase crystals, forming mafic aggregates (Figs. 11C–11F).

Backscattered images obtained via SEM-EDS show that titanomagnetite crystals are usually homogeneous in composition, with the presence of ilmenite concentrated in the margins of the crystals (Figs. 11D and 11F). Elemental analyses carried out on opaque minerals from representative samples indicate that titanomagnetites have compositions close to the Ti-poor end member (Fig. 11G; detailed results are presented in the Supplemental Material; see Table S3). These compositions are consistent with the relatively high bulk magnetic susceptibility values of the specimens (Fig. 11H).

Magnetic Fabric Results

The magnetic fabric was determined at 25 sites by anisotropy of magnetic susceptibility measurements. Detailed data are presented in Table S4. The bulk magnetic susceptibility (K_{bulk}) of all specimens presents an average value of $2.09 \times 10^{-2} \pm 1.89 \times 10^{-2}$ SI (N = 255; range between 0.43×10^{-4} and 9.06×10^{-2} SI; where >99% of the specimens have values >10^{-3} SI; Fig. 11H). The sites corresponding to the quartz-diorites and quartz-monzodiorites (most mafic compositions) have higher mean bulk magnetic susceptibility values (K_m; Fig. 12A), consistent with the higher content of mafic minerals and Fe-Ti

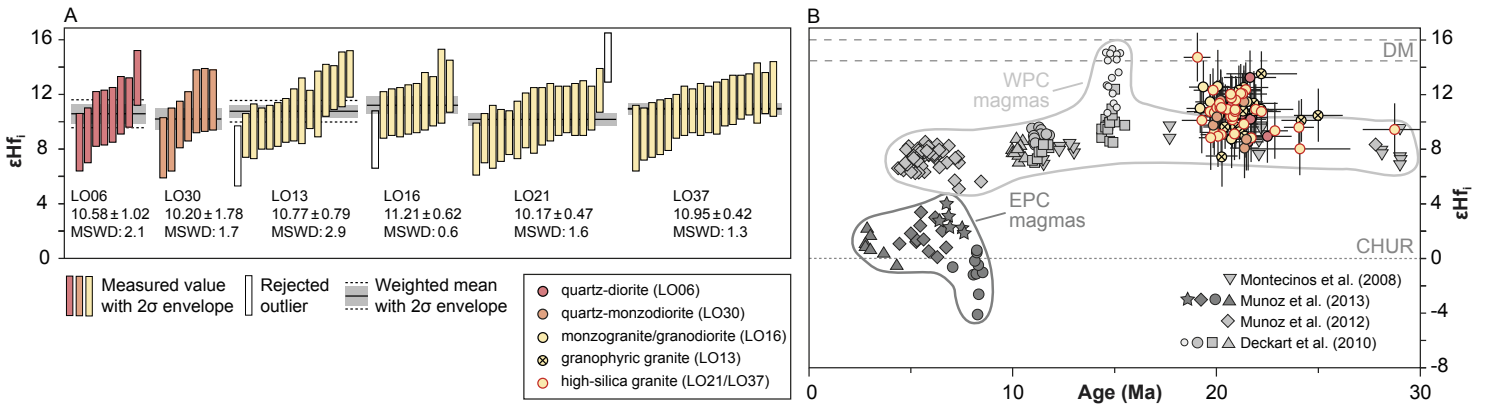

Figure 10. Results of Hf in zircon analyses. (A) Rank-order plot of initial εHf isotopic compositions for zircons from La Obra and Cerro Blanco plutons. (B) Data from this work ($\varepsilon Hf_{(t)}$) included in a compilation of available in situ Hf isotope data for zircons from Cenozoic Andean magmas from the western and eastern Principal Cordilleras (WPC and EPC). DM—depleted mantle; CHUR—chondritic uniform reservoir; MSWD—mean square of weighted deviates.

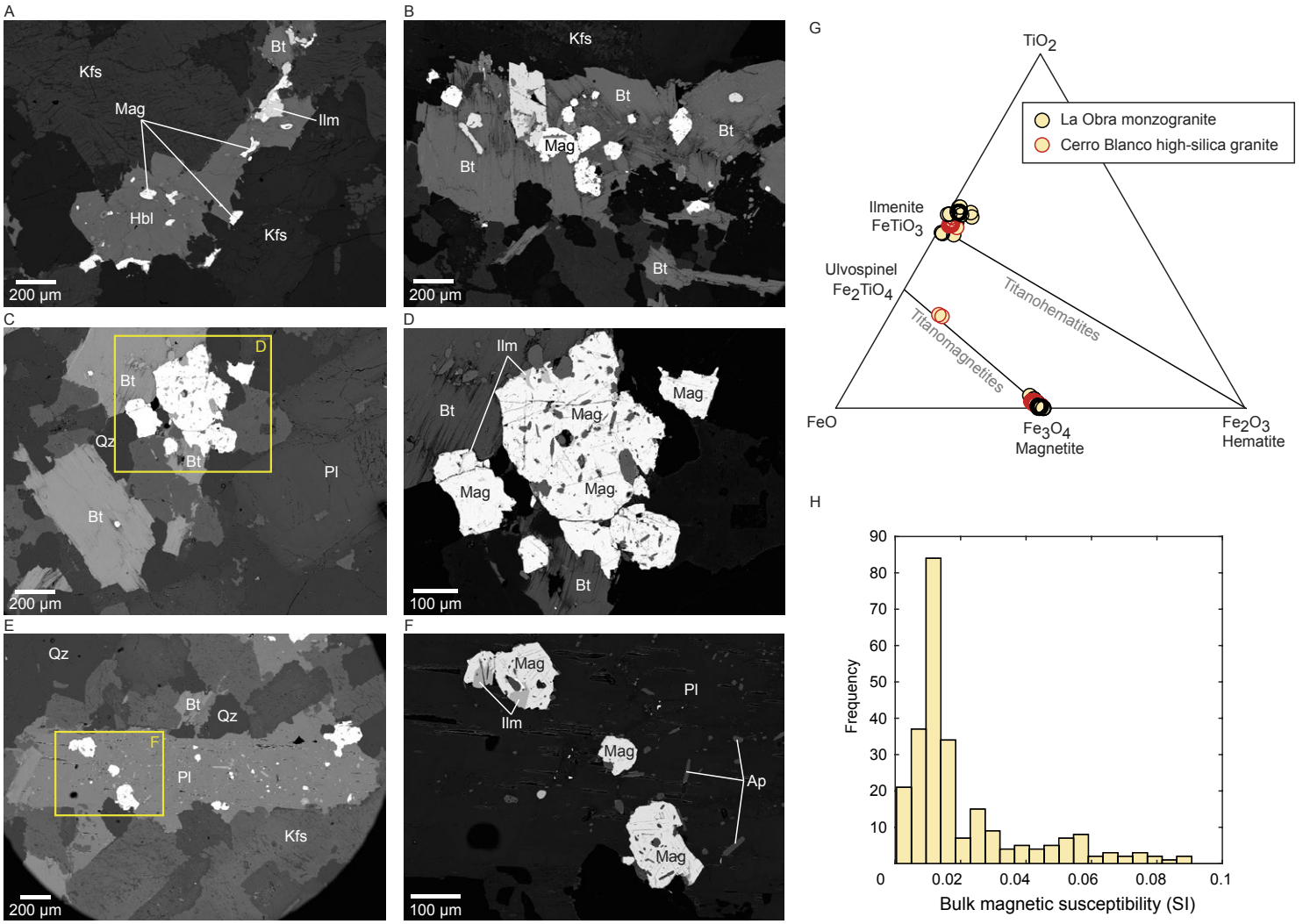

Figure 11. (A–F) Backscattered photomicrographs of the Fe-Ti–oxide crystals within selected samples from La Obra monzogranite (LO2701) and Cerro Blanco high-silica granites (LO2101 and LO3701). (A) Inter- and intracrystalline Fe-Ti oxides within a hornblende (Hbl) crystal. Fe-Ti oxides in the hornblende margins follow the shape of the surrounding crystals. (B) Fe-Ti oxides occurring within agglomerates of biotite crystals. (C–D) Representative intercrystalline Fe-Ti oxides. The compositional zoning is highlighted in D, where nearly homogeneous magnetites (Ti-poor composition) present ilmenite zones close to the margins. (E–F) Inclusions of Ti-poor titanomagnetite crystals within a plagioclase crystal, where ilmenite zones are present. (G) Ternary projection of the molar composition of the Fe-Ti–oxide crystals obtained by energy-dispersive spectroscopy and scanning electron microscope analyses, showing that most of the Fe-Ti oxides correspond to Ti-poor titanomagnetites (magnetite) with the presence of Ti-rich titanohematite (ilmenite). (H) Histogram showing the distribution of bulk magnetic susceptibility for the analyzed specimens. A peak around 0.01 SI is observed, indicating that the main magnetic carrier is Ti-poor titanomagnetite (magnetite). Mineral abbreviations are according to Whitney and Evans (2010).

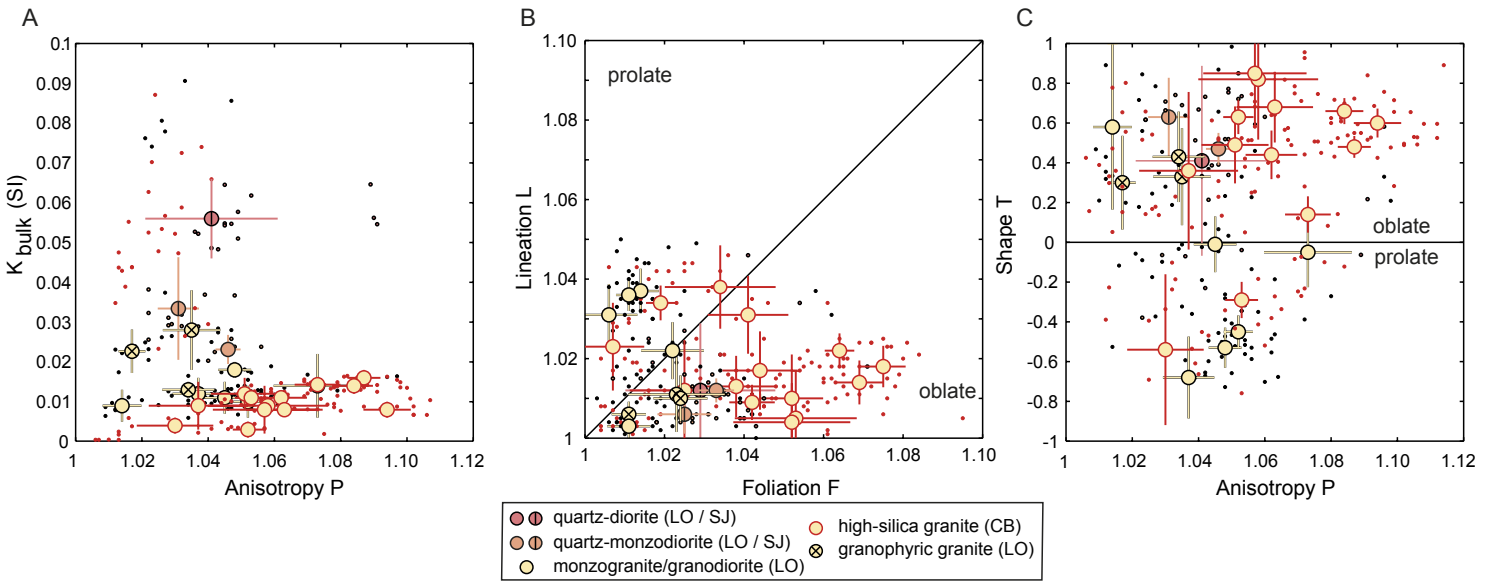

Figure 12. Scalar parameters and associated errors of the magnetic fabric ellipsoids from La Obra–Cerro Blanco plutonic suite. (A) Mean bulk magnetic susceptibility (K_m) vs. anisotropy parameter (P), showing the lower bulk susceptibility values in the most felsic samples (from Cerro Blanco pluton), which also tend to present higher anisotropy. (B) Flinn's diagram comparing the lineation and foliation magnitudes, which show that magnetic fabric ellipsoids tend to be oblate. (C) Shape parameter of Jelinek (1981) (T) vs. anisotropy parameter (P), reinforcing the relatively high anisotropy values and oblate shapes for the magnetic fabric tensors of most felsic samples. Error bars of the shape parameters correspond to 95% confidence error calculated by propagation of the error of anisotropy axis magnitudes. Error bar of K_{bulk} corresponds to the 2σ value of the specimens per site. The individual specimen values are also plotted (red dots are samples from Cerro Blanco pluton, mostly high-silica granites). Abbreviations: LO—La Obra pluton; CB—Cerro Blanco; SJ—San Juan stock.

oxides. In contrast, K_m values are similar for granites/granodiorites from La Obra pluton and the high-silica granites from Cerro Blanco pluton. However, it is interesting to observe that the granophyric granites (both in the bottom and upper levels of La Obra pluton) present relatively higher K_m values than the rest of the granites (0.015–0.03 SI; Fig. 12B).

In general, foliation values (F) vary between 1.01 and 1.08, at the expense of magnetic lineation (L), which has maximum values of 1.038 (Fig. 12A). About 80% of the sites have a magnetic fabric represented by a triaxial to oblate ellipsoid, as indicated by the predominantly positive values of Jelinek's shape parameter (T; Jelinek, 1981; Fig. 12C), and U values predominantly between 0 and 0.82 (6 sites have U < –0.3). Five sites have a pronounced prolate fabric and correspond to monzogranites from both La Obra (sites 5, 6, 7) and Cerro Blanco (sites 18 and 23). The anisotropy values (P) exhibit variations based on site location, ranging from 1.01 to 1.06 for sites within La Obra pluton, while reaching values as high as 1.09 in the case of the high-silica granites within Cerro Blanco pluton (Figs. 12B and 12C). The granophyric granites have relatively low anisotropy degree values compared to the other granites, with values between 1.018 and 1.04 (Fig. 12C).

The orientation of magnetic lineation shows contrasting behavior depending on the analyzed pluton. In La Obra pluton and the two sites from the San Juan stock, the magnetic lineation typically exhibits N and NNE trends with inclinations of less than 30° (Figs. 13A and 13C), except for sites 2 and 25, which exhibit a steeper lineation that plunges between 40° and 60° (Fig. 13D). In the contrasting case of Cerro Blanco pluton, the magnetic lineation tends to be steeper than the lineation in the north, typically plunging >30° in the NE direction (Figs. 13A and 13C). In addition, four sites have a steep magnetic lineation that plunges >60°, two of which are in the upper levels of Cerro Blanco pluton (sites 20 and 21; Figs. 13A and 13D). This defines a pattern of variation that becomes steeper moving southward across the pluton.

Magnetic foliation also shows contrasting patterns between La Obra pluton (including the San Juan stock) in the north and Cerro Blanco pluton in the south of the plutonic system. In general, magnetic foliation planes in La Obra pluton tend to strike NE and exhibit dips >55°, even reaching dip values >80° at eight sites (Figs. 13B and 13E). It is worth noting that sites 3, 4, and 5, which are in the uppermost part of La Obra pluton (near the roof and magmatic contacts), present less steep foliation planes that dip between 55° and 20° (Fig. 13B).

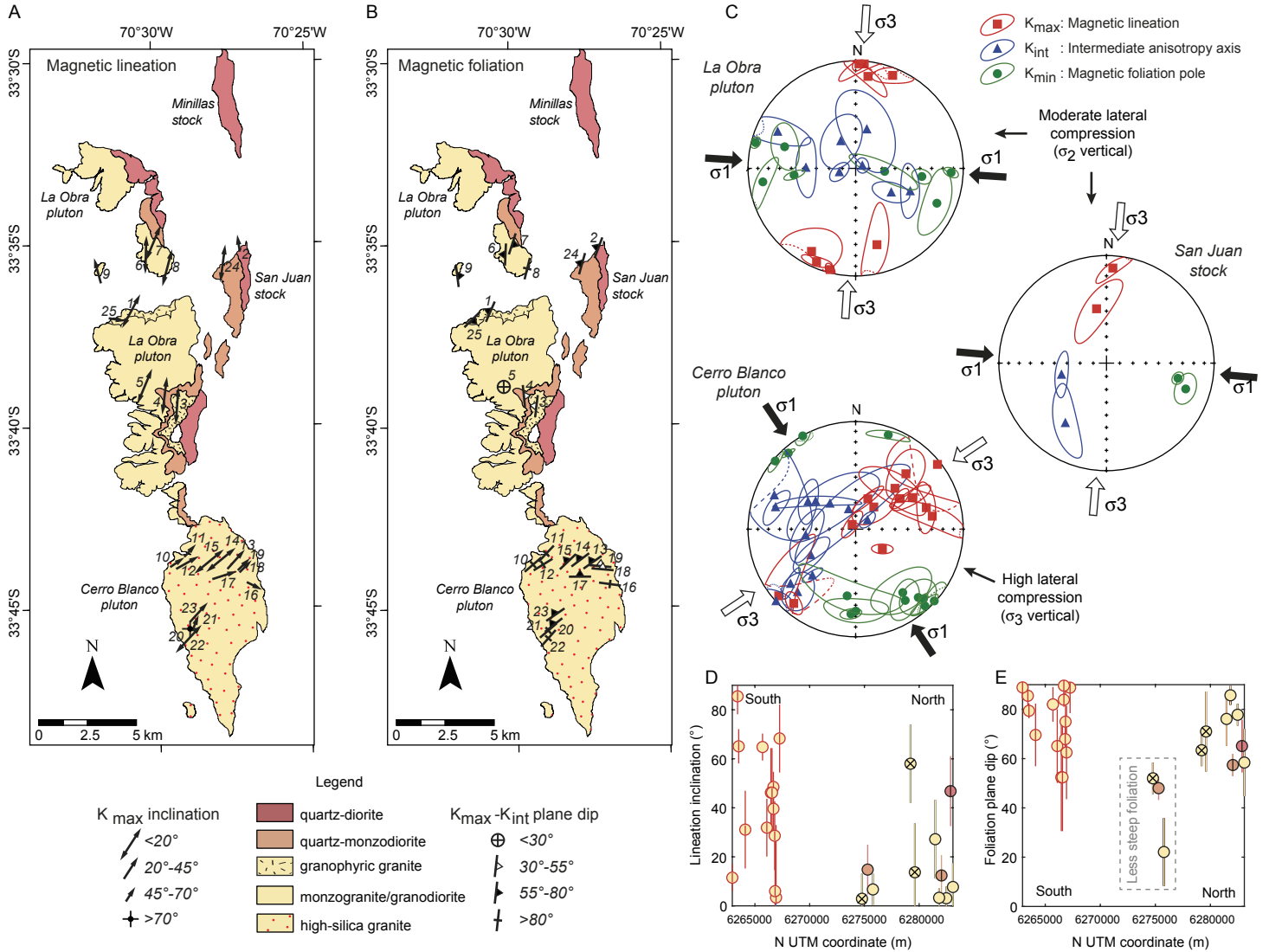

Figure 13. Orientation of the magnetic fabric tensors obtained through anisotropy of magnetic susceptibility analyses. (A) Map of the magnetic lineation (K_{max}) orientation represented with arrows, showing the declination. Arrows point to the direction of inclination. Numbers indicate the site. (B) Map of the magnetic foliation (defined by the plane containing K_{int} and K_{min}). Numbers indicate the site. (C) Equal-area stereographic projections (lower hemisphere) of the specimens' K_{max} (lineation in red), K_{int} (intermediate anisotropy axis), and K_{min} (pole of the foliation plane in green) orientation grouped by intrusion. Ellipses represent 95% confidence angles. The orientation of the expected principal stresses is shown for La Obra pluton and San Juan stock (moderate lateral compression) and Cerro Blanco pluton (high lateral compression), assuming that the magnetic fabrics record the synmagmatic coaxial deformation caused by far-field tectonic forces (Burton-Johnson et al., 2019). Projections were obtained by using Stereonet version 10.2.9 (Allmendinger et al., 2013; Cardozo and Allmendinger, 2013). (D) Variation of the inclination of the magnetic lineation along the axis of the intrusive bodies. Error bars represent the 95% confidence interval. (E) Variation of the dip of the magnetic foliation plane along the axis of the intrusive bodies. Error bars represent the 95% confidence interval. Coordinates correspond to Universal Transverse Mercator (UTM) Zone 19H South.

Magnetic foliation planes in Cerro Blanco pluton present a NE trend, typically with subvertical disposition in the western part of the pluton and less steep north-dipping trends in the eastern part (sites 16, 17, 18, and 19; Fig. 13B).

DISCUSSION

The integration and analysis of the results presented here allow us to propose a conceptual model for the construction of the magma reservoir that would have given rise to the La Obra–Cerro Blanco suite at the emplacement level. We envision the evolution of the suite through a conceptual model that includes magma formation in deeper crustal environments, emplacement at upper-crustal levels, and in situ differentiation. These steps of magmatic evolution are discussed in order in the following sections. Our interpretations are based on field relationships, compositional variations, magnetic fabrics, and ages, contrasting with well-documented case studies, as well as simple geochemical modeling of the trace-element distribution in the magmas involved (see footnote 1).

The discussion opens with an examination of the genesis of the magmas injected at the emplacement level of the intrusive suite, which are postulated to have been generated by the fractionation of a plagioclase-dominated assemblage (with minor amphibole) within a transcrustal mush-type magmatic system. The first pulses sourced from deeper levels of the transcrustal magmatic system to reach the emplacement level were quartz-diorite and quartz-monzodiorites, which gave rise to the amalgamation of stocks and the mafic layer of La Obra pluton. Subsequently, monzogranitic magmas fed from deeper levels intruded subhorizontally, producing a series of crystal-poor silicic caps. In the late stages, highly differentiated, high-silica granites were concentrated in the Cerro Blanco area to form a single thick magma chamber (convective crystal-poor magma chamber). These high-silica melts were extracted and redistributed after the formation of a mushy reservoir, giving rise to a swarm of both crystal-poor and crystal-rich dikes that likely fed a subaerial volcanic system.

Below the Emplacement Level: Genesis of the Compositional Variability and Cogeneticity of the Magmatic Suite

The variability in magmatic compositions observed in arc systems is driven by multiple magmatic processes in which both the magma itself and the host lithologies can be involved as magmas ascend through the lithosphere. These processes include crystal fractionation and shifts in the partial melting conditions and degree of crustal assimilation, among others (for an exhaustive review, see Ducea et al., 2015). The intrusive and volcanic record of Miocene magmatic rocks in central Chile only represents the upper-crustal level (<5 km depth) of a translithospheric magmatic system. Reconstructing the ascent path of these magmas and the series of processes they underwent along this path thus remains a challenging proposition.

To resolve these questions, geochemistry and isotopes are the most commonly used proxies (Ratschbacher et al., 2024). In the Andean segment that is subject of this study, the influence of terrigenous material on the asthenospheric source has been proposed to explain the incorporation of crustal material in arc magmas, as suggested by crustal isotopic signatures (Stern, 1991). Alternatively, researchers have proposed contamination of pristine subduction-derived magmas by crustal lithologies at lower-crustal levels, where the resulting hybrid magmas were homogenized, as an explanation for the observed compositional and isotopic variability (e.g., Hildreth and Moorbath, 1988; Muñoz et al., 2012). In addition, during the Miocene, the Andean orogen in central Chile underwent major changes in the tectonic configuration, which triggered an accelerated crustal thickening around 21–15 Ma, accompanied by a multiple-stage arc migration (generally trending eastward; Giambiagi and Ramos, 2002; Farías et al., 2010; Jara and Charrier, 2014). These changes are evidenced, for instance, by the progressive increase of La/Yb ratios, indicating a deeper magmatic source with residual garnet (Kay and Mpodozis, 2002; Muñoz et al., 2012). Furthermore, during this interval, modifications in the compositional constituents of the continental crust occurred, which would have affected the composition of the arc magmas. This is indicated by the crustal affinity of isotopic signatures observed in zircons (relatively low εHf values) of intrusive rocks emplaced in the Principal Cordillera of central Chile. The crustal affinity has been associated to the higher influence of the Cuyania terrain rocks in deep crustal levels, because of the tectonic configuration changes since 8 Ma (Muñoz et al., 2013). Furthermore, these changes have been observed both in regional and single magmatic system scales, such as the San Francisco Batholith, which holds an ~13.5 m.y. record of arc magma evolution (Large et al., 2024).

For the case of La Obra–Cerro Blanco intrusive suite, our data support the hypothesis that the diversity of magmas that gave rise to the system was generated by crystal fractionation during the ascent or stagnation across a transcrustal mushy magmatic system (Cashman et al., 2017), both by gravitational settling and crystal-melt separation by removal of interstitial melts or other mechanism (e.g., reactive flow; Jackson et al., 2018), depending on the thermomechanical properties (Dufek and Bachmann, 2010). The magmatic evolution of the igneous suite included limited changes in the deep magmatic source. Crustal assimilation, if present, was limited to older arc magmatic rocks similar in composition and isotopic signature, as suggested by the relatively flat and parallel whole-rock light rare earth element (LREE) patterns, which would have shown enrichment in highly incompatible elements even at low degrees of assimilation of non-cogenetic material. The flat REE patterns and low REE ratios (La/Yb, La/Sm, and Dy/Yb) also suggest that the residual mineralogy at lower-crustal levels was plagioclase- and amphibole-dominated mineralogy and remained the same (with variable proportions) throughout the generation of the intrusive suite. Based on the REE budget across the La Obra lithologies, we discard the influence of other residual phases in the deep crustal levels, such as garnet, the influence of which at deeper crustal levels has been recorded only in economic porphyry associated with the San Francisco

Batholith after 8 Ma (Large et al., 2024). In addition, the trace-element ratios such as La/Nb and Ba/Th suggest that there were no differences in the addition of fluid phases and/or mobile elements from the slab as inferred for other systems (Kay et al., 2005; Müntener et al., 2018). Moreover, relatively higher increments in Ba/Th ratios (>100), not observed here, have been interpreted in this region as evidence for partial melting of different crystalline basement rocks (Large et al., 2024), allowing us to discard these processes as controlling the compositional variability of this intrusive suite.

In this sense, we propose a common origin for the entire La Obra–Cerro Blanco intrusive suite. The transcrustal magmatic system was dominated by fractionation of plagioclase and minor amphibole (MREEs and HREEs; Nandedkar et al., 2016; Smith, 2014). These phases were fractionated in variable proportions, likely at deeper crustal levels, during generation and ascent of the magma, as suggested by the absence at the emplacement level of plagioclase- or amphibole-rich cumulates. A simple fractional crystallization model that combines the trace-element distribution with a major-element mass balance can replicate the compositional trends observed in the bulk-rock geochemistry (for modeling details, see Text S1; Table S5). Modeling results indicate that mineral fractionation was dominated in the early stages by plagioclase to produce the least-evolved lithologies of the intrusive suite (~90% of the fractionated solid to generate quartz-diorites and quartz-monzodiorites), whereas amphibole fractionation was crucial to the production of the most felsic magmas (i.e., monzogranites and high-silica granites). The fractionating mineralogy is suggested by the marked negative Eu anomalies (most pronounced in monzogranites and high-silica granites) observed both in whole-rock and zircon compositions (Fig. 9E), the high variability in Sr, Rb, and Ba, and the slight depletion in MREEs as SiO_2 increases (Figs. 8F–8I). However, fractionation of minor pyroxene (which also fractionates MREEs and HREEs; Ulmer et al., 2018), iron oxides, and accessory phases such as titanite and zircon (as indicated by decreasing tendency of Zr and the Dy/Yb ratio in monzogranites and high-silica granites; Fig. S1) is required to explain the MgO and FeO_t content and the MREE and HREE depletion of monzogranites and high-silica granites compared to the rest of the suite. The fractionation of a plagioclase-dominated mineral assemblage has been proposed to occur in relatively low-pressure conditions (up to 10 kbar; Villiger et al., 2007; Marxer et al., 2023), which is consistent with the thin continental crust setting proposed for that period in central Chile before the tectonic inversion of the Abanico basin (Farías et al., 2010; Jara et al., 2015; Muñoz et al., 2012). We propose that the fractionation of these phases must have occurred at deep crustal levels, as has been proposed for arc-related hydrous magmatic systems via experimental studies (Müntener and Ulmer, 2018; Nandedkar et al., 2016).

The only elements that show a constantly increasing trend across the entire magmatic suite are K_2O, Ba, and Rb, contrary to the decreasing Sr tendency with increasing SiO_2 content (Fig. 8). This suggests that K-feldspar and biotite were late crystallizing phases (supported by petrographic observations). However, the wider trace-element compositional ranges exhibited by aplitic dikes indicates that their generation was controlled by the fractionation of those phases, in variable proportions. In general, they are enriched in REEs, showing the most pronounced negative Eu anomalies and HREE enrichment, suggesting significant plagioclase fractionation, with minor mafic phase and accessory mineral (zircon and titanite) fractionation, during the production of aplitic magmas. Although aplitic dikes have lower Ba than granites and high-silica granites, which could be associated with orthoclase fractionation, we suggest that this would have been generated either by biotite fractionation (consistent with the euhedral crystal shapes observed in high-silica granites) and/or Ba mobilization by volatile phases common in the late-magmatic stages of hydrated granitic systems (Morgan and London, 2003).

Mafic enclaves observed in La Obra–Cerro Blanco intrusive suite are variable in textures and compositions and can be classified into two groups: the coarse-grained mafic enclaves and microgranular mafic enclaves. The similitude in texture and REE patterns between the composition of the quartz-diorites and quartz-monzodiorites and the coarse-grained mafic enclaves (represented by samples LO0605 and LO1803), with no evidence for flow in a magmatic condition, suggests that they are autoliths formed from the reworking of previously crystallized initial pulses (for a detailed discussion on autoliths, see Pascual et al., 2008; Clemens et al., 2017). The straight monzogranitic dikes intruding some of coarse-grained mafic enclaves (Fig. 3F) indicate that this small group was mostly crystallized at the time of interaction with the monzogranitic magma, suggesting that the enclaves might be the result of incorporation in the monzogranitic intrusion of previously crystallized mafic units (i.e., magmatic erosion; Paterson et al., 2016; Žák et al., 2010). Conversely, the microgranular mafic enclaves, which are enriched in HREE content and have a marked negative Eu anomaly, can be interpreted as mafic magma globules that probably exchanged mass with the host magma and witnessed concentration of mafic phases as hornblende and clinopyroxenes (i.e., cumulates), as interpreted by Barbarin (2005) for some microgranular mafic enclaves preserved in granitoids of the central Sierra Nevada Batholith, California, USA. It is important to note that interpreting the nature of the chemical interaction between microgranular mafic enclaves and host granites based on whole-rock and textural data only, without information on mineral composition, is difficult and inherently speculative. The presence in microgranular mafic enclaves of coarse-grained plagioclase and mafic phase phenocrysts similar to those present in the host granitoids and the Na_2O and total alkali enrichment compared to diorites lead to the possibility that phenocrysts may have been physically transferred from the host. Alternatively, these phenocrysts might correspond to minerals that crystallized within the enclaves after chemical diffusion of elements from the host granitoid (Lesher, 1990; Barbarin, 2005).

The cogenetic nature of the magmas that fed the entire La Obra–Cerro Blanco suite is supported by the tight temporal window of emplacement and crystallization (Fig. 9), the bulk-rock compositional trends, zircon geochemistry (e.g., the continuous trends in Eu/Eu^*_N, Ti, Hf), and Hf isotopic signature. The restricted range in εHf_i values indicates a significant juvenile component in the source magmas where zircons were equilibrated, as previously identified in late Cenozoic (30–4 Ma) magmatic products of the western Principal Cordillera (Fig. 10B; Deckart et al., 2010; Large et al., 2024; Montecinos et al., 2008; Muñoz

et al., 2012, 2013). The absence of a significant inherited component in U-Pb ages in La Obra–Cerro Banco rocks (Fig. 9A) indicates that assimilation of older crust-derived material, relatively lower in εHf, was limited. Alternatively, this conspicuous feature of La Obra–Cerro Blanco intrusive suite might be related to transient zirconium undersaturation of magmas in the upper-crustal staging area, which might have erased the xenocrystic component of the zircon record (Szymanowski et al., 2020).

At the Emplacement Level: Origin of the Magnetic Fabrics and the Magma Flow Record

Anisotropy of magnetic susceptibility has been extensively used to approach the petrofabrics and investigate the strain record in plutonic rocks (Aranguren et al., 2003; Archanjo et al., 1995; Garibaldi et al., 2018; Liu et al., 2018; McNulty et al., 2000). However, its interpretation is typically obscured by the multiple sources of the magnetic anisotropy, such as the combination of ferromagnetic and paramagnetic signals (Grégoire et al., 1995; Biedermann et al., 2018). Based on the relatively high bulk susceptibility values (K_{bulk}), our results are consistent with Ti-poor titanomagnetite (i.e., magnetite; Parés, 2015) controlling the magnetic properties of La Obra–Cerro Blanco intrusive suite. However, the origin of the magnetic anisotropy requires a deeper analysis (Biedermann and Bilardello, 2021), which is beyond the scope of this paper. Although more analyses are required to confirm the anisotropy carrier and, ideally, separate the ferromagnetic and paramagnetic signals, here we try to shed some light on its most probable origin.

Microscopic observations indicate that magnetite occurs mostly as equant euhedral to subhedral crystals filling the intercrystalline spaces within mafic agglomerates (typically biotite and pyroxene; Fig. 5). The presence of anhedral magnetite crystals, with elongated faces defined by the boundaries of euhedral feldspar crystals, can result in anisotropy of grain shape for magnetite grains (Figs. 11A and 11B). Furthermore, magnetite crystals exhibit an anisotropy in their spatial distribution, especially within elongated plagioclase crystals (Fig. 11E). These observations, as reported by Biedermann and Bilardello (2021), suggest that magnetite may be the principal magnetic anisotropy carrier.

Microtextures indicative of solid-state deformation are preserved mainly along the inner parts of La Obra pluton. These microstructures are restricted to microscopic shear zones as kink bands on biotite (250 µm width) and internal crystal fractures in plagioclase (Fig. 14), indicating that plastic deformation has affected (at least locally) the intrusive suite. However, Fe-Ti–oxide crystals appear to be unaffected by plastic deformation, suggesting that the magnetic fabric was acquired in the suprasolidus state.

Even though the intrusive suite was emplaced in spatial association with the tectonic structures along the West Andean thrust system, we reject the idea that the magnetic fabric records the deformation produced by the tectonic activity related to thrust development. The magnetic fabric of La Obra–Cerro Blanco intrusive suite displays anisotropy values up to 1.1 (Fig. 12), which are much lower than those values measured in granites affected by fault systems causing synmagmatic shearing. For instance, in the case of the Mono Creek intrusive suite, where magnetite is also the main magnetic carrier, the magnetic anisotropy degree reaches values of 1.6, which is interpreted as strain recorded by a fault system (de Saint Blanquat and Tikoff, 1997). This indicates that the emplacement of La Obra–Cerro Blanco intrusive suite effectively postdated the fault systems of the western margin of the Principal Cordillera, as also indicated by crosscutting relationship with the host-rock structures and stratification (Figs. 3A and 4A).

An alternative scenario for attributing a tectonic origin to the magnetic fabric is the influence of far-field stress, typically associated with plate convergence in subduction environments. Exhaustive analysis of compiled anisotropy of magnetic susceptibility data reveals that the synmagmatic tectonic strain field may be accurately determined from the orientation of magnetic fabrics in plutons (Burton-Johnson et al., 2019). For example, in the Huemul–Risco Bayo plutons (in southern central Chile), the magnetic fabric has been interpreted from the preferred orientation of crystals as due to the plate-convergence stress recorded in a suprasolidus state (Garibaldi et al., 2018). In this exemplary intrusion, the far-field stress induced the redistribution of residual silicic melts throughout the magma reservoir, ultimately causing the compositional zoning of the intrusive suite (Schaen et al., 2018).

In a similar framework, we can infer the orientation of the principal stress to replicate the magnetic fabric orientation of La Obra–Cerro Blanco intrusive suite, assuming the scheme for coaxial pure shear presented by Burton-Johnson et al. (2019). The subhorizontal magnetic lineations and predominantly subvertical foliations of La Obra pluton and San Juan stock may be replicated by moderate lateral compression, with σ_1 in an E-W orientation parallel to K_3 and horizontal σ_3 (Fig. 13C). This setting is consistent with that expected for the compressional regime in central Chile during the Miocene, when the tectonic inversion of Abanico basin, dominated by the N-S thrust system, took place (Charrier et al., 2002; Farías et al., 2010; Piquer et al., 2017). Along the same line, the orientation of magnetic fabric in the Cerro Blanco pluton shows discordant patterns and can hardly be linked to the synmagmatic tectonic stress field record. According to the approach by Burton-Johnson et al. (2019), the horizontal K_3 axis and steep K_1 could be explained by higher lateral compression in a NW-SE direction with σ_1 parallel to K_3 and a steep σ_3 (Fig. 13C). Nevertheless, that implies an orientation of σ_1 with a NW trend, which has not been recorded in this Andean segment. Indeed, if the magnetic fabric patterns of the whole intrusive suite represent only synmagmatic tectonic deformation, it is unlikely that such contrasting directions of tectonic stress would be recorded at the same time given the similitude of cooling ages for La Obra and Cerro Blanco plutons. Moreover, no large tectonic rotations (>30°) that may explain the rotation of the Cerro Blanco fabric patterns after their acquisition have been reported for the Miocene in this segment of the Western Cordillera (Arriagada et al., 2013).

In this framework, the magnetic fabric from Cerro Blanco pluton, and to a lesser extent that of La Obra, seems to have been controlled by the geometric

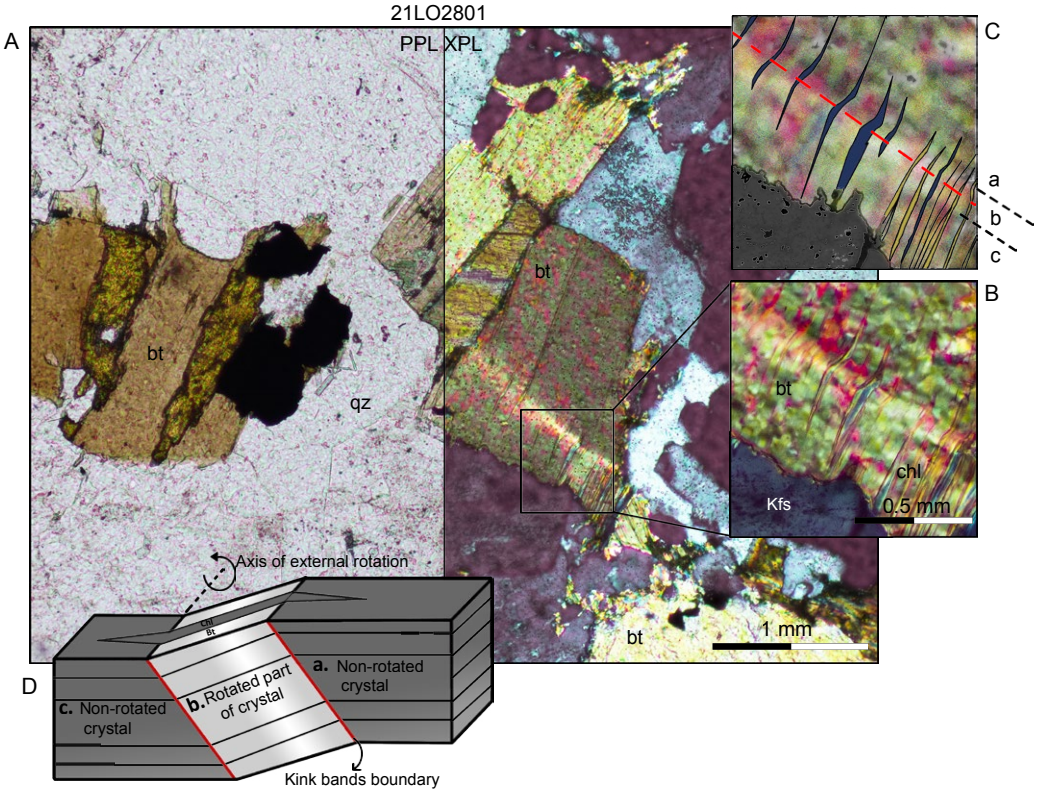

Figure 14. Photomicrograph of an example of the microtextures observed in a monzogranite sample from La Obra pluton, evidencing solid-state deformation (sample is not oriented). (A) Photomicrograph in parallel nicols (PPL) and crossed-nicols (XPL) views in the optical microscope. (B, C) Close-ups of the kink band observed in the biotite (bt) crystal. (D) Schematic of the crystal folding indicating the deformation. Kfs—K-feldspar; bt—biotite; qz—quartz; chl—chlorite.

constraints of the intrusions. This interpretation is supported by: (1) the progressive changes in the orientation of the foliation planes in Cerro Blanco pluton, which varies from NE-SW to E-W strike following the bell shape of the intrusion (Figs. 13B and 13C), and which is oblique to the expected elongation caused by pure shear due to plate convergence in this Andean segment, and (2) the gently stepped foliation planes in the upper levels of La Obra pluton (subparallel to the roof; Fig. 13E). Sites with subhorizontal dips are less frequent than steeply inclined ones, as is also the case in La Gloria pluton (Gutiérrez et al., 2013), where fluid-dynamic modeling indicated that the concentric pattern of the magnetic fabric was generated by shearing of convective flows within the reservoir. However, it is possible that there is a sampling bias due to limited access to the upper zones of the plutons and limited preservation of their roofs. Based on these observations, we suggest a minor influence of the far-field stress component in orienting the magnetic fabric of the plutons. However, this mechanism allowed the development of the N-S–oriented tectonic structures through which the magma was emplaced, ultimately controlling the contrasting geometry of the two intrusions. Following the interpretation of a magmatic origin for the magnetic fabric in plutonic rocks when the fabric is parallel to the pluton's margins (Paterson et al., 1998), we interpret that the magnetic fabrics record magmatic flow during the assembly of the magma reservoir that gave rise to La Obra–Cerro Blanco suite.

Time Scales and Multistage Assemblage of the Granitic Suite

The emplacement ages of intrusive bodies can be accurately determined by employing zircon single-grain, high-precision (chemical abrasion [CA]) isotope dilution–thermal ionization mass spectrometry (ID-TIMS) U-Pb techniques (e.g., Coleman et al., 2004; Schoene et al., 2012; Barboni et al., 2015; Samperton et al., 2017). In the absence of CA-ID-TIMS data, the emplacement age is routinely approximated by taking the weighted mean of in situ U-Pb dates (e.g., Gutiérrez et al., 2018; Rezeau et al., 2016). However, the extended time scale of zircon crystallization recognized in silicic systems and the nonlinear precipitation of zircon mass during the emplacement and cooling of an

intrusive body (Watson, 1996; Keller et al., 2017) make the weighted mean a measure of the average zircon crystallization age rather than of the emplacement age (Large et al., 2020). We thus recognize that the weighted mean ages obtained in this study, rather than providing a faithful record of the timing of emplacement of successive intrusive pulses, outline a broad interval of zircon crystallization across the magmatic system. In this context, the similarity between the weighted mean ages derived from both La Obra and Cerro Blanco plutons indicates that they are part of a single system that experienced sequential emplacement and crystallization.

Specifically, in the case of La Obra–Cerro Blanco intrusive suite, U-Pb ages indicate that the entire plutonic system was constructed during a temporal interval of 1.45 ± 0.78 m.y. (calculated by propagating the uncertainties of the maximum and minimum weighted mean ages; Gutiérrez et al., 2018). Previous compilations of high-precision (CA-ID-TIMS), medium-precision (sensitive high-resolution ion microprobe [SHRIMP]), and low-precision (LA-ICP-MS) U-Pb zircon ages for a single magmatic system (e.g., Chelle-Michou et al., 2014; Correa et al., 2016; Large et al., 2020) have shown that minor amounts of Pb loss or common Pb can produce outliers undetectable (and unmitigable) with lower-precision, in situ techniques, which artificially extend the overall duration of zircon crystallization. The calculated temporal interval (1.45 ± 0.78 m.y.) of magmatic activity at La Obra–Cerro Blanco magmatic center is thus just a measure of the maximum lifespan of the system. In combination with uncertainties associated with the in situ U-Pb methodology, critical quantitative parameters like the instantaneous or average magmatic flux are impossible to determine, as no clear contacts identifying individual pulses are visible in the main granitic mass, and the floor of the plutons is unexposed. In any case, we propose that the crystallization time scale of the entire system was probably prolonged by the thermal effects of the initial intrusions (i.e., quartz-diorites and monzodiorites), which preheated the country rock that hosted the granitic reservoir.

Regardless of the limitations concerning the exposure level of the intrusion and the accuracy and precision of new temporal constraints on the system assembly, by integrating the information presented so far, which includes: (1) the subhorizontal magnetic lineations observed within La Obra–Cerro Blanco intrusive suite, (2) the vertical compositional zoning of La Obra pluton (defined by layers hundreds to thousands of meters thick), (3) the crosscutting relationships suggesting that mafic/intermediate intrusions preceded monzogranitic intrusions, and (4) the observed similarities between quartz-monzodioritic layers and stocks, we propose a multistage construction model for La Obra–Cerro Blanco intrusive suite.

Early Stage: Discrete Magma Injections (Quartz-Diorite and Quartz-Monzodiorite)

The earliest recorded stages of the magmatic evolution of La Obra–Cerro Blanco intrusive suite correspond to the initial construction of the magmatic reservoir at the level of exposure, which would have been dominated by the injection and amalgamation of multiple pulses of intermediate mafic magma. The early discrete intrusions were emplaced as subhorizontal sheets, represented by layers of quartz-diorite and quartz-monzodiorites within La Obra pluton, as well as vertical dikes as inferred for the San Juan and Minillas stocks from geologic mapping (Fig. 15A). This intrusion mode has been widely recognized in other natural cases and appears to be an important mechanism for constructing magma reservoirs at upper-crustal levels (Rocchi et al., 2002), where the initial mafic magmas prepare the thermal conditions to host felsic magma reservoirs (e.g., Memeti et al., 2010; Otamendi et al., 2012; Bachmann and Huber, 2016).

We suggest that quartz-diorites represent the parental magma of the entire system and contributed to the thermal priming of the crust to accommodate the subsequent formation of the granite-dominated reservoir. This intrusion mode has been invoked to explain the thermal survival of granitic magma reservoirs in upper-crustal levels, where the relatively cold environment should induce fast cooling and hinder magmatic convection. This condition depends highly on the volume of the magma reservoir, which is difficult to constrain in this case because the floor of the intrusions is unexposed.

Textural evidence suggests that multiple pulses of quartz-dioritic to quartz-monzodioritic magmas successively intruded the crust, favoring magmatic mingling and reheating of the first pulses as new injections of similar composition were injected. This is supported by the abundant presence of mafic enclaves in the San Juan stock with dioritic composition, as well as the frequent presence of sieve textures in plagioclase crystals in quartz-diorites and quartz-monzodiorites. The early intrusion of mafic/intermediate magmas has been recognized in a number of normally zoned plutons (e.g., Searchlight pluton—Bachl et al., 2001; Guadalupe igneous complex—Ratschbacher et al., 2018, 2024).

Second Stage: Felsic Magma Reservoir (Monzogranites)

After the quartz-dioritic and quartz-monzodioritic magma injections, the construction of La Obra–Cerro Blanco magma reservoir transitioned to the periodic intrusion of monzogranitic magma batches emplaced as tabular, elongated bodies, as suggested by the subhorizontal magnetic lineations recorded in La Obra pluton (Fig. 15B). The monzogranites intruded the quartz-monzodiorites when they were completely crystallized or contained but a volumetrically limited interstitial melt fraction, as suggested by the sharp and straight contacts between granitic dikes and quartz-monzodiorites (Fig. 3). This allows us to propose that the latter stage of the magmatic evolution of La Obra–Cerro Blanco plutonic system was dominated by cooling and crystallization of the monzogranites located in the inner parts of the magma reservoir at the exposure level (i.e., away from the contact with the host rock). Two possible scenarios could explain this observation: (1) The inner granites represent late magma injections that intruded the previously emplaced monzogranitic pulses, continuing the incremental growth of the reservoir, or, alternatively, (2) the inner

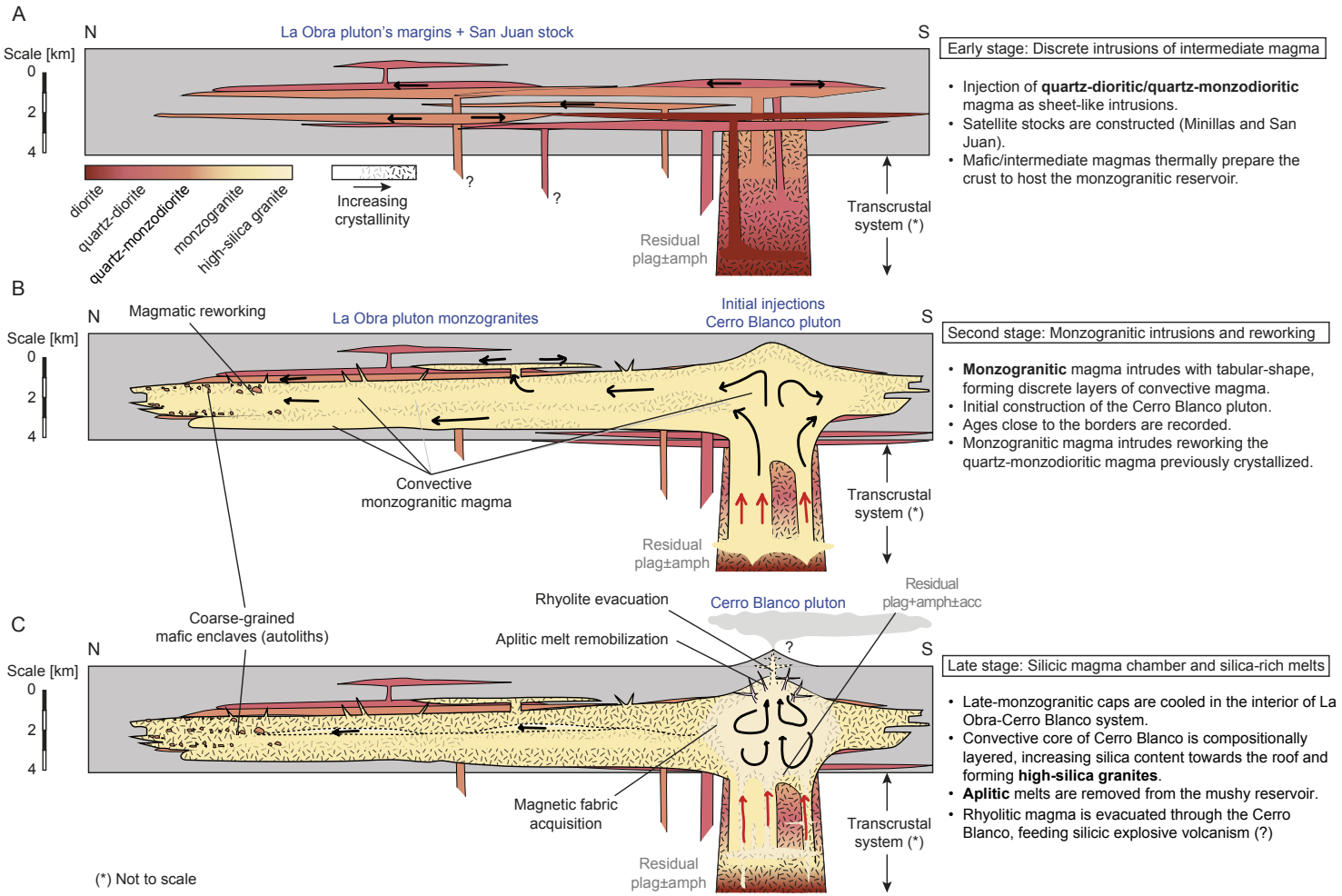

Figure 15. Conceptual model for the construction of La Obra–Cerro Blanco intrusive suite. (A) The early stage was dominated by the injection of discrete magma pulses, which varied in composition, ranging from quartz-diorite to quartz-monzodiorite. Subhorizontal sheet-like intrusions produced the initial architecture of La Obra pluton and satellite stocks. Plagioclase (plag) and minor amphibole (amph) accumulated at deeper crustal levels to generate quartz-diorites and quartz-monzodiorites. (B) The second stage was dominated by the intrusion of monzogranitic magmas generated at deeper crustal levels by plagioclase- and amphibole-dominated fractionation, giving rise to the dominant facies of La Obra pluton. These magmas intruded as discrete tabular-shaped intrusions, probably varying in crystal content and allowing the concentration of coarse-grained mafic enclaves (autoliths) in the middle parts. The initial construction of Cerro Blanco pluton occurred during this stage. (C) During the late-stage evolution of the intrusive suite, the final crystallization of the inner monzogranites and the late convection of the magma chamber formed in Cerro Blanco pluton took place. High-silica granites that composed the Cerro Blanco magma chamber were extracted from a mushy reservoir. Rhyolitic melts (represented by aplitic dikes) were extracted from the chamber in this stage through the upper parts of the pluton, fractionating plagioclase, amphibole, and probably some accessory phases (acc).

monzogranites represent the core of a large, compositionally homogeneous intrusion that remained lower in crystallinity until the last stages of reservoir cooling. The second scenario has been refuted by multiple studies based on geologic mapping, geochronologic data, and thermal modeling of plutons, which favor the first scenario (Glazner et al., 2004; Annen, 2009; Coleman et al., 2012). For example, based on observations from the Sierra Nevada Batholith (USA), Coleman et al. (2012) proposed that the batholith-scale geochemical variations are explained by changes of the magmatic deep source, while the in situ magma differentiation is expressed by compositional changes at the scale of plutons or lithologic domains. We envision the La Obra monzogranitic domain as a series of monzogranitic intrusions fed from deeper crustal zones, but with internal variations that may reflect differentiation processes at the emplacement level, which we explain in the following section.

We propose that the construction mechanism of La Obra pluton involved protracted emplacement of monzogranitic magma batches. This piecemeal assembly eventually produced an elongated magma reservoir at the exposure level, which probably had the ability to convect (as opposed to the initial mafic intrusions; Fig. 15B). The spatial extent of these (short-lived?) convective, monzogranitic magma bodies was probably restricted to one or multiple reservoirs following the main orientation of La Obra pluton, with a thickness of a few hundred meters (Fig. 15B), as suggested by the vertical zonation and inferred from comparably sized intrusions (e.g., Farina et al., 2012; Li et al., 2013; Barboni et al., 2015; Liu et al., 2018). This interpretation is based on the presence of coarse-grained mafic enclaves in the middle levels of La Obra monzogranites (Figs. 3D and 3E), which we interpreted as autoliths (as stated in the first section of this discussion) that were transported by settling into the reservoir and remained stagnant at certain levels due to changes in the effective viscosity of the host magma (Paterson and Miller, 1998).

Late Stage: Cooling of a Single Silicic Magma Chamber (High-Silica Granites)

Although the precision allowed by in situ U-Pb zircon geochronology is not sufficient to detect marked differences between the diverse lithologies composing the plutonic suite, two observations are noteworthy: (1) The quartz-diorites that comprise the San Juan stock (I: sample LO06), located at the periphery of the system, are distinctly older than the monzogranites and high-silica granites located in the lower central parts of La Obra and Cerro Blanco plutons (III: samples LO16 and LO21, for which the 2σ uncertainty of zircon U-Pb weighted mean ages do not overlap). (2) Samples situated in close proximity to the margins of La Obra and Cerro Blanco plutons (II: LO13, LO30, and LO37) appear to have crystallized in a time span between the crystallization of the quartz-diorites and the crystallization of the monzogranites located in the inner (lower) parts of the major intrusions.

It is noteworthy that a similar pattern is also present in Cerro Blanco pluton. The zircon U-Pb weighted mean ages obtained for the upper margin of Cerro Blanco pluton are within uncertainty of weighted mean ages from samples collected at the margins of La Obra pluton (samples LO30 and LO13; Fig. 9B). Insofar as low-precision U-Pb ages and crosscutting relationships can resolve, this observation suggests that Cerro Blanco assembly began concurrently with the intrusion of La Obra monzogranitic magmas and the northern quartz-monzodiorites. Lower Ti contents of zircon grains from monzogranites, and especially high-silica granites, suggest lower crystallization temperatures (700–775 °C at a_{SiO2} = 1.0 and a_{TiO2} = 0.6) compared to quartz-diorites and quartz-monzodiorites (Fig. 9D). Since the Cerro Blanco pluton is more homogeneous in composition (high-silica granites) and records a magnetic fabric pattern differing from the N-S tendency of the La Obra monzogranites, we propose that it might represent a crystal-poor reservoir dominated by mobile magma (Fig. 15B). According to its spatial distribution, this reservoir would have had a more bell-shaped geometry, unlike the elongated, tabular La Obra pluton, thus representing a zone of silicic magma concentration. Piquer et al. (2021) suggested the presence of a significant NW-trending fault system in this particular Andean segment, which intersects the major N-S–trending thrusts in correspondence to the Cerro Blanco pluton, and this would have promoted the upward migration of magma from deeper crustal levels. If the source zone of the entire system was located beneath Cerro Blanco pluton, it could be expected that a single magma reservoir was formed in that area. The existence of a shared, tectonically controlled source and ascent pathway for magmas feeding both intrusions is supported by the homogeneous zircon Hf isotopic values between the northern (La Obra) and southern (Cerro Blanco) segments of this latitudinally extensive magmatic suite (Fig. 10).

The last stage in the evolution of the plutonic system was dominated by the crystallization of Cerro Blanco high-silica granites, which represent the most voluminous accumulation of evolved, silica-rich granitic magma in the whole system at the emplacement level (Fig. 15C). Based on the magnetic fabric patterns recorded in this intrusion, with subvertical foliation forming a concentric pattern surrounding the central part of the pluton, and the subvertical lineation recorded in the upper levels, we interpret Cerro Blanco pluton as the terminal phase of the evolution of a single, crystal-poor granitic magma chamber emplaced at the exposure level. This is supported by the discordant magnetic fabric compared to the orientations observed in La Obra pluton and the absence of clear magmatic internal contacts. The magnetic fabric would have been acquired as the crystallization fronts advanced inward as the magma chamber cooled down from the margins, probably recording the magma flow along the rheological transition between crystal-rich (i.e., rigid sponge, plutonic rind) and crystal-poor magmas as inferred in other case studies (Gutiérrez et al., 2013; Picard et al., 2013). As previously discussed, the trace elements and REE concentrations indicate that these magmas were produced by fractionation of a plagioclase- and amphibole-dominated association, probably from a monzogranitic mushy reservoir (also supported by the disequilibrium of some minerals observed in this unit; Fig. 5). The hypothesis of convective crystal-poor magma reservoirs with batholith-scale volumes (~1000 km^3) has been thoroughly refuted by several studies (e.g., Glazner et al., 2004; Annen,

2009; Coleman et al., 2012). However, in the case of Cerro Blanco pluton, it can be observed to have an area exposure of just over 50 km^2, which could indicate a volume of at least ~100 km^3 (assuming a conservative thickness of 2 km). Consequently, the possibility of a short-lived (10^4–10^5 yr), silicic magmatic chamber formed by crystal-poor, mobile, and eruptible magma cannot be dismissed (for examples of such short-lived, crystal-poor systems, see Eddy et al., 2016; Schaen et al., 2021; Farina et al., 2024).

Above the Emplacement Level: Cerro Blanco Pluton, A Subvolcanic Reservoir(?)

The connection between epizonal plutons and volcanic systems has been intensely debated during the last decades (Glazner et al., 2004; Bachmann and Bergantz, 2008; Clemens et al., 2022a). The contrasting visions of granitic plutons as silicic cumulates (i.e., crystal graveyards) or silicic melts that remained at depth after evacuation and eruption have been discussed in the context of rock compositions and mineralogy (Clemens et al., 2022b; Tavazzani et al., 2020; Wallrich et al., 2023). However, one of the most challenging aspects in this discussion is the scarcity of natural cases where granitic plutons are spatially and temporally connected to subvolcanic and volcanic lithologies. A well-documented case is the Reyðarártindur pluton (southeast Iceland), where multiple dikes have been interpreted as ancient volcanic conduits intruding the volcanic host rock (Rhodes et al., 2021).

La Obra–Cerro Blanco intrusive suite presents several aplitic dikes in the middle and upper levels of the Cerro Blanco pluton, suggesting that this zone has undergone intense felsic melt remobilization, focusing, and extraction. Unfortunately, no aplitic dikes from the main intrusion can be observed intruding into the volcanic host rock, probably because of erosion. However, the vertical porphyritic dikes observed in the top, similar to those observed in other case studies (Rhodes et al., 2021, 2024) and texturally similar to erupted rhyolites (Wallrich et al., 2023; Wiebe and Ulrich, 1997), support the hypothesis that the summit of Cerro Blanco represents an extraction zone of silicic magmas to upper levels of the crust. This is also supported by the steep magnetic lineations recorded in the Cerro Blanco pluton. We suggest that the magmas that formed both the aplitic and the porphyritic dikes could have been more or less efficiently extracted via crystal-melt separation from a crystalline silicic mush (consistent with REE content in dikes). The porphyritic dikes are noteworthy as they carry crystals that were disequilibrated and partially resorbed, similar to the proposed evolution of natural cases such as the Reyðarártindur pluton (Rhodes et al., 2021). Overall, it is difficult to estimate the volume of the extracted material, and further detailed studies are required to determine the intensive variables of magma evacuation (e.g., viscosity, temperature, extraction depth).

In the surrounding area, the Farellones Formation is subdivided into two members: the lower one dominated by pyroclastic rocks and subordinate sedimentary and effusive volcanic rocks, and an upper one dominated by effusive facies and less pyroclastic material. U-Pb zircon ages of 22.5 ± 0.2 Ma, 21.3 ± 0.3 Ma, and 21.41 ± 0.5 Ma have been reported from the silicic crystal-tuff from the lower member of the Farellones Formation (Fig. 1; Fock, 2005; Piquer et al., 2017). These ages are in the same age range as the new and already published weighted mean ages of La Obra–Cerro Blanco intrusive suite samples, suggesting that the plutonic system was emplaced synchronously with the occurrence of explosive, silicic volcanism. This temporal overlap indicates that La Obra–Cerro Blanco system might have been a potential feeder for silicic volcanism during the Miocene. We emphasize that further studies are needed to test this hypothesis, with emphasis on the determination of rock compositions, textures, and volcanic facies. In this sense, La Obra–Cerro Blanco intrusive suite offers new and exciting possibilities to explore not just the architecture of a complex, multistage upper-crustal magmatic reservoir, but also the ever-elusive connection between the plutonic and volcanic realms.

CONCLUSIONS

In this contribution, we provide a comprehensive data set (field observations, geochemical, isotopic, geochronologic, and magnetic fabric data) from La Obra–Cerro Blanco intrusive suite emplaced during the early Miocene in central Chile. We reconstructed the architecture of the intrusion, allowing us to propose a conceptual model for the construction of an upper-crustal silicic magmatic system. We conclude that La Obra–Cerro Blanco system is an example of a magmatic reservoir where the evolution was dominated by diverse silicic magma emplacement styles, from the amalgamation of discrete, sheet-like magma injections of intermediate to silicic composition to the construction of a larger, silicic magma chamber.

The magmatic system spanned an interval of 1.45 ± 0.78 m.y., as defined by the early mafic intrusion of the San Juan stock, the crystallization of the marginal facies, and the late-stage crystallization of the high-silica granite core of La Obra and Cerro Blanco plutons. The long-lived nature of the system, especially in the thickest portion of the reservoir, was likely favored by the thermal priming of the upper crust by early mafic magma injections. However, higher precision on age determinations is required to more accurately determine the order of emplacement and crystallization rates.

During an early stage, La Obra pluton and surrounding stocks were assembled incrementally by the injection of discrete magmatic pulses of varying composition. Specifically, from sheet-like mafic and intermediate pulses, the system shifted to granitic magmas continuously emplaced to form a large, elongated dome-shaped body. The geochemical patterns suggest that the assembled magmas were cogenetic, probably differentiated at deeper levels in the crust by fractionation of plagioclase and variable proportions of mafic phases as hornblende. The sequence of magmatic events recorded during the first stage highlights the importance of thermal priming of the country rocks to sustain long-lived, suprasolidus processes in a silicic magma reservoir (e.g., mixing, mingling, and crystal-melt separation).

The late stage of magmatic evolution was dominated by cooling and crystallization of a single granitic magma chamber recorded in Cerro Blanco pluton, which was probably capable of internal convection. We propose that the Cerro Blanco pluton had the potential to generate mobile high-silica crystal-poor magmas, which could feed the explosive volcanism recorded in the surrounding volcanic formation, where pyroclastic rocks of similar age have been reported. This makes La Obra–Cerro Blanco intrusive suite and the Farellones Formation a potential natural laboratory in which to explore the genetic connection between silicic volcanic rocks and their upper-crustal plutonic roots. These findings should stimulate further studies on the Miocene volcanic and plutonic rocks of central Chile to deepen understanding of the geochemical linkages and reconstruct the architecture of fossil volcanic plumbing systems.

ACKNOWLEDGMENTS

This research has been developed by Chilean National Commission for Science and Technology (CONICYT; currently Chilean National Research and Development Agency [ANID]) projects (FONDECYT #1180577) and the Fund for Publication Developments project (PEP I-2019071) granted by Universidad Mayor, Vicerrectoría de Investigación. We greatly thank Cristóbal Bayer for his invaluable support in the field campaigns. We also acknowledge the ranger's team, part of the Chilean Corporación Nacional Forestal (CONAF), for their valuable support in the field work to sample rocks in Río Clarillo National Park. We also acknowledge Sarah Leray for the guides to access the park and access to previously sampled rocks. We thank Juan Vargas for his support in the separation of minerals and José Galaz for his willingness and support in performing the energy-dispersive spectroscopy and scanning electron microscope analyses.

REFERENCES CITED

Alasino, P.H., Larrovere, M.A., Rocher, S., Dahlquist, J.A., Basei, M.A.S., Memeti, V., Paterson, S., Galindo, C., Macchioli Grande, M., and da Costa Campos Neto, M., 2017, Incremental growth of an upper crustal, A-type pluton, Argentina: Evidence of a re-used magma pathway: Lithos, v. 284–285, p. 347–366, https://doi.org/10.1016/j.lithos.2017.04.013.

Alasino, P.H., Paterson, S.R., Kirsch, M., and Larrovere, M.A., 2022, The role of crustal thickness on magma composition in arcs: An example from the pre-Andean, South American Cordillera: Gondwana Research, v. 106, p. 191–210, https://doi.org/10.1016/j.gr.2022.01.009.

Allmendinger, R.W., Cardozo, N.C., and Fisher, D., 2013, Structural Geology Algorithms: Vectors and Tensors: Cambridge, UK, Cambridge University Press, 289 p.

Annen, C., 2009, From plutons to magma chambers: Thermal constraints on the accumulation of eruptible silicic magma in the upper crust: Earth and Planetary Science Letters, v. 284, p. 409–416, https://doi.org/10.1016/j.epsl.2009.05.006.

Annen, C., Paulatto, M., Sparks, R.S.J., Minshull, T.A., and Kiddle, E.J., 2014, Quantification of the intrusive magma fluxes during magma chamber growth at Soufrière Hills volcano (Montserrat, Lesser Antilles): Journal of Petrology, v. 55, no. 3, p. 529–548, https://doi.org/10.1093/petrology/egt075.

Aranguren, A., Cuevas, J., Tubía, J.M., Román-Berdiel, T., Casas-Sainz, A., and Casas-Ponsati, A., 2003, Granite laccolith emplacement in the Iberian arc: AMS and gravity study of the La Tojiza pluton (NW Spain): Journal of the Geological Society, v. 160, no. 3, p. 435–445, https://doi.org/10.1144/0016-764902-079.

Aravena, A., Gutiérrez, F.J., Parada, M.A., Payacán, Í, Bachmann, O., and Poblete, F., 2017, Compositional zonation of the shallow La Gloria pluton (central Chile) by late-stage extraction/redistribution of residual melts by channelization: Numerical modeling: Lithos, v. 284–285, p. 578–587, https://doi.org/10.1016/j.lithos.2017.05.013.

Archanjo, C.J., Launeau, P., and Bouchez, J.L., 1995, Magnetic fabric vs. magnetite and biotite shape fabrics of the magnetite-bearing granite pluton of Gameleiras (northeast Brazil): Physics of the Earth and Planetary Interiors, v. 89, no. 1, p. 63–75, https://doi.org/10.1016/0031-9201(94)02997-P.

Armijo, R., Rauld, R., Thiele, R., Vargas, G., Campos, J., Lacassin, R., and Kausel, E., 2010, The West Andean thrust, the San Ramón fault, and the seismic hazard for Santiago, Chile: Tectonics, v. 29, no. 2, TC2007, https://doi.org/10.1029/2008TC002427.

Arriagada, C., Ferrando, R., Córdova, L., Morata, D., and Roperch, P., 2013, The Maipo orocline: A first scale structural feature in the Miocene to Recent geodynamic evolution in the central Chilean Andes: Andean Geology, v. 40, p. 419–437, https://doi.org/10.5027/andgeoV40n3-a02.

Bachl, C.A., Miller, C.F., Miller, J.S., and Faulds, J.E., 2001, Construction of a pluton: Evidence from an exposed cross section of the Searchlight pluton, Eldorado Mountains, Nevada: Geological Society of America Bulletin, v. 113, no. 9, p. 1213–1228, https://doi.org/10.1130/0016-7606(2001)113<1213:COAPEF>2.0.CO;2.

Bachmann, O., and Bergantz, G.W., 2004, On the origin of crystal-poor rhyolites: Extracted from batholithic crystal mushes: Journal of Petrology, v. 45, no. 8, p. 1565–1582, https://doi.org/10.1093/petrology/egh019.

Bachmann, O., and Bergantz, G.W., 2008, Rhyolites and their source mushes across tectonic settings: Journal of Petrology, v. 49, no. 12, p. 2277–2285, https://doi.org/10.1093/petrology/egn068.

Bachmann, O., and Huber, C., 2016, Silicic magma reservoirs in the Earth's crust: The American Mineralogist, v. 101, p. 2377–2404, https://doi.org/10.2138/am-2016-5675.

Bachmann, O., and Huber, C., 2019, The inner workings of crustal distillation columns: The physical mechanisms and rates controlling phase separation in silicic magma reservoirs: Journal of Petrology, v. 60, no. 1, p. 3–18, https://doi.org/10.1093/petrology/egy103.

Barbarin, B., 2005, Mafic magmatic enclaves and mafic rocks associated with some granitoids of the central Sierra Nevada batholith, California: Nature, origin, and relations with the hosts: Lithos, v. 80, p. 155–177, https://doi.org/10.1016/j.lithos.2004.05.010.

Barboni, M., Annen, C., and Schoene, B., 2015, Evaluating the construction and evolution of upper crustal magma reservoirs with coupled U/Pb zircon geochronology and thermal modeling: A case study from the Mt. Capanne pluton (Elba, Italy): Earth and Planetary Science Letters, v. 432, p. 436–448, https://doi.org/10.1016/j.epsl.2015.09.043.

Bartley, J.M., Glazner, A.F., and Mahan, K.H., 2012, Formation of pluton roofs, floors, and walls by crack opening at Split Mountain, Sierra Nevada, California: Geosphere, v. 8, no. 5, p. 1086–1103, https://doi.org/10.1130/GES00722.1.

Bergantz, G.W., 2000, On the dynamics of magma mixing by reintrusion: Implications for pluton assembly processes: Journal of Structural Geology, v. 22, no. 9, p. 1297–1309, https://doi.org/10.1016/S0191-8141(00)00053-5.

Biedermann, A., and Bilardello, D., 2021, Practical magnetism VII: Avoiding common misconceptions in magnetic fabric interpretation: The IRM Quarterly, v. 31, no. 3, p. 1–18.

Biedermann, A.R., Kunze, K., and Hirt, A.M., 2018, Interpreting magnetic fabrics in amphibole-bearing rocks: Tectonophysics, v. 722, p. 566–576, https://doi.org/10.1016/j.tecto.2017.11.033.

Black, L.P., Kamo, S.L., Allen, C.M., Aleinikoff, J.N., Davis, D.W., Korsch, R.J., and Foudoulis, C., 2003, TEMORA 1: A new zircon standard for Phanerozoic U–Pb geochronology: Chemical Geology, v. 200, p. 155–170, https://doi.org/10.1016/S0009-2541(03)00165-7.

Bouvier, A., Vervoort, J.D., and Patchett, P.J., 2008, The Lu-Hf and Sm-Nd isotopic composition of CHUR: Constraints from unequilibrated chondrites and implications for the bulk composition of terrestrial planets: Earth and Planetary Science Letters, v. 273, p. 48–57, https://doi.org/10.1016/j.epsl.2008.06.010.

Burchardt, S., Tanner, D., and Krumbholz, M., 2012, The Slaufrudalur pluton, southeast Iceland—An example of shallow magma emplacement by coupled cauldron subsidence and magmatic stoping: Geological Society of America Bulletin, v. 124, no. 1–2, p. 213–227, https://doi.org/10.1130/B30430.1.

Burton-Johnson, A., Macpherson, C.G., Muraszko, J.R., Harrison, R.J., and Jordan, T.A., 2019, Tectonic strain recorded by magnetic fabrics (AMS) in plutons, including Mt. Kinabalu, Borneo: A tool to explore past tectonic regimes and syn-magmatic deformation: Journal of Structural Geology, v. 119, p. 50–60, https://doi.org/10.1016/j.jsg.2018.11.014.

Cardozo, N., and Allmendinger, R.W., 2013, Spherical projections with OSXStereonet: Computers & Geosciences, v. 51, p. 193–205, https://doi.org/10.1016/j.cageo.2012.07.021.

Cashman, K.V., Sparks, R.S.J., and Blundy, J.D., 2017, Vertically extensive and unstable magmatic systems: A unified view of igneous processes: Science, v. 355, no. 6331, https://doi.org/10.1126/science.aag3055.

Charrier, R., Baeza, O., Elgueta, S., Flynn, J.J., Gans, P., Kay, S.M., Muñoz, N., Wyss, A.R., and Zurita, E., 2002, Evidence for Cenozoic extensional basin development and tectonic inversion south of the flat-slab segment, southern Central Andes, Chile (33°–36°SL): Journal of South American Earth Sciences, v. 15, no. 1, p. 117–139, https://doi.org/10.1016/S0895-9811(02)00009-3.

Charrier, R., Bustamante, M., Comte, D., Elgueta, S., Flynn, J.J., Iturra, N., Muñoz, N., Pardo, M., Thiele, R., and Wyss, A.R., 2005, The Abanico extensional basin: Regional extension, chronology of tectonic inversion and relation to shallow seismic activity and Andean uplift: Neues Jahrbuch für Geologie und Paläontologie–Abhandlungen, v. 236, p. 43–77, https://doi.org/10.1127/njgpa/236/2005/43.

Chelle-Michou, C., Chiaradia, M., Ovtcharova, M., Ulianov, A., and Wotzlaw, J.-F., 2014, Zircon petrochronology reveals the temporal link between porphyry systems and the magmatic evolution of their hidden plutonic roots (the Eocene Coroccohuayco deposit, Peru): Lithos, v. 198–199, p. 129–140, https://doi.org/10.1016/j.lithos.2014.03.017.

Chu, N.C., Taylor, R.N., Chavagnac, V., Nesbitt, R.W., Boella, R.M., Milton, J.A., German, C., Bayon, G., and Burton, K., 2002, Hf isotope ratio analysis using multi-collector inductively coupled plasma mass spectrometry: An evaluation of isobaric interference corrections: Journal of Analytical Atomic Spectrometry, v. 17, no. 12, p. 1567–1574, https://doi.org/10.1039/B206707B.

Clemens, J.D., 1998, Observations on the origins and ascent mechanisms of granitic magmas: Journal of the Geological Society, v. 155, no. 5, p. 843–851, https://doi.org/10.1144/gsjgs.155.5.0843.

Clemens, J.D., Elburg, M.A., and Harris, C., 2017, Origins of igneous microgranular enclaves in granites: The example of Central Victoria, Australia: Contributions to Mineralogy and Petrology, v. 172, no. 10, p. 88, https://doi.org/10.1007/s00410-017-1409-2.

Clemens, J.D., Bryan, S.E., Mayne, M.J., Stevens, G., and Petford, N., 2022a, How are silicic volcanic and plutonic systems related? Part 1: A review of geological and geophysical observations, and insights from igneous rock chemistry: Earth-Science Reviews, v. 235, https://doi.org/10.1016/j.earscirev.2022.104249.

Clemens, J.D., Bryan, S.E., Stevens, G., Mayne, M.J., and Petford, N., 2022b, How are silicic volcanic and plutonic systems related? Part 2: Insights from phase-equilibria, thermodynamic modelling and textural evidence: Earth-Science Reviews, v. 235, https://doi.org/10.1016/j.earscirev.2022.104250.

Coleman, D.S., Gray, W., and Glazner, A.F., 2004, Rethinking the emplacement and evolution of zoned plutons: Geochronologic evidence for incremental assembly of the Tuolumne intrusive suite, California: Geology, v. 32, p. 433–436, https://doi.org/10.1130/G20220.1.

Coleman, D.S., Bartley, J.M., Glazner, A.F., and Pardue, M.J., 2012, Is chemical zonation in plutonic rocks driven by changes in source magma composition or shallow-crustal differentiation?: Geosphere, v. 8, no. 6, p. 1568–1587, https://doi.org/10.1130/GES00798.1.

Cornejo, P.C., and Mahood, G.A., 1997, Seeing past the effects of re-equilibration to reconstruct magmatic gradients in plutons: La Gloria pluton, central Chilean Andes: Contributions to Mineralogy and Petrology, v. 127, no. 1–2, p. 159–175, https://doi.org/10.1007/s004100050273.

Correa, K.J., Rabbia, O.M., Hernández, L.B., Selby, D., and Astengo, M., 2016, The timing of magmatism and ore formation in the El Abra porphyry copper deposit, northern Chile: Implications for long-lived multiple-event magmatic-hydrothermal porphyry systems: Economic Geology, v. 111, p. 1–28, https://doi.org/10.2113/econgeo.111.1.1.

Deckart, K., Godoy, E., Bertens, A., Jerez, D., and Saeed, A., 2010, Barren Miocene granitoids in the Central Andean metallogenic belt, Chile: Geochemistry and Nd-Hf and U-Pb isotope systematics: Andean Geology, v. 37, no. 1, p. 1–31, https://doi.org/10.4067/S0718-71062010000100001.

DePaolo, D.J., 1981, Trace element and isotopic effects of combined wallrock assimilation and fractional crystallization: Earth and Planetary Science Letters, v. 53, no. 2, p. 189–202, https://doi.org/10.1016/0012-821X(81)90153-9.

de Saint Blanquat, M., and Tikoff, B., 1997, Development of magmatic to solid-state fabrics during syntectonic emplacement of the Mono Creek Granite, Sierra Nevada Batholith, *in* Bouchez, J.L., Hutton, D.H.W., and Stephens, W.E., eds., Granite: From Segregation of Melt to Emplacement Fabrics: Dordrecht, Netherlands, Springer, Petrology and Structural Geology 8, p. 231–252, https://doi.org/10.1007/978-94-017-1717-5_15.

de Saint Blanquat, M., Horsman, E., Habert, G., Morgan, S., Vanderhaeghe, O., Law, R., and Tikoff, B., 2011, Multiscale magmatic cyclicity, duration of pluton construction, and the paradoxical relationship between tectonism and plutonism in continental arcs: Tectonophysics, v. 500, p. 20–33, https://doi.org/10.1016/j.tecto.2009.12.009.

Ducea, M.N., Saleeby, J.B., and Bergantz, G., 2015, The architecture, chemistry, and evolution of continental magmatic arcs: Annual Review of Earth and Planetary Sciences, v. 43, p. 299–331, https://doi.org/10.1146/annurev-earth-060614-105049.

Dufek, J., and Bachmann, O., 2010, Quantum magmatism: Magmatic compositional gaps generated by melt-crystal dynamics: Geology, v. 38, no. 8, p. 687–690, https://doi.org/10.1130/G30831.1.

Eddy, M.P., Bowring, S.A., Miller, R.B., and Tepper, J.H., 2016, Rapid assembly and crystallization of a fossil large-volume silicic magma chamber: Geology, v. 44, no. 4, p. 331–334, https://doi.org/10.1130/G37631.1.

Eddy, M.P., Ibañez-Mejia, M., Burgess, S.D., Coble, M.A., Cordani, U.G., DesOrmeau, J., Gehrels, G.E., Li, X., MacLennan, S., Pecha, M., Sato, K., Schoene, B., Valencia, V.A., Vervoort, J.D., and Wang, T., 2019, GHR1 zircon—A new Eocene natural reference material for microbeam U-Pb geochronology and Hf isotopic analysis of zircon: Geostandards and Geoanalytical Research, v. 43, no. 1, p. 113–132, https://doi.org/10.1111/ggr.12246.

Eddy, M.P., Pamukçu, A., Schoene, B., Steiner-Leach, T., and Bell, E.A., 2022, Constraints on the timescales and processes that led to high-SiO_2 rhyolite production in the Searchlight pluton, Nevada, USA: Geosphere, v. 18, no. 3, p. 1000–1019, https://doi.org/10.1130/GES02439.1.

Farías, M., Charrier, R., Carretier, S., Martinod, J., Fock, A., Campbell, D., Cáceres, J., and Comte, D., 2008, Late Miocene high and rapid surface uplift and its erosional response in the Andes of central Chile (33°–35°S): Tectonics, v. 27, TC1005, https://doi.org/10.1029/2006TC002046.

Farías, M., Comte, D., Charrier, R., Martinod, J., David, C., Tassara, A., Tapia, F., and Fock, A., 2010, Crustal-scale structural architecture in central Chile based on seismicity and surface geology: Implications for Andean mountain building: Tectonics, v. 29, TC3006, https://doi.org/10.1029/2009TC002480.

Farina, F., Dini, A., Innocenti, F., Rocchi, S., and Westerman, D.S., 2010, Rapid incremental assembly of the Monte Capanne pluton (Elba Island, Tuscany) by downward stacking of magma sheets: Geological Society of America Bulletin, v. 122, no. 9–10, p. 1463–1479, https://doi.org/10.1130/B30112.1.

Farina, F., Stevens, G., and Villaros, A., 2012, Multi-batch, incremental assembly of a dynamic magma chamber: The case of the Peninsula pluton granite (Cape Granite suite, South Africa): Mineralogy and Petrology, v. 106, p. 193–216, https://doi.org/10.1007/s00710-012-0224-8.

Farina, F., Weber, G., Hartung, E., Rubatto, D., Forni, F., Luisier, C., and Caricchi, L., 2024, Magma flux variations triggering shallow-level emplacement of the Takidani pluton (Japan): Insights into the volcanic-plutonic connection: Earth and Planetary Science Letters, v. 635, https://doi.org/10.1016/j.epsl.2024.118688.

Ferry, J.M., and Watson, E.B., 2007, New thermodynamic models and revised calibrations for the Ti-in-zircon and Zr-in-rutile thermometers: Contributions to Mineralogy and Petrology, v. 154, no. 4, p. 429–437, https://doi.org/10.1007/s00410-007-0201-0.

Fock, A., 2005, Cronología y Tectónica de la Exhumación en el Neógeno de los Andes de Chile Central entre los 33° y los 34°S [M.Sc. thesis]: Santiago, Chile, Universidad de Chile, 179 p.

Garibaldi, N., Tikoff, B., Schaen, A.J., and Singer, B.S., 2018, Interpreting granitic fabrics in terms of rhyolitic melt segregation, accumulation, and escape via tectonic filter pressing in the Huemul pluton, Chile: Journal of Geophysical Research: Solid Earth, v. 123, no. 10, p. 8548–8567, https://doi.org/10.1029/2018JB016282.

Gelman, S.E., Gutiérrez, F.J., and Bachmann, O., 2013, On the longevity of large upper crustal silicic magma reservoirs: Geology, v. 41, no. 7, p. 759–762, https://doi.org/10.1130/G34241.1.

Gelman, S.E., Deering, C.D., Bachmann, O., Huber, C., and Gutiérrez, F.J., 2014, Identifying the crystal graveyards remaining after large silicic eruptions: Earth and Planetary Science Letters, v. 403, p. 299–306, https://doi.org/10.1016/j.epsl.2014.07.005.

Giambiagi, L.B., and Ramos, V.A., 2002, Structural evolution of the Andes in a transitional zone between flat and normal subduction (33°30′–33°45′S), Argentina and Chile: Journal of South American Earth Sciences, v. 15, no. 1, p. 101–116, https://doi.org/10.1016/S0895-9811(02)00008-1.

Glazner, A., Bartley, J., Coleman, D.S., Gray, W., and Taylor, R.Z., 2004, Are plutons assembled over millions of years by amalgamation from small magma chambers?: GSA Today, v. 14, p. 4–11, https://doi.org/10.1130/1052-5173(2004)014<0004.

Glazner, A., Coleman, D., and Bartley, J., 2008, The tenuous connection between high-silica rhyolites and granodiorite plutons: Geology, v. 36, no. 2, p. 183–186, https://doi.org/10.1130/G24496A.1.

Godoy, E., Yañez, G., and Vera, E., 1999, Inversion of an Oligocene volcano-tectonic basin and uplifting of its superimposed Miocene magmatic arc in the Chilean central Andes: First seismic and gravity evidences: Tectonophysics, v. 306, no. 2, p. 217–236, https://doi.org/10.1016/S0040-1951(99)00046-3.

Grégoire, V., de Saint Blanquat, M., Nédélec, A., and Bouchez, J.-L., 1995, Shape anisotropy versus magnetic interactions of magnetite grains: Experiments and application to AMS in granitic rocks: Geophysical Research Letters, v. 22, no. 20, p. 2765–2768, https://doi.org/10.1029/95GL02797.

Guillong, M., von Quadt, A., Sakata, S., Peytcheva, I., and Bachmann, O., 2014, LA-ICP-MS Pb-U dating of young zircons from the Kos-Nisyros volcanic centre, SE Aegean arc: Journal of Analytical Atomic Spectrometry, v. 29, p. 963-970, http://doi.org/10.1039/c4ja00009a.

Gutiérrez, F., Payacán, Í., Gelman, S., Bachmann, O., and Parada, M.A., 2013, Late-stage magma flow in a shallow felsic reservoir: Merging the anisotropy of magnetic susceptibility record

with numerical simulations in La Gloria pluton, central Chile: Journal of Geophysical Research: Solid Earth, v. 118, no. 5, p. 1984–1998, https://doi.org/10.1002/jgrb.50164.
Gutiérrez, F., Payacán, I., Szymanowski, D., Guillong, M., Bachmann, O., and Parada, M.A., 2018, Lateral magma propagation during the emplacement of La Gloria pluton, central Chile: Geology, v. 46, no. 12, p. 1051–1054, https://doi.org/10.1130/G45361.1.
Hawkins, D.P., and Wiebe, R.A., 2004, Discrete stoping events in granite plutons: A signature of eruptions from silicic magma chambers?: Geology, v. 32, no. 12, p. 1021–1024, https://doi.org/10.1130/G21083.1.
Hildreth, W., and Moorbath, S., 1988, Crustal contributions to arc magmatism in the Andes of central Chile: Contributions to Mineralogy and Petrology, v. 98, no. 4, p. 455–489, https://doi.org/10.1007/BF00372365.
Horstwood, M.S.A., Košler, J., Gehrels, G., Jackson, S.E., McLean, N.M., Paton, C., Pearson, N.J., Sircombe, K., Sylvester, P., Vermeesch, P., Bowring, J.F., Condon, D.J., and Schoene, B., 2016, Community-derived standards for LA-ICP-MS U-(Th-)Pb geochronology—Uncertainty propagation, age interpretation and data reporting: Geostandards and Geoanalytical Research, v. 40, p. 311–332, https://doi.org/10.1111/j.1751-908X.2016.00379.x.
Irvine, T.N., and Baragar, W.R.A., 1971, A guide to the chemical classification of the common volcanic rocks: Canadian Journal of Earth Sciences, v. 8, no. 5, p. 523–548, https://doi.org/10.1139/e71-055.
Jackson, M.D., Blundy, J., and Sparks, R.S.J., 2018, Chemical differentiation, cold storage and remobilization of magma in the Earth's crust: Nature, v. 564, p. 405–409, https://doi.org/10.1038/s41586-018-0746-2.
Jara, P., and Charrier, R., 2014, Nuevos antecedentes estratigráficos y geocronológicos para el Meso-Cenozoico de la Cordillera Principal de Chile entre 32° y 32°30′S: Implicancias estructurales y paleogeográficas: Andean Geology, v. 41, p. 174–209, https://doi.org/10.5027/andgeoV41n1-a07.
Jara, P., Likerman, J., Winocur, D., Ghiglione, M.C., Cristallini, E.O., Pinto, P., and Charrier, R., 2015, Role of basin width variation in tectonic inversion: Insight from analogue modelling and implications for the tectonic inversion of the Abanico basin, 32°–34°S, Central Andes, *in* Sepúlveda, S.A., et al., eds., Geodynamic Processes in the Andes of Central Chile and Argentina: Geological Society, London, Special Publication 399, p. 83–107, https://doi.org/10.1144/SP399.7.
Jelinek, V., 1981, Characterization of the magnetic fabric of rocks: Tectonophysics, v. 79, no. 3–4, p. T63–T67, https://doi.org/10.1016/0040-1951(81)90110-4.
Kaiser, J.F., de Silva, S., Schmitt, A.K., Economos, R., and Sunagua, M., 2017, Million-year melt–presence in monotonous intermediate magma for a volcanic-plutonic assemblage in the Central Andes: Contrasting histories of crystal-rich and crystal-poor super-sized silicic magmas: Earth and Planetary Science Letters, v. 457, p. 73–86, https://doi.org/10.1016/j.epsl.2016.09.048.
Karakas, O., Degruyter, W., Bachmann, O., and Dufek, J., 2017, Lifetime and size of shallow magma bodies controlled by crustal-scale magmatism: Nature Geoscience, v. 10, no. 6, p. 446–450, https://doi.org/10.1038/ngeo2959.
Kay, S.M., and Mpodozis, C., 2002, Magmatism as a probe to the Neogene shallowing of the Nazca plate beneath the modern Chilean flat-slab: Journal of South American Earth Sciences, v. 15, no. 1, p. 39–57, https://doi.org/10.1016/S0895-9811(02)00005-6.
Kay, S.M., Godoy, E., and Kurtz, A., 2005, Episodic arc migration, crustal thickening, subduction erosion, and magmatism in the south-central Andes: Geological Society of America Bulletin, v. 117, no. 1–2, p. 67–88, https://doi.org/10.1130/B25431.1.
Keller, C.B., Boehnke, P., and Schoene, B., 2017, Temporal variation in relative zircon abundance throughout Earth history: Geochemical Perspectives Letters, v. 3, p. 179–189, https://doi.org/10.7185/geochemlet.1721.
Kern, J.M., de Silva, S.L., Schmitt, A.K., Kaiser, J.F., Iriarte, A.R., and Economos, R., 2016, Geochronological imaging of an episodically constructed subvolcanic batholith: U-Pb in zircon chronochemistry of the Altiplano-Puna volcanic complex of the Central Andes: Geosphere, v. 12, no. 4, p. 1054–1077, https://doi.org/10.1130/GES01258.1.
Kruger, W., and Latypov, R., 2020, Fossilized solidification fronts in the Bushveld Complex argue for liquid-dominated magmatic systems: Nature Communications, v. 11, no. 1, p. 2909, https://doi.org/10.1038/s41467-020-16723-6.
Kurtz, A.C., Kay, S.M., Charrier, R., and Farrar, E., 1997, Geochronology of Miocene plutons and exhumation history of the El Teniente region, central Chile (34–35°S): Revista Geológica de Chile, v. 24, no. 1, p. 75–90, https://doi.org/10.5027/andgeoV24n1-a05.
Large, S.J.E., Wotzlaw, J.-F., Guillong, M., Von Quadt, A., and Heinrich, C.A., 2020, Resolving the timescales of magmatic and hydrothermal processes associated with porphyry deposit formation using zircon U-Pb petrochronology: Geochronology, v. 2, p. 209–230, https://doi.org/10.5194/gchron-2-209-2020.
Large, S.J.E., Nathwani, C.L., Wilkinson, J.J., Knott, T.R., Tapster, S.R., and Buret, Y., 2024, Tectonic and crustal processes drive multi-million year arc magma evolution leading up to porphyry copper deposit formation in central Chile: Journal of Petrology, v. 65, no. 4, https://doi.org/10.1093/petrology/egae023.
Lee, C.-T.A., and Morton, D.M., 2015, High silica granites: Terminal porosity and crystal settling in shallow magma chambers: Earth and Planetary Science Letters, v. 409, p. 23–31, https://doi.org/10.1016/j.epsl.2014.10.040.
Lee, C.-T.A., Morton, D.M., Farner, M.J., and Moitra, P., 2015, Field and model constraints on silicic melt segregation by compaction/hindered settling: The role of water and its effect on latent heat release: The American Mineralogist, v. 100, no. 8–9, p. 1762–1777, https://doi.org/10.2138/am-2015-5121.
Lesher, C.E., 1990, Decoupling of chemical and isotopic exchange during magma mixing: Nature, v. 344, no. 6263, p. 235–237, https://doi.org/10.1038/344235a0.
Leuthold, J., Müntener, O., Baumgartner, L.P., Putlitz, B., Ovtcharova, M., and Schaltegger, U., 2012, Time resolved construction of a bimodal laccolith (Torres del Paine, Patagonia): Earth and Planetary Science Letters, v. 325–326, p. 85–92, https://doi.org/10.1016/j.epsl.2012.01.032.
Li, S., Wilde, S.A., Wang, T., and Guo, Q., 2013, Incremental growth and origin of the Cretaceous Renjiayingzi pluton, southern Inner Mongolia, China: Evidence from structure, geochemistry and geochronology: Journal of Asian Earth Sciences, v. 75, p. 226–242, https://doi.org/10.1016/j.jseaes.2013.07.005.
Lipman, P.W., 2007, Incremental assembly and prolonged consolidation of Cordilleran magma chambers: Evidence from the Southern Rocky Mountain volcanic field: Geosphere, v. 3, no. 1, p. 42–70, https://doi.org/10.1130/GES00061.1.
Liu, H., Martelet, G., Wang, B., Erdmann, S., Chen, Y., Faure, M., Huang, F., Scaillet, B., le-Breton, N., Shu, L., Wang, R., and Zhu, J., 2018, Incremental emplacement of the Late Jurassic mid-crustal, lopolith-like Qitianling pluton, South China, revealed by AMS and Bouguer gravity data: Journal of Geophysical Research: Solid Earth, v. 123, no. 10, p. 9249–9268, https://doi.org/10.1029/2018JB015761.
López-Escobar, L., Frey, F.A., and Oyarzún, J., 1979, Geochemical characteristics of central Chile (33°–34°S) granitoids: Contributions to Mineralogy and Petrology, v. 70, p. 439–450, https://doi.org/10.1007/BF00371050.
Mahood, G.A., and Cornejo, P.C., 1992, Evidence for ascent of differentiated liquids in a silicic magma chamber found in a granitic pluton: Earth and Environmental ScienceTransactions of the Royal Society of Edinburgh, v. 83, no. 1–2, p. 63–69, https://doi.org/10.1017/S0263593300007756.
Marxer, F., Ulmer, P., and Müntener, O., 2023, Ascent-driven differentiation: A mechanism to keep arc magmas metaluminous?: Contributions to Mineralogy and Petrology, v. 178, no. 8, p. 51, https://doi.org/10.1007/s00410-023-02035-7.
Matzel, J.E.P., Bowring, S.A., and Miller, R.B., 2006, Time scales of pluton construction at differing crustal levels: Examples from the Mount Stuart and Tenpeak intrusions, north Cascades, Washington: Geological Society of America Bulletin, v. 118, no. 11–12, p. 1412–1430, https://doi.org/10.1130/B25923.1.
McNulty, B.A., Tobisch, O.T., Cruden, A.R., and Gilder, S., 2000, Multistage emplacement of the Mount Givens pluton, central Sierra Nevada Batholith, California: Geological Society of America Bulletin, v. 112, no. 1, p. 119–135, https://doi.org/10.1130/0016-7606(2000)112<119:MEOTMG>2.0.CO;2.
Memeti, V., Paterson, S., Matzel, J., Mundil, R., and Okaya, D., 2010, Magmatic lobes as "snapshots" of magma chamber growth and evolution in large, composite batholiths: An example from the Tuolumne intrusion, Sierra Nevada, California: Geological Society of America Bulletin, v. 122, no. 11–12, p. 1912–1931, https://doi.org/10.1130/B30004.1.
Menand, T., de Saint-Blanquat, M., and Annen, C., 2011, Emplacement of magma pulses and growth of magma bodies: Tectonophysics, v. 500, no. 1–4, p. 1–2, https://doi.org/10.1016/j.tecto.2010.05.014.
Menand, T., Annen, C., and de Saint Blanquat, M., 2015, Rates of magma transfer in the crust: Insights into magma reservoir recharge and pluton growth: Geology, v. 43, no. 3, p. 199–202, https://doi.org/10.1130/G36224.1.
Michel, J., Baumgartner, L., Putlitz, B., Schaltegger, U., and Ovtcharova, M., 2008, Incremental growth of the Patagonian Torres del Paine laccolith over 90 k.y.: Geology, v. 36, no. 6, p. 459–462, https://doi.org/10.1130/G24546A.1.
Middlemost, E.A.K., 1994, Naming materials in the magma/igneous rock system: Earth-Science Reviews, v. 37, no. 3, p. 215–224, https://doi.org/10.1016/0012-8252(94)90029-9.

Montecinos, P., Schärer, U., Vergara, M., and Aguirre, L., 2008, Lithospheric origin of Oligocene–Miocene magmatism in central Chile: U-Pb ages and Sr-Pb-Hf isotope composition of minerals: Journal of Petrology, v. 49, no. 3, p. 555–580, https://doi.org/10.1093/petrology/egn004.

Morel, M.L.A., Nebel, O., Nebel-Jacobsen, Y.J., Miller, J.S., and Vroon, P.Z., 2008, Hafnium isotope characterization of the GJ-1 zircon reference material by solution and laser-ablation MC-ICPMS: Chemical Geology, v. 255, p. 231–235, https://doi.org/10.1016/j.chemgeo.2008.06.040.

Morgan, G.B., and London, D., 2003, Trace-element partitioning at conditions far from equilibrium: Ba and Cs distributions between alkali feldspar and undercooled hydrous granitic liquid at 200 MPa: Contributions to Mineralogy and Petrology, v. 144, no. 6, p. 722–738, https://doi.org/10.1007/s00410-002-0425-y.

Morgan, S., Stanik, A., Horsman, E., Tikoff, B., de Saint Blanquat, M., and Habert, G., 2008, Emplacement of multiple magma sheets and wall rock deformation: Trachyte Mesa intrusion, Henry Mountains, Utah: Journal of Structural Geology, v. 30, no. 4, p. 491–512, https://doi.org/10.1016/j.jsg.2008.01.005.

Moyen, J.F., Janoušek, V., Laurent, O., Bachmann, O., Jacob, J.B., Farina, F., Fiannacca, P., and Villaros, A., 2021, Crustal melting vs. fractionation of basaltic magmas: Part 1. Granites and paradigms: Lithos, v. 402–403, https://doi.org/10.1016/j.lithos.2021.106291.

Muñoz, M., Charrier, R., Fanning, C.M., Maksaev, V., and Deckart, K., 2012, Zircon trace element and O-Hf isotope analyses of mineralized intrusions from El Teniente ore deposit, Chilean Andes: Constraints on the source and magmatic evolution of porphyry Cu-Mo related magmas: Journal of Petrology, v. 53, no. 6, p. 1091–1122, https://doi.org/10.1093/petrology/egs010.

Muñoz, M., Farías, M., Charrier, R., Fanning, C.M., Polvé, M., and Deckart, K., 2013, Isotopic shifts in the Cenozoic Andean arc of central Chile: Records of an evolving basement throughout cordilleran arc mountain building: Geology, v. 41, no. 8, p. 931–934, https://doi.org/10.1130/G34178.1.

Müntener, O., and Ulmer, P., 2018, Arc crust formation and differentiation constrained by experimental petrology: American Journal of Science, v. 318, no. 1, p. 64–89, https://doi.org/10.2475/01.2018.04.

Müntener, O., Ewing, T., Baumgartner, L.P., Manzini, M., Roux, T., Pellaud, P., and Allemann, L., 2018, Source and fractionation controls on subduction-related plutons and dike swarms in southern Patagonia (Torres del Paine area) and the low Nb/Ta of upper crustal igneous rocks: Contributions to Mineralogy and Petrology, v. 173, no. 5, 38, https://doi.org/10.1007/s00410-018-1467-0.

Nyström, J.O., Vergara, M., Morata, D., and Levi, B., 2003, Tertiary volcanism during extension in the Andean foothills of central Chile (33°15′–33°45′S): Geological Society of America Bulletin, v. 115, no. 12, p. 1523–1537, https://doi.org/10.1130/B25099.1.

Otamendi, J.E., Ducea, M.N., and Bergantz, G.W., 2012, Geological, petrological and geochemical evidence for progressive construction of an arc crustal section, Sierra de Valle Fértil, Famatinian arc, Argentina: Journal of Petrology, v. 53, no. 4, p. 761–800, https://doi.org/10.1093/petrology/egr079.

Parés, J.M., 2015, Sixty years of anisotropy of magnetic susceptibility in deformed sedimentary rocks: Frontiers of Earth Science, v. 3, https://doi.org/10.3389/feart.2015.00004.

Pascual, E., Donaire, T., and Pin, C., 2008, The significance of microgranular enclaves in assessing the magmatic evolution of a high-level composite batholith: A case on the Los Pedroches Batholith, Iberian Massif, Spain: Geochemical Journal, v. 42, no. 2, p. 177–198, https://doi.org/10.2343/geochemj.42.177.

Paterson, S., Memeti, V., Mundil, R., and Žák, J., 2016, Repeated, multiscale, magmatic erosion and recycling in an upper-crustal pluton: Implications for magma chamber dynamics and magma volume estimates: The American Mineralogist, v. 101, no. 10, p. 2176–2198, https://doi.org/10.2138/am-2016-5576.

Paterson, S.R., and Miller, R.B., 1998, Stoped blocks in plutons: Paleo-plumb bobs, viscometers, or chronometers?: Journal of Structural Geology, v. 20, no. 9, p. 1261–1272, https://doi.org/10.1016/S0191-8141(98)00066-2.

Paterson, S.R., Fowler, T.K., Schmidt, K.L., Yoshinobu, A.S., Yuan, E.S., and Miller, R.B., 1998, Interpreting magmatic fabric patterns in plutons: Lithos, v. 44, p. 53–82, https://doi.org/10.1016/S0024-4937(98)00022-X.

Paterson, S.R., Zák, J., and Janousek, V., 2008, Growth of complex sheeted zones during recycling of older magmatic units into younger: Sawmill Canyon area, Tuolumne batholith, Sierra Nevada, California: Journal of Volcanology and Geothermal Research, v. 177, p. 457–484, https://doi.org/10.1016/j.jvolgeores.2008.06.024.

Paterson, S.R., Okaya, D., Memeti, V., Economos, R., and Miller, R.B., 2011, Magma addition and flux calculations of incrementally constructed magma chambers in continental margin arcs: Combined field, geochronologic, and thermal modeling studies: Geosphere, v. 7, no. 6, p. 1439–1468, https://doi.org/10.1130/GES00696.1.

Paterson, S.R., Ardill, K., and Vernon, R., 2019, A review of mesoscopic magmatic structures and their potential for evaluating the hypersolidus evolution of intrusive complexes: Journal of Structural Geology, v. 125, p. 134–147, https://doi.org/10.1016/j.jsg.2018.04.022.

Paton, C., Woodhead, J.D., Hellstrom, J.C., Hergt, J.M., Greig, A., and Maas, R., 2010, Improved laser ablation U-Pb zircon geochronology through robust downhole fractionation correction: Geochemistry, Geophysics, Geosystems, v. 11, no. 3, https://doi.org/https://doi.org/10.1029/2009GC002618.

Paton, C., Hellstrom, J., Paul, B., Woodhead, J., and Hergt, J., 2011, Iolite: Freeware for the visualisation and processing of mass spectrometric data: Journal of Analytical Atomic Spectrometry, v. 26, no. 12, p. 2508–2518, https://doi.org/10.1039/C1JA10172B.

Payacán, I., Gutiérrez, F., Bachmann, O., and Parada, M.Á., 2023, Differentiation of an upper crustal magma reservoir via crystal-melt separation recorded in the San Gabriel pluton, central Chile: Geosphere, v. 19, no. 2, p. 348–369, https://doi.org/10.1130/GES02535.1.

Petford, N., Cruden, A.R., McCaffrey, K.J.W., and Vigneresse, J.L., 2000, Granite magma formation, transport and emplacement in the Earth's crust: Nature, v. 408, no. 6813, p. 669–673, https://doi.org/10.1038/35047000.

Petrus, J.A., and Kamber, B.S., 2012, VizualAge: A novel approach to laser ablation ICP-MS U-Pb geochronology data reduction: Geostandards and Geoanalytical Research, v. 36, no. 3, p. 247–270, https://doi.org/10.1111/j.1751-908X.2012.00158.x.

Picard, D., Arbaret, L., Pichavant, M., Champallier, R., and Launeau, P., 2013, The rheological transition in plagioclase-bearing magmas: Journal of Geophysical Research: Solid Earth, v. 118, no. 4, p. 1363–1377, https://doi.org/10.1002/jgrb.50091.

Piquer, J., Skármeta, J., and Cooke, D.R., 2015, Structural evolution of the Rio Blanco–Los Bronces District, Andes of central Chile: Controls on stratigraphy, magmatism, and mineralization: Economic Geology, v. 110, no. 8, p. 1995–2023, https://doi.org/10.2113/econgeo.110.8.1995.

Piquer, J., Berry, R.F., Scott, R.J., and Cooke, D.R., 2016, Arc-oblique fault systems: Their role in the Cenozoic structural evolution and metallogenesis of the Andes of central Chile: Journal of Structural Geology, v. 89, p. 101–117, https://doi.org/10.1016/j.jsg.2016.05.008.

Piquer, J., Hollings, P., Rivera, O., Cooke, D.R., Baker, M., and Testa, F., 2017, Along-strike segmentation of the Abanico basin, central Chile: New chronological, geochemical and structural constraints: Lithos, v. 268–271, p. 174–197, https://doi.org/10.1016/j.lithos.2016.10.025.

Piquer, J., Rivera, O., Yáñez, G., and Oyarzún, N., 2021, The Piuquencillo fault system: A long-lived, Andean-transverse fault system and its relationship with magmatic and hydrothermal activity: Solid Earth, v. 12, no. 1, p. 253–273, https://doi.org/10.5194/se-12-253-2021.

Ratschbacher, B.C., Keller, C.B., Schoene, B., Paterson, S.R., Anderson, J.L., Okaya, D., Putirka, K., and Lippoldt, R., 2018, A new workflow to assess emplacement duration and melt residence time of compositionally diverse magmas emplaced in a sub-volcanic reservoir: Journal of Petrology, v. 59, no. 9, p. 1787–1809, https://doi.org/10.1093/petrology/egy079.

Ratschbacher, B.C., Ardill, K., Keller, C.B., Schoene, B., Paterson, S.R., Putirka, K.D., Lackey, J.S., and Paige, M.L., 2024, Multi-scale, open-system magmatic and sub-solidus processes contribute to the chemical and isotopic characteristics of the Jurassic Guadalupe igneous complex, Sierra Nevada, California, USA: Geosphere, v. 20, p. 1005–1029, https://doi.org/10.1130/GES02689.1.

Rezeau, H., Moritz, R., Wotzlaw, J.-F., Tayan, R., Melkonyan, R., Ulianov, A., Selby, D., d'Abzac, F.-X., and Stern, R.A., 2016, Temporal and genetic link between incremental pluton assembly and pulsed porphyry Cu-Mo formation in accretionary orogens: Geology, v. 44, p. 627–630, https://doi.org/10.1130/G38088.1.

Rhodes, E., Burchardt, S., Greiner, S.H.M., Mattsson, T., Sigmundsson, F., Schmiedel, T., Barker, A.K., and Witcher, T., 2024, Volcanic unrest as seen from the magmatic source: Reyðarártindur pluton, Iceland: Scientific Reports, v. 14, no. 1, 962, https://doi.org/10.1038/s41598-023-50880-0.

Rhodes, E.L., Barker, A.K., Burchardt, S., Hieronymus, C.F., Rousku, S.N., McGarvie, D.W., Mattsson, T., Schmiedel, T., Ronchin, E., and Witcher, T., 2021, Rapid assembly and eruption of a shallow silicic magma reservoir, Reyðarártindur pluton, southeast Iceland: Geochemistry, Geophysics, Geosystems, v. 22, no. 11, https://doi.org/10.1029/2021GC009999.

Rocchi, S., Westerman, D.S., Dini, A., Innocenti, F., and Tonarini, S., 2002, Two-stage growth of laccoliths at Elba Island, Italy: Geology, v. 30, no. 11, p. 983–986, https://doi.org/10.1130/0091-7613(2002)030<0983:TSGOLA>2.0.CO;2.

Samperton, K.M., Bell, E.A., Barboni, M., Keller, C.B., and Schoene, B., 2017, Zircon age-temperature-compositional spectra in plutonic rocks: Geology, v. 45, no. 11, p. 983–986, https://doi.org/10.1130/G38645.1.

Schaen, A.J., Singer, B.S., Cottle, J.M., Garibaldi, N., Schoene, B., Satkoski, A.M., and Fournelle, J., 2018, Textural and mineralogical record of low-pressure melt extraction and silicic cumulate formation in the late Miocene Risco Bayo–Huemul plutonic complex, southern Andes: Journal of Petrology, v. 59, no. 10, p. 1991–2016, https://doi.org/10.1093/petrology/egy087.

Schaen, A.J., Schoene, B., Dufek, J., Singer, B.S., Eddy, M.P., Jicha, B.R., and Cottle, J.M., 2021, Transient rhyolite melt extraction to produce a shallow granitic pluton: Science Advances, v. 7, https://doi.org/10.1126/sciadv.abf0604.

Scherer, E., Münker, C., and Mezger, K., 2001, Calibration of the lutetium-hafnium clock: Science, v. 293, no. 5530, p. 683–687, https://doi.org/10.1126/science.1061372.

Schoene, B., Schaltegger, U., Brack, P., Latkoczy, C., Stracke, A., and Günther, D., 2012, Rates of magma differentiation and emplacement in a ballooning pluton recorded by U-Pb TIMS-TEA, Adamello batholith, Italy: Earth and Planetary Science Letters, v. 355, p. 162–173, https://doi.org/10.1016/j.epsl.2012.08.019.

Selles, D., and Gana, P., 2001, Geología del área Talagante–San Francisco de Mostazal, Regiones Metropolitana de Santiago y del Libertador General Bernardo O'Higgins: Servicio Nacional de Geología y Minería, Carta Geológica de Chile, Serie Geología Básica 74, 30 p., 1 map, scale 1:100,000.

Shand, S.J., 1927, On the relations between silica, alumina, and the bases in eruptive rocks, considered as a means of classification: Geological Magazine, v. 64, no. 10, p. 446–449, https://doi.org/10.1017/S0016756800103760.

Silva, M.P., Giuliani, A., Schaltegger, U., Chiaradia, M., Nowak, A., Schoene, B., Ulmer, P., and Müntener, O., 2024, Tracing lower crustal contamination in continental arc magmas using Sr-Nd-Hf isotopes: A combined in-situ and bulk rock approach applied to the Adamello Batholith: Journal of Petrology, v. 65, https://doi.org/10.1093/petrology/egae084.

Sláma, J., Košler, J., Condon, D.J., Crowley, J.L., Gerdes, A., Hanchar, J.M., Horstwood, M.S.A., Morris, G.A., Nasdala, L., Norberg, N., Schaltegger, U., Schoene, B., Tubrett, M.N., and Whitehouse, M.J., 2008, Plešovice zircon—A new natural reference material for U-Pb and Hf isotopic microanalysis: Chemical Geology, v. 2491, no. 1, p. 1–35, https://doi.org/10.1016/j.chemgeo.2007.11.005.

Sliwinski, J.T., Guillong, M., Horstwood, M.S.A., and Bachmann, O., 2022, Quantifying long-term reproducibility of zircon reference materials by U-Pb LA-ICP-MS dating: Geostandards and Geoanalytical Research, v. 46, p. 401–409, https://doi.org/10.1111/ggr.12442.

Smith, D.J., 2014, Clinopyroxene precursors to amphibole sponge in arc crust: Nature Communications, v. 5, no. 1, p. 4329, https://doi.org/10.1038/ncomms5329.

Sparks, R.S.J., Annen, C., Blundy, J.D., Cashman, K.V., Rust, A.C., and Jackson, M.D., 2019, Formation and dynamics of magma reservoirs: Philosophical Transactions of the Royal Society A, v. 377, no. 2139, https://doi.org/10.1098/rsta.2018.0019.

Stern, C.R., 1991, Role of subduction erosion in the generation of Andean magmas: Geology, v. 19, no. 1, p. 78–81, https://doi.org/10.1130/0091-7613(1991)019<0078:ROSEIT>2.3.CO;2.

Szymanowski, D., Fehr, M.A., Guillong, M., Coble, M.A., Wotzlaw, J.-F., Nasdala, L., Ellis, B.S., Bachmann, O., and Schönbächler, M., 2018, Isotope-dilution anchoring of zircon reference materials for accurate Ti-in-zircon thermometry: Chemical Geology, v. 481, p. 146–154, https://doi.org/10.1016/j.chemgeo.2018.02.001.

Szymanowski, D., Forni, F., Wolff, J.A., and Ellis, B.S., 2020, Modulation of zircon solubility by crystal-melt dynamics: Geology, v. 48, p. 798–802, https://doi.org/10.1130/G47405.1.

Tavazzani, L., Peres, S., Sinigoi, S., Demarchi, G., Economos, R.C., and Quick, J.E., 2020, Timescales and mechanisms of crystal-mush rejuvenation and melt extraction recorded in Permian plutonic and volcanic rocks of the Sesia magmatic system (southern Alps, Italy): Journal of Petrology, v. 61, no. 5, https://doi.org/10.1093/petrology/egaa049.

Tavazzani, L., Wotzlaw, J.F., Economos, R., Sinigoi, S., Demarchi, G., Szymanowski, D., Laurent, O., Bachmann, O., and Chelle-Michou, C., 2023, High-precision zircon age spectra record the dynamics and evolution of large open-system silicic magma reservoirs: Earth and Planetary Science Letters, v. 623, https://doi.org/10.1016/j.epsl.2023.118432.

Tavazzani, L., Economos, R.C., Peres, S., Demarchi, G., Sinigoi, S., and Bachmann, O., 2024, The role of latent heat buffering in the generation of high-silica rhyolites: Journal of Petrology, v. 65, no. 7, https://doi.org/10.1093/petrology/egae072.

Thiele, R., 1980, Geología de la Hoja Santiago, Región Metropolitana: Servicio Nacional de Geología y Minería, Carta Geológica de Chile 29, 21 p., 1 map, scale 1:250,000.

Townsend, M., and Huber, C., 2020, A critical magma chamber size for volcanic eruptions: Geology, v. 48, no. 5, p. 431–435, https://doi.org/10.1130/G47045.1.

Ulmer, P., and Müntener, O., 2016, Amphibole-melt trace element partitioning of fractionating calc-alkaline magmas in the lower crust: An experimental study: Contributions to Mineralogy and Petrology, v. 171, no. 8, 71, https://doi.org/10.1007/s00410-016-1278-0.

Ulmer, P., Kaegi, R., and Müntener, O., 2018, Experimentally derived intermediate to silica-rich arc magmas by fractional and equilibrium crystallization at 1.0 GPa: An evaluation of phase relationships, compositions, liquid lines of descent and oxygen fugacity: Journal of Petrology, v. 59, p. 11–58, https://doi.org/10.1093/petrology/egy017.

Vergara, M., Charrier, R., Munizaga, F., Rivano, S., Sepúlveda, P., Thiele, R., and Drake, R., 1988, Miocene volcanism in the central Chilean Andes (31°30′S–34°35′S): Journal of South American Earth Sciences, v. 1, no. 2, p. 199–209, https://doi.org/10.1016/0895-9811(88)90038-7.

Vergara, M., López-Escobar, L., Palma, J.L., Hickey-Vargas, R., and Roeschmann, C., 2004, Late Tertiary volcanic episodes in the area of the city of Santiago de Chile: New geochronological and geochemical data: Journal of South American Earth Sciences, v. 17, no. 3, p. 227–238, https://doi.org/10.1016/j.jsames.2004.06.003.

Vermeesch, P., 2018, IsoplotR: A free and open toolbox for geochronology: Geoscience Frontiers, v. 9, no. 5, p. 1479–1493, https://doi.org/10.1016/j.gsf.2018.04.001.

Vigneresse, J.L., and Clemens, J.D., 2000, Granitic magma ascent and emplacement: Neither diapirism nor neutral buoyancy, *in* Vendeville, B.C., et al., eds., Salt, Shale and Igneous Diapirs In and Around Europe: Geological Society, London, Special Publication 174, p. 1–19, https://doi.org/10.1144/GSL.SP.1999.174.01.01.

Villiger, S., Ulmer, P., and Müntener, O., 2007, Equilibrium and fractional crystallization experiments at 0.7 GPa: The effect of pressure on phase relations and liquid compositions of tholeiitic magmas: Journal of Petrology, v. 48, no. 1, p. 159–184, https://doi.org/10.1093/petrology/egl058.

Wallrich, B.M., Miller, C.F., Gualda, G.A.R., Miller, J.S., Hinz, N.H., and Faulds, J.E., 2023, Volcano-pluton connection: Perspectives on material and process linkages, Searchlight pluton and Highland Range volcanic sequence, Nevada, USA: Earth-Science Reviews, v. 238, https://doi.org/10.1016/j.earscirev.2023.104361.

Watson, E.B., 1996, Dissolution, growth and survival of zircons during crustal fusion: Kinetic principals, geological models and implications for isotopic inheritance: Earth and Environmental Science Transactions of the Royal Society of Edinburgh, v. 87, p. 43–56, https://doi.org/10.1017/S0263593300006465.

Weinberg, R.F., Vernon, R.H., and Schmeling, H., 2021, Processes in mushes and their role in the differentiation of granitic rocks: Earth-Science Reviews, v. 220, https://doi.org/10.1016/j.earscirev.2021.103665.

Whitney, D.L., and Evans, B.W., 2010, Abbreviations for names of rock-forming minerals: The American Mineralogist, v. 95, no. 1, p. 185–187, https://doi.org/10.2138/am.2010.3371.

Wiebe, R.A., and Collins, W.J., 1998, Depositional features and stratigraphic sections in granitic plutons: Implications for the emplacement and crystallization of granitic magma: Journal of Structural Geology, v. 20, no. 9/10, p. 1273–1289, https://doi.org/10.1016/S0191-8141(98)00059-5.

Wiebe, R.A., and Ulrich, R., 1997, Origin of composite dikes in the Gouldsboro granite, coastal Maine: Lithos, v. 40, no. 2–4, p. 157–178, https://doi.org/10.1016/S0024-4937(97)00008-X.

Wiedenbeck, M., Allé, P., Corfu, F., Griffin, W.L., Meier, M., Oberli, F., von Quadt, A., Roddick, J.C., and Spiegel, W., 1995, Three natural zircon standards for U-Th-Pb, Lu-Hf, trace element and REE analyses: Geostandards Newsletter, v. 19, no. 1, p. 1–23, https://doi.org/10.1111/j.1751-908X.1995.tb00147.x.

Woodhead, J.D., and Hergt, J.M., 2005, A preliminary appraisal of seven natural zircon reference materials for in situ Hf isotope determination: Geostandards and Geoanalytical Research, v. 29, no. 2, p. 183–195, https://doi.org/10.1111/j.1751-908X.2005.tb00891.x.

Žák, J., Hrouda, F., and Holub, F.V., 2010, Plane-confined magnetic lineations in mingled mafic and felsic magmas, the Sázava pluton, Bohemian Massif: Journal of Volcanology and Geothermal Research, v. 190, no. 3–4, p. 312–324, https://doi.org/10.1016/j.jvolgeores.2009.12.002.